# NON-LINEAR PROPAGATION OF COSMIC RAYS AROUND THEIR SOURCES

Phd Candidate
MARTA D'ANGELO

Advisor
PASQUALE BLASI

co-Advisor

GIOVANNI MORLINO

PhD Thesis

Submitted 16 April, 2017

**Gran Sasso Science Institute**

Ciclo XXIX – A.A 2013-2016


Marta D'Angelo: *Non-linear propagation of Cosmic Rays around their sources,* Advisor Pasquale Blasi, co-Advisor Giovanni Morlino, PhD Thesis, © 2017, June.

WEBSITE:
http://www.gssi.infn.it/

E-MAIL:
marta.dangelo@gssi.infn.it

# ABSTRACT

The cosmic ray spectrum observed at the Earth's surface is the result of two concurring processes: particle acceleration at the source and transport from the sources to Earth. In this work we investigate a particular aspect of the transport process, which consists in the generation of hydromagnetic turbulence by the accelerated particles streaming outside the parent source. When these particles leave the acceleration site, they propagate in a magnetized environment where they interact with the background plasma. This interaction leads to the excitation of streaming instabilities. We show that in near source regions particle propagation is dominated by non-linear self-generation of the unstable waves. As a consequence, the scattering properties of the medium become dependent upon the spectrum and spatial distribution of the energetic particles. The enhancement of the magnetic turbulence forces particles to be self-confined in these near-source regions for a period of time, which can be non-negligible relative to the propagation time to the Earth. This self-confinement process can have important consequences from both the theoretical and observational points of view.

In case of propagation around Galactic supernova remnants we calculate the amount of matter accumulated by self-confined accelerated protons. Then, we compare this quantity with the total amount of matter traversed by cosmic rays in the Galaxy, namely the cosmic ray grammage. The latter quantity is usually inferred from the measurement of the ratio of secondary-to-primary nuclei, as for instance the boron (B)/carbon (C) ratio, and used to estimate parameters of Galactic particle propagation, such as the residence time in the Galaxy. In this work we show that, depending on the level of ionization of the medium, the grammage accumulated in the source vicinity can be a non-negligible fraction of the cosmic ray grammage. Moreover, there is an irreducible grammage that cosmic rays traverse while trapped downstream of the shock that accelerated them, though this contribution is rather uncertain. We conclude that some caution should be used in inferring parameters of Galactic cosmic ray propagation from measurements of the B/C ratio. A possible signature of this self-confinement process is the formation of extended halos of gamma ray emission from $\pi^0$-meson decay around sources. The sum of these halos over the distribution of supernova remnants located into the Galactic disc can be a non negligible contribution to the diffuse gamma-ray emission from the Galactic disc, measured by the *Fermi*-LAT telescope over 7 years of data acquisition. We estimate this contribution assuming that cosmic ray sources are supernova remnants

with a rate of explosion of $1/30\,\mathrm{yr}^{-1}$. We find that the results strongly depend on the type of interstellar medium where the sources are located. In case of a fully ionized medium we show that the halos emission almost saturates the observed Galactic one. However, if the medium is partially ionized, we show that the effect of ion-neutral damping is to strongly reduce the confinement time and consequently the gamma-ray emission. In this case, the contribution to the Galactic emission is non negligible only for energies of $\gamma$-rays around 100 GeV.

The effect of self-confinement appears to be important even in the proximity of Extra-Galactic sources of cosmic rays. In this context we show that the self-confinement process forces cosmic rays to be trapped in the source proximity. In addition, we find that particles with energies less than a critical value $E_c$ are not able to reach the Earth, because the time of their confinement in the source proximity exceeds the Age of the Universe. As a consequence, the spectrum of cosmic rays leaving these sources and eventually reaching the Earth must have a low-energy cutoff at an energy $E_c$. In particular we show that, if the background magnetic field is extremely low, i.e. $\ll$ nG, the value of this critical energy $E_c$ depends only on the source luminosity $L_{CR}$ as $\propto L_{CR}^{2/3}$. We consider as typical value of $L_{CR}$ about $10^{44}$erg/s and we obtain $E_c \approx 10^7$ GeV. For larger values of the background magnetic field we find that $E_c$ depends also on the field strength $B_0$ and on its coherence length $l_c$ and, considering as typical values of $B_0 \approx 0.1$ nG and of $l_c \approx 10$ Mpc, we obtain $E_c \approx 2 \times 10^8$ GeV. In both these scenarios the cut-off energy $E_c$ is in the energy range where the transition from Galactic to Extra-Galactic origin is assumed to take place.

# ACKNOWLEDGEMENTS

This work would not have been possible without my advisor, Pasquale Blasi, and my co-advisor Giovanni Morlino. I would like to express my gratitude to them for the discussions on the various aspects of cosmic ray physics, and most importantly for their advises on how to become a good researcher. My heartfelt thanks.

I also want to thank the referees Felix A. Aharonian and Stefano Gabici for their precious comments which improve the quality of this work.

I thank Damiano Caprioli for his effort to collaborate with me and providing me his continuos support.

In addition, I would like to thank the Arcetri Group for the lovely time spent at the "Osservatorio di Arcetri" and in particular Elena Amato for her collaboration.

A special mention goes to Francesco Vissani, especially for showing me his incredible passion for Science which helped me so many times.

I owe a lot to all the staff and students of the GSSI, above all: Michele, Lucia, Maria, Giancarlo and my flat mate Sarah. Thanks from the bottom of my heart guys! This important period of my life would not have been possible without the continuos support from all of you.

# CONTENTS

# INTRODUCTION

Cosmic rays (CRs) are very energetic charged particles produced somewhere in the Universe that hit the Earth with an almost perfect isotropic flux. They are composed primarily of protons with about 10% fraction of helium nuclei and smaller abundances of heavier elements. There is also a very small fraction of electrons-positrons of the order of 1%. One of the most noticeable features is that these particles are detected over twelve decades of energy: from fractions of GeV up to more than $10^{11}$ GeV (see Ref. [1–4] for general reviews). More than one century after the discovery of cosmic rays, a theory of their origin is still being developed, accommodating new pieces of observation and new theoretical ideas. One of the open problems is the description of the connection between the accelerated particles leaving the sources and what we observe as CRs.

The standard paradigm of Galactic CR propagation (see Ref. [1, 5]) describes particle transport in the Galaxy as diffusive with a momentum dependent diffusion coefficient $D(p)$. In this picture the propagation time $\tau_d(p)$ is dominated by diffusion in the magnetized halo of size $H$, i.e. $\tau_d(p) = H^2/D(p)$, and the thinner disc is traversed occasionally. The estimate of $\tau_d$ is usually inferred from the measurement of the ratio of secondary to primary nuclei, as for instance Boron over Carbon nuclei (B/C), because this observable is directly releted to the grammage [1, 6, 7]. The grammage $X$ is defined as the amount of matter traversed by CRs during their propagation and it is proportional to the residence time in the Galaxy. Indeed, CRs accumulate the grammage during their journey to the Earth, in particular when they cross the disc. We note that in this scenario the halo is considered almost empty and the gas density $n_d$ is distributed mostly in the disc, where CR sources are located. Thus, this quantity can be estimated as $X(p) \approx 1.4 m_p n_d (h/H) c \tau_d(p)$, where $m_p$ is the proton mass (in this work we consider only relativistic protons as accelerated particles), $c$ is the speed of light and $h$ is the size of the disc. The numerical factor 1.4 accounts for the fact that both protons and helium nuclei in the interstellar medium serve as target for the particle collisions that define $X$. This implies that the grammage scales as $1/D(p)$ where $D(p)$ is assumed the same throughout the disc and halo regions [1, 6, 7]. In this paradigm the measurement of B/C ratio, which is proportional to the grammage, provides important information on the parameters of Galactic propagation, such as the slope of the diffusion coefficient.

The Galactic diffusive description, discussed above, is expected to be accurate on spatial scales much larger than the coherence scale of the Galactic magnetic field, which is of the order of $\sim 100\,\mathrm{pc}$ [8].

However, it becomes questionable on smaller scales, as it is for instance in the close surroundings of a source [9–11]. Near sources one may expect that the CR density and density gradient may be large enough to affect the environment in which CRs propagate, through the excitation of electromagnetic instabilities. Such phenomena can in turn affect particles propagation, forcing their confinement in the near-source region to be longer than naively expected and with important implications on CR transport on the Galactic scale.

The investigation of the role of self-generated magnetic turbulence due to CR-driven instabilities goes back to the '70s. In the theory of diffusive shock acceleration [12–16], for instance, large magnetic field amplification is required close to the shock front in order to explain particle acceleration up to $10^6$ - $10^7$ GeV (as expected from observations of CRs at Earth). Also the presence of narrow filaments of non-thermal X-ray radiation in virtually all young supernova remnants can be produced by this mechanism [17, 18]. The self-generation of turbulence, in addition, can be relevant for CR propagation over the whole Galaxy, especially in the prediction of the spectra of several nuclei and of the B/C ratio in order to well reproduce the available data [19, 20].

Within a distance from the source of the order of the coherence scale of the background magnetic field, particle propagation is dominated by the non-linear effects of self-generated turbulence via the excitation of CR streaming instability. The aim of this work is to study these effects and discuss the possible phenomenological implications in both Galactic and Extra-Galactic environments. The streaming instability is characterized by two branches: the resonant branch and the non-resonant one. The resonant branch [21–23] takes place when a spatial gradient is present in the CR distribution. This gradient generates Alfvén waves (hydromagnetic waves propagating parallel to the background field) moving in the direction of the decreasing CR density. When accelerated particles stream faster that the local Alfvén speed, waves having wavelengths comparable to particle Larmor radii become unstable. The importance of such instability relies on the fact that these resonant modes slow down CRs propagation. This process is considered to play a major role in CR transport across the Galaxy (see Ref. [24] for a general review). The non-resonant brach [25, 26] requires a condition more stringent than the one necessary for the resonant branch to take place. In this case, indeed, accelerated particles must drift at a velocity greater than the ratio of the background magnetic energy density to the CR kinetic energy density times the speed of light. If this condition is satisfied, the electric current carrying by energetic particles generates unstable magnetic waves with an especially fast growth rate. Thanks to this feature, the non-resonant streaming instability, also refereed to as the Bell's instability, has been proposed as responsible for the magnetic field

amplification implied by X-ray observations [17] a condition which is required to accelerate particles up to $\sim$ PeV energies in supernova remnants.

In case of Galactic supernova remnants (SNRs, considered as the most important CR source population in the Milky Way), within a distance of about the coherence scale of the Galactic magnetic field, of the order of $\sim 100\,\mathrm{pc}$ [8], the density of particles leaving the acceleration site stays larger than the Galactic mean density for relatively long time, so that a strong gradient in the CR distribution is present and the resonant branch can develop. In addition to this requirement there is also the fact that some mechanisms can damp the unstable waves, especially the ion-neutral damping [27, 28] due to the presence of neutral atoms in the background plasma. Indeed, depending on the level of ionization of the surrounding medium, this damping can be so efficient to prevent the growth of the unstable waves. Thus, a second important condition is that resonant unstable waves grow faster than damping processes. In this context the non-resonant branch cannot be excited because the energy density of the Galactic magnetic field is larger than particles energy density. In case of Extra-Galactic sources, instead, the upper limits on the cosmological magnetic field are extremely low, i.e. $\leqslant$ nG [29], so that within the coherence scale, which is of the order of 10 Mpc [30, 31], and for the typical luminosities invoked for such sources, about $10^{44}$ erg/s [32], the velocity requirement for the development of the non-resonant branch can be satisfied. Nevertheless, a second condition has to be satisfied that is the time scale of the fastest growing mode must be smaller than the Age of the Universe.

The excitation of the streaming instability leads to self-confine particles near the accelerator in both Galactic and Extra-Galactic environments. This phenomenon can have important consequences in terms of CR propagation to the Earth.

First we discuss the possible implications for the Galactic transport. The particle self-confinement in regions near SNRs can produce a non negligible contribution to the Galactic grammage in the energy range where the resonant modes are effectively excited. Moreover, there is another contribution to take into account, namely the irreducible grammage accumulated by the accelerated particles while trapped downstream of the shock during the acceleration process. The presence of these two contributions does not imply that the confinement time in the near source region is close to the escape time of CRs from the Galaxy, because most of the matter is distributed into the disc while the halo (where in the standard paradigm particles spent most of the time) is almost empty. What this scenario suggests is that the assumption of the Galactic diffusion coefficient to be equal throughout the disc and halo regions is too simple to describe the Galactic transport in a suitable way. Thus, a combination of the stan-

dard Galactic propagation plus one of the two phenomena described above can be more appropriate to reproduce the available data. A possible signature of the self-confinement can be the formation of an extended halo of $\gamma$-ray emission due to the decay of $\pi^0$-mesons produced by the interaction between CRs and nucleons of the Interstellar Medium. The emission from a single halo is too faint to be detected with the current gamma-ray telescopes. However, the sum of these halos over the whole CR source population can produce a non negligible contribution to the diffuse gamma-ray emissivity from the Galactic disc. The diffuse Galactic emission has been measured by the *Fermi*-LAT telescope over 7 years of data acquisition. Therefore, the predicted emission from the total halo's population can be compared with the available data. A clear understanding of the diffuse gamma-ray emission is essential to infer the correct CR distribution in the whole Galactic volume, hence it is important to disentangle the actual diffuse gamma ray emission from the one coming from the sources and the near-source regions. Part of this work has been devoted to address this issue. The development of the streaming instability in its non-resonant form around Extra-Galactic sources can lead also to self-confinement, as previously mentioned. This can have important implications on Extra-Galactic CR propagation. In a situation in which particles remain self-confined for times exceeding the age of the Universe, they cannot propagate to the Earth. This means that the self-confinement process can introduce a critical energy so that CRs with energies less than this value do no reach the Earth. In other terms, the self-generation of magnetic turbulence via the excitation of the non-resonant streaming instability gives rise to a cutoff in the spectrum of Extra-Galactic CRs reaching the Earth. Indeed, a low energy cutoff in the Extra-Galactic CR spectrum has been proposed by several models in order to describe in a phenomenological way the transition between Galactic and Extra-Galactic CRs. For instance a cut-off is required by the dip model [33, 34] as well as by models requiring a mixed composition [35]. Such a cut-off is usually interpreted as a consequence of the existence of a "magnetic horizon" around the Extra-Galactic sources, namely a region where CRs are confined on the timescale of the age of the Universe [36]. Nevertheless the existence of a magnetic horizon requires a quite arbitrary assumption on magnetic field properties. In the scenario depicted in this work the presence of a low-energy cutoff in the UHECR spectrum is a natural consequence of the self-confinement process and could be a crucial element to describe the transition region between Galactic and Extra-Galactic CRs.

## STRUCTURE OF THE THESIS

In Ch. 1 we start the discussion with a brief review on cosmic ray phenomenology focusing on the basic aspects of the actual paradigm of Galactic cosmic ray propagation as well as the actual models of the transition from Galactic to Extra-Galactic CRs.

In Ch. 2 we describe the mathematical tools necessary to model the non-linear propagation around CR sources. We discuss the growth rate of both the resonant and the non-resonant branch of streaming instability and the most important damping mechanisms.

In Ch. 3 we consider the context of Galactic sources. We solve the CR transport equation numerically together with the time evolution of the self-generated turbulence considering different levels of ionization of the medium surrounding the parent start. We estimate the residence time spent by the accelerated protons near their sources and the related grammage. Then we calculate the sum of the gamma-ray halos over the whole SNR distribution in the Galactic disc and we compare our predicted emission with the diffuse Galactic emission measured by the *Fermi*-LAT telescope.

In Ch. 4 we consider the context of extragalactic sources. We analyze the conditions for the development of non-resonant modes of the streaming instability which lead to particle's self-confinement. Then we show that particles with energies less than a critical energy are confined inside a distance of few Mpc from the source for times exceeding the age of the Universe, thereby introducing a cutoff in the spectrum of CRs reaching the Earth.

The conclusions are described in Ch. 5.

# 1 COSMIC RAY PHENOMENOLOGY

In Sec. 1.1 we briefly discuss the main features of the cosmic ray spectrum observed at the Earth. Then, in Sec. 1.2 we describe the current paradigm for the origin of Galactic cosmic rays, focusing on the diffusive model of their propagation across the Galaxy. In particular, we discuss the importance of the measurement of the ratio of secondary to primary nuclei, as for instance Boron over Carbon nuclei (B/C), in order to infer parameters of Galactic transport. In Sec. 1.3 we explore the effects of the self-generation of magnetic turbulence due to CR streaming instability on particle propagation around sources and the possible implications on the Galactic transport. In Sec. 1.4, we discuss the possible origin of Extra-Galactic CRs, in particular focusing on the current models of the transition from Galactic to Extra-Galactic CRs. The effects of CR streaming instability on particle propagation around sources and the relative implications on the transport to the Earth are discussed in Sec. 1.5.

## 1.1 COSMIC RAY SPECTRUM

Cosmic Rays are very energetic charged particles which are produced somewhere in the Universe and propagate to the Earth. The all-particle spectrum is very close to a broken power-law and ranges over twelve decades of energy: from fractions of GeV up to $\sim 10^{11}$ GeV.

In figure 1 we report the all particle differential flux (number of particles per unit time, energy, surface and per unit solid angle) as measured by different experiments. We note that the behavior of the curve is approximately fitted by a power-law $\sim E^{-3}$. For energies lower than 10 GeV the differential flux curves down. This is due to the interaction of CRs with the magnetized wind originated from our Sun, which prevents the arrival of very low energy particles [37].

In the energy range from 10 GeV to $10^6$ GeV the slope of the differential flux is $\propto E^{-2.7}$. Around 3 - 5 $\times 10^6$ GeV it changes becoming $\propto E^{-3.1}$ (see Ref. [1–4] for general reviews). This is the most prominent feature in the CR spectrum, clearly visible in Fig. 1, and it is usually referred to as the *knee*. This peculiarity is commonly explained as the result of rigidity dependent acceleration processes [2, 38]. Indeed, if protons are accelerated up to a maximum energy $E_{max,p} \sim 5 \times 10^6$ GeV, then iron nuclei are accelerated up to $E_{max,Fe} \simeq Z_{Fe} \times E_{max,p}$. At such high energies Fe is expected to be fully ionized and consequently the unscreened charge is $Z_{Fe} = 26$,

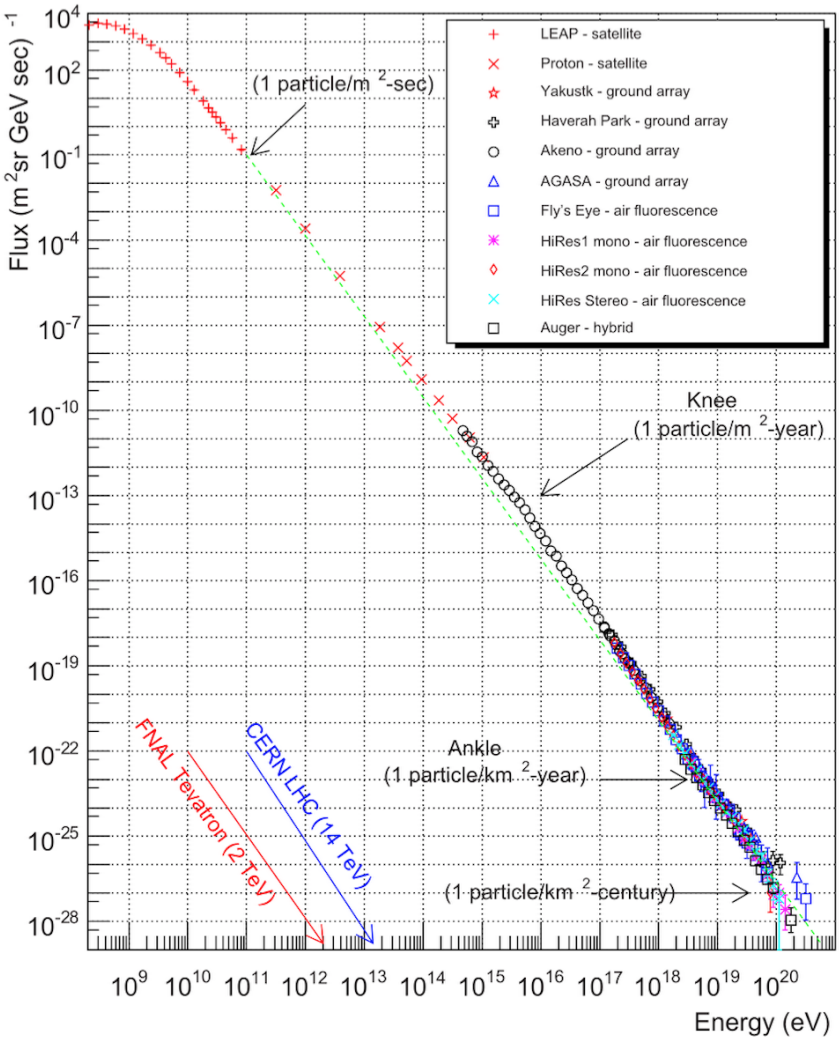


**Figure 1:** All particle CR flux measured by different experiments at the Earth. We show the energies reached by the Tevatron and LHC accelerators in order to give the idea of the impressive energy range in which CRs are detected. (Image: Telescope Array Project Commons)

so that $E_{max,Fe} \sim 10^8$ GeV. Thus, the superposition of the cut-offs in the spectra of different elements results in a knee in the all particle spectrum [2, 38, 39].

Recently, PAMELA [40] and AMS-02 [41] revealed an hardening of both the proton and helium spectra around 200 GeV/nucleon. The experiments found a quite abrupt flattening of about 0.14 (AMS-02) and 0.22 (PAMELA) in their spectral slope. Moreover, the proton spectrum presents a slightly different slope than that of the He [42]. For energies above 300 GeV/nucleon the spectral slopes measured by PAMELA and AMS-02 are in agreement with those measured by previous experiments also for heavier nuclei, as for instance CREAM [42], TRACER [43] and BESS [44]. This feature can either be connected to a break in the spectrum injected by sources (possibly only by local ones [45]) or to the transport process throughout the Galaxy. In the context of the latter scenario, a relevant role could be played by turbulence self-generated by CRs that try to escape from the Galaxy, as discussed in Ref. [19] and Ref. [46]. In these works the authors suggest that the diffusion process is dominated by the self-generated turbulence up to a particle rigidity of $\sim$ 200GV, while for larger energies the galactic turbulence dominates. As a consequence the spectral hardening could reflect the change in the slope of the magnetic turbulence.

The differential flux presents two other spectral features: a change in the slope occurring around 3 - 5 $\times$ $10^9$ GeV, also known as the *ankle*, where the flux flattens again towards a value close to $E^{-2.7}$ and an evident suppression around $\approx 10^{11}$ GeV. The ankle is usually interpreted as the energy at which the transition from Galactic to Extra-Galactic origin occurs [47, 48]. Nevertheless, in the last years this scenario has been questioned [31, 49].

The problem of the transition from Galactic to Extra-Galactic origin is strictly related with the measurements on the spectrum and chemical composition of particles with energies greater than $10^9$ GeV, also referred to as ultra-high energy CRs (UHECRs). At energy $\sim$ $10^9$ GeV all the three largest experiments, Pierre Auger Observatory (PAO) [50, 51], Telescope Array (TA) [52, 53] and High Resolution Fly's Eye experiment (HiRes) [54], agree that the flux is dominated by a light component, while at higher energies the situation is less clear. TA [52] and HiRes [54] found that the chemical composition is compatible with being proton-dominated up to the highest energies. The PAO, instead, spots a somewhat different scenario where a gradual transition from light to heavy component takes place above $\sim 5 \times 10^9$ GeV [50]. The KASCADE-GRANDE experiment has recently presented the measurements of the spectrum and chemical composition in the energy range $10^7$ - $10^9$ GeV [55], showing that the light component, presumably formed by protons and helium nuclei with a small fraction of carbon nitrogen and oxygen (CNO), has an ankle

like structure at $10^8$ GeV. The authors propose that this features is related with the transition of the light nuclei component from Galactic to Extra-Galactic origin. The problem of the transition from Galactic to Extra-Galactic origin is of the utmost importance in order to understand the global picture of CR physics, especially in connection with the aspect of CR transport, and will be discussed in Sec. 1.4.1.

There is no clear consensus even on the physical interpretation of the flux suppression [56, 57], which is measured by HiRes, TA and PAO with good statistical significance beyond $4 \times 10^{10}$ GeV. This suppression was predicted almost a half a century ago by Greisen [58] and independently by Zatsepin and Kuz'min (GZK) [59]. Their idea is based on the assumption that UHECRs are made essentially by protons. In this scenario, protons propagating through Extra-Galactic distances suffer energy losses due to the interaction with the cosmic microwave background (CMB), giving rise to a sharp decrease in the CR flux, a feature than called GZK cut-off. Currently, the HiRes collaboration has associated its measurement on the flux suppression of the protonic component with the GZK cut-off model [60]. The PAO's measurement of mass composition at the highest energies, instead, is not consistent with a pure proton composition [61]. In this latter case the suppression could either be due to nuclei fragmentation in collision with CMB photons, or reflect the maximum acceleration energy of Extra-Galactic sources (or a combination of both processes [56]).

The non-linear interaction of CRs with the environment in which they propagate can play a key role in the generation of spectral breaks or any other feature in power law trends. The aim of this work is to study a particular aspect of the non-linear particle transport, that is the non-linear propagation around CR sources. Indeed, the energetic particles can excite the streaming instability which has the effect of self-confine particles into near-source regions. In Sec. 1.2 we discuss the actual diffusive paradigm of CR transport across the Galaxy. Then we explain the possibile implications of our study within this framework in Sec. 1.3. In Sec. 1.4 we describe the different models of the transition from Galactic to Extra-Galactic origin and we conclude this Chapter with the possible implications of self-confinement.

## 1.2 PARADIGM OF THE ORIGIN AND PROPAGATION OF GALACTIC COSMIC RAYS

Supernova remnants (SNRs) are the most reliable factories for Galactic CRs [1, 5]. This idea has been put forward for the first time by Baade and Zwicky in 1934 [62], even though they argued for an Extra-Galactic origin of all the CRs. Hence, they concluded that a SNR scenario could not be possible because SN do not produce enough power to fill the whole Universe with the measured density of CRs. In the

'60s Ginzburg and Syrovatsky [63] discussed the energy requirement necessary to accelerate CRs only in the Galactic context. They found that a fraction around 10% of the energy released by SN blast waves must be channeled into accelerated particles, in order to explain the energy density of Galactic CRs of about $\sim$ 1eV/cm$^3$. Their assumptions for this energetic argument are: the amount of kinetic energy released during the explosion of a SN is $\sim 10^{51}$ erg and the rate of explosion in our Galaxy is $1/30\text{yr}^{-1}$.

The mechanism which is generally accepted to work in SNRs is the diffusive shock acceleration (DSA) process [12, 13, 64–66]. The DSA mechanism is based on the fact that charged particles undergo repeated reflections due to the magnetic irregularities present in the shock region (see Ref. [67] for a recent review). For each cycle in which particles cross the shock from one side to the other and come back, they subtract energy from the bulk motion of the plasma. In this scenario the magnetic irregularities serve as diffusive scattering centers. Moreover, the magnetic turbulence confines particles around the shock, allowing them to cross the shock repeatedly. As a result the spectrum is a power-law, completely independent of the details of particle scattering [12]. For strong shocks (i.e. shock velocity much larger than the ISM sound speed) the slope of the power-law is $\propto E^{-2}$. Nevertheless, the DSA mechanism has several limitations. For instance, this theory does not account for the dynamical reaction of accelerated particles which can have important effects on the shock structure [68, 69]. Moreover, non linear processes are required, such as the generation of plasma instabilities by the same energetic particles, in order to explain the magnetic field amplification at the shock necessary to accelerate up to the knee energy [12–16]. These aspects are examined in the non-linear theory of DSA and we refer to Ref. [1, 5, 70] for detailed reviews.

There are several observational evidences of SNRs being the main factories of Galactic CRs. In the Radio and X-ray frequency range observed from young SNRs a relevant contribution comes from synchrotron emission of relativistic electrons propagating in magnetic fields. This multi-frequency emission provides important information both about the spectrum of the accelerated electrons and about the presence of magnetic field amplification near the remnant [17, 18]. In the case of hadrons $\gamma$-ray emission in the TeV range, instead, can be used as a powerful test for their acceleration in SNRs, as pointed out by O'C. Drury et al. in 1994 [71]. Indeed, such an emission might derive from the decay of $\pi^0$s produced by nuclear collisions of accelerated protons, i.e. $p_{CR} + p_{ISM} \rightarrow \pi^0 \rightarrow \gamma\gamma$, with material present in the shocked circumstellar medium. As a consequence of this process, a bump-like feature is produced in the associated gamma-ray spectrum, around the threshold for the pion production. Detections of the pion bump in the gamma-ray spectrum of some SNRs near

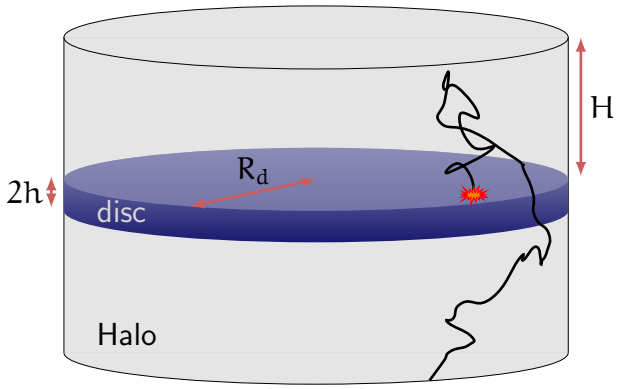


**Figure 2:** Sketch of the diffusive model for CR propagation into the Galaxy.

molecular clouds have been claimed both by the AGILE collaboration [72, 73] and the Fermi-LAT collaboration [74–78]. It is important to mention that SNRs near molecular clouds are fundamental astrophysical laboratories where to investigate not only CR acceleration but also the process of particle escape from the sources which is the bridge that connect the accelerated spectrum with the one injected into theGalaxy, as pointed out in Ref. [79–81].

We have briefly summarized the basic aspects of the SNR paradigm of the origin of Galactic CRs. Now we discuss the diffusive model of CR propagation throughout the Galaxy, focusing on the standard predictions.

### 1.2.1 Cosmic ray propagation throughout the Galaxy

In the current view of CR transport, particles diffusse in an almost empty and magnetized halo of size $H \sim 3\,\mathrm{kpc}$ and occasionally traverse the dense disc. Here we assume that the disc is a thin region with an half width $h$ of about $\sim 150\,\mathrm{pc}$ where CRs sources are located [1, 6, 7]. The diffusion transport is due to scattering by the irregularities in the Galactic magnetic field [6], in analogy with the diffusion off magnetic waves in DSA theory. Other processes can affect CR propagation, such as advection due the motion of the scattering waves or bulk motion of the plasma, energy gain and/or loss and nuclear fragmentation. This simplified version of the diffusive model describing Galactic propagation is sketched in Fig. 2. It is worth noticing that in this model the diffusion coefficient is assumed to be the same in the whole Galaxy and it is treated as a fitting parameter. Usually, this parameter is inferred from the measurement of the ratio of secondary to primary CR flux, in particular from the boron over carbon (B/C) ratio [1, 6, 7].

The secondary CRs are charged particles produced by nuclear interactions between energetic nuclei, accelerated directly at CR sources, and nuclei composing the ISM. This process is also referred to as *spal-*

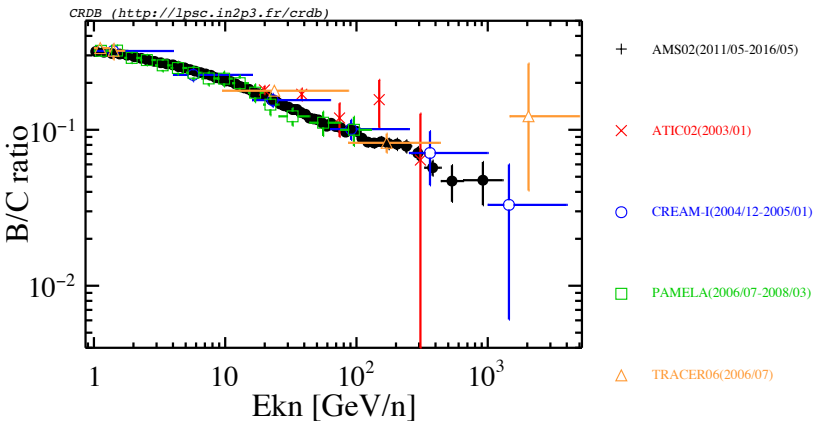


**Figure 3:** B/C ratio as a function of energy per nucleon for different experiments, as listed on the plot legend (data taken from the Cosmic Ray Database, see Ref. [82]).

*lation*. For instance, carbon nuclei in CRs are thought to be mainly primary particles while boron nuclei are entirely secondary particles produced by the spallation of heavier nuclei, such as carbon and oxygen. The ratio of secondary to primary fluxes, as the B/C ratio, is proportional to the average amount of interstellar material traversed by CRs, which, in turn, can be used to constrain the Galactic diffusion coefficient. This fact has motivated a huge collection of B/C data over the last 30 years and we refer to Ref. [82] for a comprehensive literature. In Fig. 3 we report the B/C ratio as a function of particle energy per nucleon for different experiments, using a bi-logarithmic scale. A power-law behavior is clearly visible for energies greater than 1 GeV per nucleon. The AMS collaboration has recently published a very precision measurement in the rigidity range from 1.9 GV to 2.6 TV, finding that for rigidity $> 65$ GV the B/C ratio is well described by a single power law with slope $\delta = 0.333 \mp 0.014(\text{fit}) \mp 0.005(\text{syst})$ [83]. This result is in good agreement with the Kolmogorov theory of turbulence which predicts $\delta = 1/3$ asymptotically [84].

The B/C ratio is proportional to the average amount of interstellar material traversed by CRs per unit surface, namely the grammage X, as shown in Ref. [1, 6, 7]. In the diffusive model of Galactic propagation this latter quantity is directly related to the CR residence time in the Galaxy through a simple relation, namely

$$X = \bar{n}\mu v\tau_{esc}\,, \tag{1}$$

where $\bar{n}$ is the mean gas density in the whole Galaxy, $\mu$ is the mean mass of particles composing the gas, $v$ is the speed of CRs and $\tau_{esc}$ is the confinement time into the Galaxy. In this scenario the mean gas density in the whole Galaxy can be evaluated as $\bar{n} \approx n_{disc}h/H$, where $n_{disc}$ represents the density of the disc. For a standard chemical composition of ISM mainly made of hydrogen and a smaller

fraction of helium (about $n_{He} \approx 0.15 n_H$, with $n_H$ and $n_{He}$ the hydrogen density and the helium density, respectively) the mean mass $\mu = (n_H + 4n_{He})/(n_H + n_{He})m_p \approx 1.4 m_p$ with $m_p$ the proton rest mass. The Galactic confinement time $\tau_{esc}$ can be rewritten in terms of the Galactic diffusion coefficient $D_g$ as $\tau_{esc} = H^2/D_g$. The basic assumption of this estimate is that $D_g$ is the same in the whole Galaxy. Substituting $\tau_{esc}$ in Eq. (1) we obtain that the grammage scales as $1/D_g(p)$. In other terms, the paradigm of CR transport describes the propagation as diffusive throughout the Galaxy with an energy-dependent diffusion coefficient $D_g(R) \propto R^\delta$, where the slope $\delta$ can be inferred from the B/C ratio.

The basic expectation on how the spectrum at Earth relates to that injected by the sources is easily obtained in this diffusive model. Using the DSA power-law result, the spectrum $q_{inj}(p)$ injected by a CR source into the ISM has the following form

$$q_{inj}(p) = \frac{\xi E_{SN}}{m^2} I(\beta) \left(\frac{p}{mc}\right)^{-\beta} . \tag{2}$$

Here $\beta \geqslant 4$ is the slope of the differential spectrum expressed in particle momentum $p$, $\xi$ is the fraction of the kinetic energy $E_{SN}$ of the SNR shock converted into CRs and $m$ is the particle rest mass. The function $I(\beta)$ is a normalization factor obtained by imposing that the total CR energy equals $\xi E_{SN}$. We normalize the CR spectrum to the observed proton one, since the latter is not expected to be affected by spallation reactions. Moreover, in case of CR protons (in this work we only deal with protons), for sufficiently high-energies, ionization losses can be neglected as well as the effects of solar modulation. Thus, the proton spectrum observed at the Earth can be evaluated as

$$\begin{aligned} N_{Earth} =& \frac{c}{4\pi} \frac{q_{inj} \mathcal{R}_{SN}}{2\pi R_d^2 H} \tau_{esc} \\ =& 8 \times 10^5 \, \xi \, I(\beta) \left(\frac{\mathcal{R}_{SN}}{30 yr^{-1}}\right) \left(\frac{E}{m_p}\right)^{-\beta-\delta} \\ & \times \left(\frac{E^*}{m_p}\right)^{\delta} m^{-2} s^{-1} sr^{-1} GeV^{-1} , \end{aligned} \tag{3}$$

where $R_d$ is the Galactic radius assumed to be 10 kpc, $\mathcal{R}_{SN}$ is the rate of SNR explosion in the Galaxy assumed to be $1/30\,yr^{-1}$, $m_p$ is the proton rest mass and $E^*$ corresponds to the energy at which the B/C ratio is normalized, typically 10 GeV for protons. It is important to note that in this simple diffusive model of CR Galactic propagation both the proton flux and the grammage scale as the ratio $1/D_g(R)$.

One on the main purpose of this thesis is to investigate the impact of non linear propagation of CRs around their sources onto the current picture of Galactic propagation. In near-source regions, we consider the interplay of accelerated particles with the ambient medium. This non-linear interaction gives rise to streaming instability [21–23]

that amplifies the magnetic turbulence. As a consequence particles become self-confine in the near-source region for a time longer than naively expected, as recently investigated in Ref. [9–11]. This self-confinement process can have important implications on the Galactic CR transport which we are going to discuss in the next section.

## 1.3 SELF-CONFINEMENT AROUND GALACTIC SOURCES AND POSSIBLE IMPLICATIONS

In the standard diffusive paradigm of Galactic propagation the diffusion coefficient is assumed to be the same as in the whole Galaxy. It is treated as a fitting parameter, usually inferred from the measurement of the ratio of secondary to primary fluxes, especially the B/C ratio. Indeed, as we discussed in the previous section, the B/C ratio is proportional to the grammage which scales as the inverse of the Galactic diffusion coefficient. Nevertheless, this way to infer Galactic transport parameters could be revised once the phenomenon of non-linear propagation is taken into account. When energetic particles escape from their acceleration site, they interact with the magnetized ISM. In near-source regions, one may expect that the CR gradient may be large enough to excite the streaming instability. As a consequence, the self-generated turbulence leads to an increase of the confinement time in these near-source regions. The time spent by particles in such regions can be longer than naively expected implying that the accumulated grammage might be a non-negligible fraction of the observed one (from B/C). Another important contribution to the total grammage can derive also from the transport inside the source during the acceleration process. At the energies where the observed grammage is affected by either non-linear propagation in the near-source region or transport inside the source, one should account for these processes in order to derive a correct estimate of the Galactic diffusion coefficient. Thus, the CR flux measured at the Earth reflects more a combination of Galactic propagation plus the two above phenomena, instead of the simple product of the acceleration times the pure Galactic CR transport derived in Eq. (3).

As we will discuss in Ch. 3, the effectiveness of the self-confinement is strongly affected by the density of neutral Hydrogen around the sources. Therefore it is of outermost importance to be able to estimate independently the effectiveness of the self-confinement, possibly through some observations. A possible signature that we will analyze and discuss is the formation of extended halo of gamma-ray emission around the galactic sources, due to the decay of $\pi^0$-mesons produced by the interaction between CRs and nucleons of the ISM. The emission from a single halo is too faint to be detected with current gamma-ray telescopes. However, the sum of these halos over the

whole CR source population could produce a significant contribution to the diffuse gamma-ray radiation from the Galactic disc. This diffuse Galactic emission has been measured by the *Fermi*-LAT telescope over 7 years of data acquisition. Thus, it is important to predict the emission from the total halo's population in order to compare it with the available data. If this contribution were a non-negligible fraction of the observed one, this would imply that the standard way used to infer the CR Galactic density from the gamma-ray emission should be revised. In particular, the present estimates of the parameters used to determine the normalization of CR flux, such as SN efficiency, the rate of SN explosion, would be underestimated.

It is worth mentioning that there are scenarios of CRs propagation which are alternative to the standard diffusive paradigm. Among the others we cite the so called "Nested leaky box" model suggested by [85–87]. In this model most of the grammage is assumed to be accumulated in cocoon-like regions surrounding the sources with an energy-dependent profile. At the same time, a minor grammage fraction, energy independent, is accumulated during propagation throughout the Galaxy. These two quantities become comparable around few hundred GV. In this model the B/C ratio is expected to decrease with energy at $\leqslant 10^2$ GeV/nucleon, in order to reflect the grammage accumulated near sources, and to flatten at higher energies. The recent measurement of the B/C ratio performed by AMS [83] up to 2.6 TV does not show a flattening at rigidities $> 10^2$ GV. Nevertheless the idea suggested by [85] could be related, to some extend, to the CRs self-confinement around Galactic sources that we propose here.

In Chapter 3 we investigate the non-linear propagation around SNRs. We study the evolution of both particle distribution and self-generated turbulence considering different levels of ionization of the medium surrounding the parent source. We will show that the grammage traversed by CRs with energies up to a few TeV is heavily affected by the self-induced confinement close to the sources, to an extent that depends on the number density of neutral hydrogen in the Galactic disc. Then we calculate the sum of the gamma-ray halos over the whole SNR distribution in the Galactic disc and we compare our predicted emission with the diffuse Galactic emission measured by the *Fermi*-LAT telescope and recently analyzed in Ref. [88, 89].

## 1.4 ORIGIN OF THE EXTRA-GALACTIC COSMIC RAYS

The non-linear propagation around sources can affect the transport of Extra-Galactic CRs and have important implications on their spectrum observed at the Earth. To understand these implications, in this section we discuss what we know about the origin of Extra-Galactic

CRs. In particular, we focus on the current models of the transition from Galactic to Extra-Galactic origin.

Cosmic rays with energy $\geqslant 10^9$ GeV are also referred to as ultra-high energy CRs (UHECRs). A simple argument shows that UHECRs cannot originate in the Milky Way. Indeed, their Larmor radius calculated in the typical Galactic magnetic field is of the same order of magnitude or larger than the size of our Galaxy. This implies that, if UHECRs were produced in the Galaxy, the particle deflection should be small so as to result in large anisotropy. The spatial distribution of UHECRs, instead, is nearly isotropic in contrast with the assumption of a galactic origin [49]. Following this argument we can conclude that CRs with energies above $\sim 10^9$ GeV have to be Extra-Galactic but the exact position where the transition between Galactic and Extra-Galactic CRs occurs is not well constrained.

Although we still don't know what are the possible UHECR sources some lower limits on their average luminosity can be posed, as presented in the Ref. [32]. In that paper the author shows that only high luminosity sources can produce UHECRs. The argument put forward by [32] and re-elaborated in Ref. [31] is described below considering stationary acceleration sites moving both in a non-relativistic and in a relativistic regime. In the non-relativistic regime the Hillas criterion [30] can be used to put a limit on the energy density of the background magnetic field $\epsilon_B = B^2/(4\pi)$, obtaining

$$\epsilon_B > \frac{E^2}{\pi (Z\beta_s R)^2}\,, \tag{4}$$

where $R$ is the size of the acceleration region. The total source ram pressure $\rho(\beta_s c)^2$, where $\rho$ si the source mass density, has to be greater than the background magnetic energy density. This condition translates in the requirement that the source luminosity $L$ has to be larger than the magnetic energy flux, giving

$$L = 4\pi R^2 \frac{\rho(\beta_s c)^2}{2}\beta_s c > 2\pi R^2 \epsilon_B \beta_s c\,. \tag{5}$$

The above equation provides a lower limit on the source luminosity which is

$$L > 1.6 \times 10^{45} Z^{-2} \beta_s \left(\frac{E}{10^{11}\,\mathrm{GeV}}\right)^2 \mathrm{erg\,s^{-1}}\,. \tag{6}$$

In the relativistic regime the argument is basically the same but one has to pay attention to the fact that the Hillas criterion [30] is valid in the comoving frame. Hence, defining $\Gamma_s$ as the source Lorentz factor, the lower limit on the source luminosity becomes

$$L > 10^{47} Z^{-2} \Gamma_s^2 \left(\frac{E}{10^{11}\,\mathrm{GeV}}\right)^2 \mathrm{erg\,s^{-1}}\,. \tag{7}$$

Although in both cases these estimates are rather approximated, it is clear that UHECR sources require very high luminosities in order to accelerate extra-galactic CRs up to the flux suppression observed at $\sim 10^{11}$ GeV.

The are two types of extreme luminous objects which might be possible Extra-Galactic CRs sources: active galactic nuclei (AGN) and gamma ray bursts (GRBs) (for a detailed discussion about both AGN and GRBs see Ref. [90] and references therein). AGN form central cores of galaxies able to produce more radiation than the rest of the host galaxy. This radiation is believed to be originated by the accretion of a supermassive black hole located at the center of the host galaxy. These objects are the brightest steady sources in the sky [32, 91] with a Lorentz factor between 3 and 10. Thus, only some of them may fulfill the luminosity requirement expressed in Eq. (7). GRBs are extremely energetic explosions which produce the brightest electromagnetic events in the Universe. These bursts are identified by an initial flash of gamma rays followed by a longer-lived emission at longer wavelengths (such as X-ray, ultraviolet, optical, microwave and radio). Their sources are still unknown, but there are some hints regarding high-mass stars or binary systems collapsing into neutron stars or black holes. These transient sources have a Lorentz factor $\Gamma_s \simeq 10^{2.5}$ [32] implying a luminosity $L_{GRBs} > 10^{50.5} \mathrm{erg\,s^{-1}}$ well above the limit expressed in Eq. (7) (even though the above estimate refers to stationary sources). These astrophysical objects are considered to be possible sources of UHECRs. We refer to Ref. [92] for a detailed discussion about the generale requirements, set by classical electrodynamics, on the sources of UHECRs.

The non-linear propagation around Extra-Galactic sources can have profound implications for the description of the transition region between Galactic and Extra-Galactic CRs [33–35]. In order to understand why, in the next section we discuss the actual models of transition.

### 1.4.1 Transition from Galactic to Extra-Galactic origin

For long time it has been taken for granted that the ankle in the CR spectrum is the spectral signature of the transition from a steep Galactic spectrum to a flatter extragalactic one [47, 48, 93]. In this ankle model CRs are assumed of Galactic origin up to rigidities of about $\sim 10^9$ GV while for higher rigidities CRs are thought to be of Extra-Galactic origin. The ankle appears as a natural feature due to the intersection of the steep Galactic component with the flatter Extra-Galactic one. The highest energy particles reaching the ankle are generally considered to be iron nuclei. This model predict a transition from a Galactic Iron-dominated composition to an Extra-Galactic proton-dominated around $\sim 10^9$ GeV.

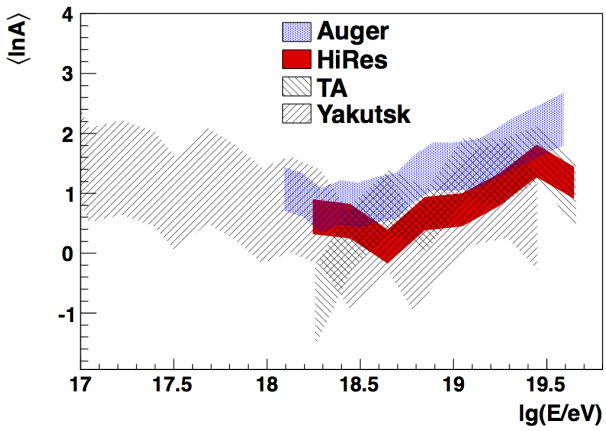


**Figure 4:** Averaged composition in terms of the logarithmic mass inferred from measurements of the mean atmospheric depth $\langle X_{max} \rangle$ at the PAO, HiRes, TA and Yakutsk experiments, taken from Ref. [61]). The shaded regions correspond to the systematic uncertainties range.

In the last years the nature of the ankle has been questioned [31, 49]. From the theoretical point of view, the non-linear theory of DSA in SNRs predicts a maximum rigidity of a few $10^6$ GV which for Fe nuclei translates into a maximum energy of $10^7$-$10^8$GeV, at least one order of magnitude below the ankle. Unless one invoke others more powerful source than the standard SNRs the transition region should be located close to $10^8$GeV [94]. Recent measurements of the CR energy spectrum between $10^8$ GeV and $10^9$ GeV, as performed by KASCADE-GRANDE experiment [95] and the Tunka-133 Cherenkov light array (for the detection of extensive air showers) [96], have revealed an important spectral feature at $\simeq 10^8$ GeV, namely the *iron knee* (or the second knee). At this energy they found that the mass composition is dominated by iron-nuclei elements. This feature corresponds to a softening of the all-particle energy spectrum, in a similar way to the knee feature, so that supports the rigidity-dependent acceleration paradigm [49]. In addition, KASCADE-GRANDE experiment managed to separate the energy spectrum of light and heavy component above $\simeq 10^8$ GeV [55]. As a result, the collaboration found that the light component presents an ankle-like structure while the heavy component presents a softening of the spectrum. Another important information is provided by the observation of the chemical composition of UHECRs. In Fig. 4 the averaged composition is reported as function of energy in logarithmic scale, for 4 different experiments: PAO [51], HiRes [97], TA [52] and Yakutsk [98]. In this plot $\langle \ln A \rangle = 0$ corresponds to a proton dominated composition while the iron-dominated composition corresponds to $\langle \ln A \rangle \simeq 4$. While at energy $\sim 10^9$ GeV the four experiments agree that the flux is domi-

nated by a light component, at higher energies PAO found a mixed composition, as it is visible from Fig. 4.

Before the publication of all these experimental findings, it was proposed the so called "dip model" [33, 34]. In this model the UHECRs are assumed to be mainly protons. The ultra high-energy protons produce electron-positron pairs through collisions with the photons of the CMB. This Bethe-Heitler pair production can have an important effect on the spectrum of CRs propagating on cosmological scales, as noticed in Ref. [99]. Indeed, it leaves a distinct feature which takes the form of a dip. The shape fits very well the observed modification factor for all experiments, with the possible exception of the one measured by the Pierre Auger Observatory. In the dip model the transition begins at the second knee and is completed at the beginning of the dip around $\simeq 1$ EeV [33, 34]. In this scenario the ankle is interpreted as an intrinsic part of the dip. The dip predicts an almost pure proton composition above $10^9$ GeV and a pure Iron composition below this energy, in contrast to the ankle and mixed composition models. A different model thought to be able to account for the complex composition scenario observed by different experiments is the mixed composition model [100]. In this model the authors discussed the possibility that UHECRs may be nuclei of various types. The transition occurs from Iron to lighter nuclei of mixed composition and it can occur below the ankle. A special case of the mixed composition model has been presented in Ref. [101] called the disappointing model. In this case the maximum proton energy is approximately $\sim 4 \times 10^9$ GeV and the iron spectrum extends to $\sim 10^{11}$ GeV. The adjective disappointing derives from the fact that the flux suppression at $\sim 10^{11}$ GeV is the intrinsic cutoff in the source spectrum rather than the GZK feature and no correlation is expected because of the heavy composition at the highest energies.

It is worth to mention here that the second knee has been interpreted as the signature of the transition from Galactic to Extra-Galactic components. Nevertheless this feature is particularly smooth and requires that the Extra-Galactic components sharply decreases below $10^8$GeV. As already mentioned, such a low energy cut-off could be explained invoking a magnetic horizon [36, 102]. In this scenario the Extra-Galactic spectrum shuts off below the second knee because the diffusion time from the closest Extra-Galactic sources of particles with energies greater than the second knee becomes larger than the age of the Universe.

As mentioned before, non-linear propagation around Extra-Galactic sources which, as in the Galactic case, can lead to self-confinement in the source vicinity giving a physically motivated picture for the existence of a magnetic horizon. Hence, in the last Section we discuss these implications, in particular relative to transition between Galactic and Extra-Galactic origin.

## 1.5 SELF-CONFINEMENT AROUND EXTRA-GALACTIC SOURCES AND POSSIBLE IMPLICATIONS

In extra-galactic environments the interaction between CRs and the ambient medium can give rise, under certain conditions, to the *non-resonant streaming* instability, first proposed by Bell [25, 26]. When the accelerated particles stream away from their source, they form an electric current to which the background plasma reacts generating a return current. This return current can lead to generate unstable modes only if the associated energy density is comparable to the magnetic energy density of the background field. Moreover, a second condition has to be satisfied that is the time scale of the fastest growing mode must be smaller than the Age of the Universe. If these conditions are fulfilled the non-resonant streaming instability can produce large turbulent magnetic fields and enhance particles scattering. As a consequence the accelerated particles are confined near their sources, as in the Galactic case. In a situation in which particles remain self-confined for times exceeding the age of the Universe, they cannot reach the Earth. Such condition will be satisfied only up to some critical energy, while above the critical energy particles will not be confined. In other terms, the self-generation of magnetic turbulence via the excitation of the non-resonant streaming instability gives rise to a cutoff in the spectrum of Extra-Galactic CRs.

As discussed in Sec. 1.4.1, a cutoff in the low-energy part of UHECR spectrum is introduced in the literature in order to avoid some phenomenological complications that affect models for the origin of ultra-high energy CRs (UHECRs). For instance, the ankle model [47, 48, 93] postulates that the cut-off is around the energy of the ankle to describe appropriately the transition from Galactic to extragalactic CRs. In the dip model [33, 34], instead, the transition is postulated to begins at the second knee and is completed at the beginning of the dip around $\simeq 1\,\mathrm{EeV}$. A similar feature is required by models with a mixed composition [35], where the transition is expected below the ankle. The existence of a magnetic horizon is invoked to justify an energy cut-off in the case that propagation of UHECRs is diffusive in the low-energy part of the spectrum [36, 102]. In the scenario depicted in this work the presence of a low-energy cutoff in the UHECR spectrum is a natural consequence of the self-confinement process and could be a crucial element to describe the transition region between Galactic and extra-galactic CRs. Finding the energy where the transition occurs, could provide a strong argument to discriminate between the proposed scenarios.

# 2 NON-LINEAR THEORY OF COSMIC RAY PROPAGATION

## 2.1 COSMIC RAY TRANSPORT EQUATION

The propagation of accelerated particles into the magnetized ISM is described by the transport equation derived by Skilling in 1975 [103] (see Ref. [6, 90, 104, 105] for a detailed discussion). This transport equation describes the evolution in phase space $(\boldsymbol{x}, \boldsymbol{p})$ of the distribution function $f(\boldsymbol{x}, \boldsymbol{p}, t)$ of accelerated particles, here assumed to be only protons. The distribution function is defined as the number of particles $dn$ in an infinitesimal volume of phase space $dV = d^3x d^3p$, i.e. $dn = f(\boldsymbol{x}, \boldsymbol{p}, t) dV$. The form of the CR transport equation is

$$\frac{\partial f}{\partial t} + (\boldsymbol{u} \cdot \nabla) f - \nabla \cdot (D \nabla f) - \frac{1}{3} (\nabla \cdot \boldsymbol{u}) p \frac{\partial f}{\partial p} = 0 \,, \tag{8}$$

where $\boldsymbol{u}$ is the advection velocity along the field lines and $D$ is the spatial diffusion coefficient. In Appendix A we derive Eq. (8) following the treatment given by Blandford and Eichler in Ref. [104].

The second term in Eq. (8) describes particles' advection (convection) along the field lines while the third term represents spatial scattering of accelerated particles as due to magnetic fluctuations. For this reason the transport equation is also referred to as the CR diffusion-convection equation. The last term describes the change in particle energy due to the adiabatic compression of the field lines frozen in the plasma. The assumption made here for simplicity that accelerated particles are mainly protons implies that we do not include spallation terms and radiative loss terms in the transport equation.

The diffusion process results from particle scattering on random magnetohydrodynamic (MHD) waves [6, 103, 104] which arise in magnetized plasmas in response to perturbations. In principle, these MHD fluctuations can be either Alfvén waves[1], namely magnetic waves moving at the Alfvén speed $v_A = B_0/\sqrt{4\pi n_i m_i}$, where $B_0$ is the background field, $n_i$ is the number density of the ions composing the plasma and $m_i$ is the ion rest mass, or fast magnetosonic waves (magnetic waves propagating perpendicular to the ordered magnetic field with phase velocity $\geqslant v_A$). However, the Alfvén waves

1 These waves have been named after Hannes Alfvén who discovered them in 1942, see Ref. [106]. Their origin is due to the oscillations of the ions of the background plasma which are subject to a restoring force yielded by magnetic tension on the field lines and are transverse to the direction of the background field.

are expected to dominate over the magnetosonic ones because the latter are damped more efficiently than the former, as explained in Ref. [103]. We notice that the role of Alfvén waves in scattering CRs has been questioned by some authors, as Yan and Lazarian [107] or Chandran [108]. The authors argued that the MHD turbulence responsible for particles scattering could be mainly dominated by three wave interactions that transfer energy from Alfvén waves parallel to the background magnetic field towards magnetosonic waves orthogonal to it. When this reasoning is applied to the cascade of waves at the single frequency towards higher frequencies the resulting power spectrum can be mainly dominated by perpendicular magnetosonic waves. Nevertheless, in the case of self-generated turbulence Alfvén waves are continuously generated at each frequency by CRs at the right resonant energy, therefore, the density of these waves is large enough to contribute to the scattering process. In this scenario magnetosonic waves may still provide a contribution to particle scattering but we consider this contribution negligible with respect to one provided by Alfvén waves.

In order to estimate the spatial diffusion coefficient, we assume that particles move in a weak magnetic turbulence [109], which corresponds to assume that the magnetic perturbation $\delta B \ll B_0$, as discussed for instance in Ref. [1] and references therein. A charged particle moving in the presence of a constant magnetic field $B_0$ simply gyrates around it with a frequency $\Omega = qB_0/(m\gamma c)$ ($q$ is the charge, $m$ is the rest mass and $\gamma$ is the Lorentz factor), and with a radius $r_L = v/\Omega$ being the Larmor radius. When a small perturbation $\delta B \ll B_0$ is added to the background field, particles are subjected to pitch angle scattering in a resonant manner. In fact, an accelerated particle is scattered predominantly by those irregularities having a wavelength comparable to the particle Larmor radius. Consequently, the pitch angle $\theta$, namely the angle between the incident particle velocity and the direction of $B_0$, suffers a small deviation from its initial value which upon time average leads to a diffusive propagation along $B_0$. We introduce $P(k)dk$ as the wave energy density in the wave number range $dk$ characterizing the power spectrum of the weak turbulence. The total pitch angle scattering rate $\nu_\theta$ due to this wave-particle interaction can be estimated as [1]

$$\nu_\theta = \frac{\pi}{4}\left(\frac{k_{res}P(k_{res})}{B_0^2/8\pi}\right)\Omega\,, \tag{9}$$

where $k_{res} = 1/r_L$ indicates the resonant wave-number. The time required to change the particle direction by $\delta\theta \sim 1$ is about the inverse of the total pitch angle scattering rate $\tau_\theta \sim 1/\nu_\theta$, therefore the spatial diffusion coefficient $D$ can be estimated as

$$D(p) = \frac{1}{3}v(v\tau_\theta) \simeq \frac{1}{3}r_L\frac{v}{\mathcal{F}(k_{res})}\,, \tag{10}$$

where $\mathcal{F}(k_{res}) = k_{res}P(k_{res})/(B_0^2/8\pi)$. This is the expression of spatial diffusion coefficient in the standard quasi-linear theory of plasma turbulence [110, 111].

In the next Section we will describe one of the mechanisms that produces the turbulence. This mechanism is considered to be responsible for pitch angle scattering. As a consequence, magnetic field is amplified while particles propagation in near-source regions, after their release from the acceleration site.

## 2.2 MAGNETIC FIELD AMPLIFICATION

Magnetic field amplification is extremely relevant at shocks in order to accelerate CRs up to the knee in the SNR paradigm [12–16]. Indeed, if the diffusion coefficient relevant for particle acceleration at SNR shocks is that inferred from the measurement of B/C ratio, the acceleration time $\tau_{acc}$ reads [1]

$$\tau_{acc}(E) \simeq \frac{D_g(E)}{cV_{sh}} \approx 10^5 \left(\frac{E}{10\,\mathrm{GeV}}\right)^{\delta} \left(\frac{V_{sh}}{10^3\,\mathrm{km/s}}\right)^{-2} \mathrm{yr}\,, \qquad (11)$$

where $D_g$ is the Galactic diffusion coefficient and $V_{sh}$ is the shock velocity. This estimate exceeds by several orders of magnitude the duration of the free-expansion phase of a SNR[2] even for low energies at any value of $\delta$ in the range 0.3 - 0.6 (see Ref. [1] for a detailed discussion). Thus, a huge amplification of the turbulence is required around the shock in order to shorten the acceleration time. In the case of an amplification factor of about $\sim 10^2$ the diffusion coefficient can be estimated assuming Bohm regime (i.e. $D(E) \simeq cr_L(E)/3$) and the acceleration time becomes

$$\tau_{acc} \approx 10^{-3} \left(\frac{E}{1\,\mathrm{GeV}}\right) \left(\frac{V_{sh}}{10^3\,\mathrm{km/s}}\right)^{-2} \left(\frac{B}{10^2\mu\mathrm{G}}\right)^{-1} \mathrm{yr}\,. \qquad (12)$$

The estimate of the maximum achievable energy $E_{max}$ can be derived by the comparison of $\tau_{acc}$ with the duration of the free-expansion phase $T_{ST} \approx 300\,\mathrm{yr}$ [1, 90] and the result is

$$E_{max} \approx 3 \times 10^5 \left(\frac{B}{10^2\mu\mathrm{G}}\right) \left(\frac{V_{sh}}{10^3\,\mathrm{km/s}}\right)^{2} \left(\frac{T_{ST}}{300\,\mathrm{yr}}\right) \mathrm{GeV}\,, \qquad (13)$$

which is one order of magnitude smaller than the knee energy [1].

The magnetic field amplification is one of the leading aspects of the non-linear theory of DSA and can be inferred from several observational facts, as for instance the detection of narrow filaments of non-thermal X-ray emission in virtually all young SNRs (see Ref. [17]

2 In phase of adiabatic expansion it is unlikely that the maximum energy can be achieved due to the decreasing velocity of the shock [1, 90].

and Ref. [112] for recent reviews). These filaments are produced by multi-TeV electrons radiating in magnetic fields as large as $\sim 10^2\,\mu$G. Another observational fact is the variability of X-ray hotspots in the shell of the SNR RX J1713.7-3946 on a timescale of few years. The existence of X-ray hotspots may imply the presence localized magnetic fields with amplitude $\leqslant$ 1mG [113]. In the non-linear theory of DSA the key mechanism responsible for magnetic field amplification is presumed to be the generation of plasma instabilities by the interaction between the accelerated particles and the plasma composing the ISM, in which both CRs and the shock are propagating (see Ref. [16] for a detailed discussion on CR driven plasma instabilities). As direct consequence, the diffusion coefficient becomes non-linearly dependent upon the distribution function of energetic particles, which is in turn determined by the diffusion coefficient in the acceleration region.

The self-generation of magnetic turbulence can play a fundamental role not only in the explanation of how to reach the knee energy but also in the study of how the accelerated particles leave the acceleration region and propagate throughout the whole Galaxy [24, 114–116]. Immediately outside the source one may expect that there is a local excess of energetic particles density with respect to the average CR density which can drive plasma instabilities and eventually leads particles to self-confinement in those regions where the contribution by the source dominates over the Galactic CR population [9–11, 117]. The phenomenon of CR self-generated turbulence can play an important role also in the CRs self-confinement in our Galaxy, in particular for predictions on the Galactic diffusion coefficient and on the level of anisotropy in particle arrival directions (see Ref. [118] and references therein).

In this thesis work we concentrate on the study of particles self-confinement in the source vicinity due to the generation of CR streaming instability, which in the context of Galactic sources develops in the *resonant* regime while in the context of Extra-Galactic sources develops in the *non-resonant* regime, as we will discuss in the next Section.

### 2.2.1 Cosmic Ray Streaming Instability

In the magnetized ISM the Alfvén speed is in general orders of magnitude smaller than the streaming speed of CRs which is close to the speed of light. For instance, in the region surrounding a SNR it is reasonable to assume that $B_0 \sim \mu$G and $n_i \sim 1\,\mathrm{cm}^{-3}$ (see Ref. [119]) which implies $v_A \sim 2 \times 10^5$ cm/s $\ll c$. This superAlfvénic streaming of CRs drives the generation of plasma instabilities among which the most important is believed to be the streaming instability, as outlined in Ref. [12, 22, 23, 120]. The principle at the base of this instability relies on the fact that particles are able to excite those Alfvén waves resonant with their Larmor radii, if they stream with super-Alfvénic

speed along the field lines. The efficiency of this excitation is proportional to the CR density gradient, so that the higher is the gradient the more efficient is the excitation of these resonant modes and the stronger is the amplification of magnetic fluctuations. This mechanism has a feedback on the same accelerated particles because they can scatter off these excited waves in the way explained in Sec. 2.1. In terms of diffusive motion, the amplification of the magnetic field implies a reduction of the spatial diffusion coefficient such that particles become self-trapped in those regions where the streaming instability is very efficient.

For the sake of clarity, it is more appropriate to define the mechanism just described as the resonant branch of the streaming instability. Indeed, there is also a non-resonant branch [25] of the streaming instability able to amplify magnetic turbulence at high levels which actually has been proposed to explain the large magnetic fields implied by X-ray observations [17]. A necessary condition for the growth of this instability is that the energy density of the bulk of streaming particles must be larger than the background magnetic energy density $B_0^2/(8\pi)$. The electric current carrying CRs induces the plasma to neutralize it by the generation of a return current[3]. This return current, in turn, excites magnetic fluctuations which start to grow exponentially on scales much smaller than CR Larmor radii (the scales of the resonant modes). This happens because the return current is composed of background electrons which react more promptly than background protons ($m_e \ll m_p$). The background electrons have very small energy (compared to CRs) so these unstable modes are excited on smaller scales than CR Larmor radii. In the vicinity of SNRs we study the non-linear propagation of the accelerated particles due to the excitation of the resonant branch of the streaming instability. Around extra-galactic sources, instead, we analyze under which conditions the non-resonant streaming instability may play the leading role on particle self-confinement.

From the analytical point of view the equation describing how the self-generated turbulence is produced by the escaping accelerated particles, which has to be solved together with the CR transport equation (8), is of the form [12, 21]

$$\frac{\partial \mathcal{F}}{\partial t} + \boldsymbol{u} \cdot \nabla \mathcal{F} = (\Gamma_{CR} - \Gamma_d)\, \mathcal{F}\,, \tag{14}$$

where $\mathcal{F}$ is the power spectrum per unit logarithmic wavenumber of the turbulence, as defined in Sec. 2.1. The first term on the rhs side of the above equation represents the growth rate $\Gamma_{CR}$ of the streaming instability while the second term $\Gamma_d$ represents the sum of the rates of those mechanisms which can damp the instability.

3 It is important to remember that a plasma is an electrically neutral medium where the overall charge and electric current are roughly zero.

In this work three processes are considered as the most probable damping mechanisms: the non-linear damping, the ion-neutral damping and the MHD cascade. These processes will be discussed in Sec. 2.3.

### 2.2.2 Resonant Modes

The expression for the growth rate $\omega_I$ of the unstable electromagnetic waves characterizing the resonant branch of the streaming instability is derived in Appendix C where is reported in Eq. (145) . The growth rate $\Gamma_{CR}$ is equals to $2\omega_I$ because the turbulence $\mathcal{F}$ is essentially the magnetic energy density $\delta B^2$, which grows as $\exp(2\omega_I)$. For the scope of this work we rewrite $\Gamma_{CR}$ in terms of the spatial diffusion coefficient. To do this we consider the fact that resonant particles carry an electric current $J_{res} = ecN(p > p_{res})$ aligned with the background magnetic field which we have assumed oriented along the $z$-axis. The particle motion is diffusive along $B_0$ so that this current can be also calculated as

$$J_{res} = 4\pi e \left| p^3 D(p) \frac{\partial f}{\partial z} \right|_{p=eB_0/(kc)} . \tag{15}$$

Using the expression reported in Eq. (10) for the diffusion coefficient, we can re-write $J_{res}$ as a function of the turbulence power spectrum $\mathcal{F}$ and the growth rate becomes

$$\Gamma_{CR} = \frac{16\pi^2}{3} \frac{v_A}{\mathcal{F} B_0^2} \nu(p) p^4 \left| \frac{\partial f}{\partial z} \right|_{p=eB_0/(kc)} . \tag{16}$$

There are some points relevant for the discussion about this instability. First of all, for a fixed particle momentum $p$ the unstable waves are the modes with the resonant wavenumber $k = 1/r_L(p)$. Second, the strength of the instability strictly depends on the spatial gradient of CR density, in fact the stronger is the gradient the more efficient is the generation of unstable waves. The third point regards the two parameters characterizing the ISM in which the accelerated particles propagate which are the background magnetic field $B_0$ and the ion density $n_i$. Indeed, $\Gamma_{CR} \propto 1/(B_0\sqrt{n_i})$, which means for instance that at fixed $B_0$ the waves grow faster in a medium with low ion density with respect to one with high ion density or considering two media with same $n_i$ the growth is faster in the medium with a lower value of $B_0$. The last aspect concerns the dependence on the inverse of the turbulence itself, because this implies that at the beginning of the process the fluctuations increase very fast, but when $\mathcal{F}$ becomes larger than the initial fluctuations this development becomes slower. However, it is important to remember that this formula holds in the quasi-linear approximation where $\mathcal{F} \ll 1$. In the case this approximation does not hold this formula is no longer valid. Nevertheless, the

intrinsic resonant nature of this instability would lead to expect that the growth stops when $\delta B$ becomes of the same order as $B_0$, so that the saturation level has often been assumed to occur when $\delta B/B_0 \sim 1$.

### 2.2.3 Non-Resonant Modes

As for the resonant branch, we derive the expression for the growth rate of the unstable non-resonant waves in Appendix C and report it in Eq. (150). As previously mentioned, resonant unstable modes are always excited as long as accelerated particles stream with super-Alfvénic speed along the field lines. For the non-resonant ones there is a more stringent condition which has to be satisfied, namely the particle drift must occur at a speed

$$\frac{v_d}{c} > \frac{w_B}{w_{CR}}\,, \tag{17}$$

where $w_B$ and $w_{CR}$ represent the magnetic energy density and the particle energy density, respectively. The electric current $J_{CR}$ carried by the streaming induces the background plasma to react generating a return current. This return current, in turn, excites magnetic fluctuations which become unstable. In this scenario the condition (17) can be rewritten as $n_{CR}/n_p \geqslant v_A^2/c^2$ [121], where we have used the fact that CRs are relativistic particles so that $v_d \approx c$. In addition to the above requirement there is another condition to satisfy due to the fact that these non-resonant streaming modes are excited by the background electrons. The background electrons forming the return current have lower energy than CRs so that the unstable modes are characterized by length scales much smaller than the CR Larmor radius. For this reason we refer to theses modes as non-resonant unstable waves. Thus, in this regime $k \gg 1/r_{L,0} \geqslant 1/r_L$ and the condition expressed in Eq. (149) becomes

$$1 < k r_{L,0} < \xi\,, \tag{18}$$

where the parameter $\xi = \frac{n_{CR}}{n_p}\frac{c^2}{v_A^2} = \frac{B_0 J_{CR} r_{L,0}}{m_p n_p v_A^2}$ has been introduced to recall the same result obtained by Bell in 2004 [25]. In this regime the growth rate (150) simplifies and becomes

$$\omega_I \approx \Omega_p^* \sqrt{\frac{n_{CR}}{n_p} k r_{L,0}}\,. \tag{19}$$

The non-resonant branch has a maximum growth rate in correspondence to the wavenumber

$$k_{max} = \frac{\xi}{r_{L,0}} = \frac{4\pi J_{CR}}{c B_0} \tag{20}$$

for which the maximum growth is

$$\Gamma_{max} = \frac{\xi}{r_{L,0}} = \frac{4\pi}{c}\frac{v_A}{B_0} J_{CR}\,. \tag{21}$$

In the work presented in Ref. [25] the author studies the CR streaming instability in case of particle acceleration at shocks with high Alfvén Mach number, namely shocks with velocity $v_s \gg v_A$, showing that if the condition $1 < kr_{L,0} < \xi v_s^2/v_A^2$, with $\xi$ defined as $B_0 J_{CR} r_{L,0}/(m_p n_p v_s^2)$, is fulfilled the magnetic fluctuations are amplified by the non-resonant streaming instability instead of the resonant one. Bell's calculation differs from the one described in this Section because the author uses a hybrid approach where the equation for the magnetic field and for the background plasma are those of the MHD theory while the CR current is treated using the kinetic Vlasov theory in the linear approximation. The growth rate obtained by Bell differs by a factor 1/2 from the one shown in Eq. (19).

## 2.3 DAMPING MECHANISMS OF MAGNETIC TURBULENCE

The CR streaming instability is, in general, subject to some mechanisms which can reduce the efficiency of magnetic field amplification. The most important consequence of a reduced magnetization is the reduction of particle diffusion and resulting into an increase of the confinement time around their sources. In this section we will concentrate on three mechanisms that are considered among the most relevant damping processes for the growth of this instability, which are: non-linear Landau damping, ion-neutral damping and an MHD damping suggested by [122].

### 2.3.1 Non-Linear Landau Damping

The non-linear Landau damping (NLLD) corresponds to the dissipation of a fraction of the energy of the Alfvén waves into thermal energy of the plasma. The growth rate is reported in Ref. [123] and reads

$$\Gamma_{NLLD}(k) = (2c_k)^{-3/2} k v_A \sqrt{\mathcal{F}(k)}\,, \tag{22}$$

where $c_k \approx 3.6$. This is an empirical formula derived from observations of both solar and interstellar turbulence which are consistent with a Kolmogorov spectrum. From a physical point of view this damping occurs when thermal protons (or generally thermal ions) interact with beat waves formed by two interfering Alfvén waves [124, 125]. The protons propagating with a speed slightly slower than that the beat envelope will take energy from the waves, instead the protons propagating faster will give energy to the waves. One might expect that in a thermal distribution there are more of the slower particles, so that the net result is damping. The name non-linear

Landau probably comes in analogy with the Landau damping mechanism [126] very important in plasma physics where a wave loses its energy due to interactions with those charged particles having a speed approximately equal to the phase velocity of the wave. It is worth noticing that this process is a non-linear mechanism which is mathematically expressed by the dependence of the growth rate on $\sqrt{\mathcal{F}(k)}$. In addition, this dependence implies that when the turbulence increases $\Gamma_{NLLD}$ increases too and the damping may become more efficient at odds with the growth rate of the resonant streaming instability being $\Gamma_{CR} \propto 1/\mathcal{F}$.

### 2.3.2 Ion-Neutral Damping

A very efficient mechanism for linear damping of Alfvénic turbulence is due to ion-neutral collisions. When Alfvén waves propagate in a partially ionized medium, their energy is dissipated because of momentum-exchanging collisions between the ions and the neutral particles composing the background plasma. The propagation of Alvén waves in a partially ionized medium consisting of one species of singly-charged ions and one species of neutral particles has been among others treated by [27] using a two fluid theory. Here we follow their treatment to determine the dispersion relation.

The neutral fluid represents the neutral species of the gas with $n_n$ indicating the neutral number density and $v_n$ the fluid velocity, the ion fluid, instead, represents the ion species composing the gas with $n_i$ the ion number density and $v_i$ its fluid velocity. The equation for the conservation of the fluid velocity characterizing the neutral species is determined solely by the friction due to neutral-ion collisions

$$\frac{d\boldsymbol{v}_n}{dt} = \nu_{in}(\boldsymbol{v}_n - \boldsymbol{v}_i)\,, \tag{23}$$

where the neutral-ion collision frequency is $\nu_{in} = n_i \langle\sigma v\rangle$ with $\langle\sigma v\rangle$ being the average over the velocity distribution of the collisional velocity $v$ times the charge exchange cross section $\sigma$. An approximation of $\langle\sigma v\rangle$ is given in Ref. [127] where it is

$$\langle\sigma v\rangle \approx 8.4 \times 10^{-9} \left(\frac{T}{10^4\ K}\right)^{0.4} cm^3 s^{-1} \tag{24}$$

valid for the temperature $T$ in the range $10^2\,k$ to $10^5\,k$. The equation for the conservation of the fluid velocity characterizing the ions species contains the same frictional term as for the neutrals plus the magnetic force due to the interaction with Alfvén waves

$$\frac{d\boldsymbol{v}_i}{dt} = \nu_{ni}(\boldsymbol{v}_i - \boldsymbol{v}_n) + \frac{1}{m_i n_i c}\boldsymbol{J}_i \times \boldsymbol{B}_0\,, \tag{25}$$

where $\nu_{ni} = n_n(m_n/m_i)\langle\sigma v_{th}\rangle$ and $\boldsymbol{J}_i$ is the ion electric current induced by the Alfvén turbulence. As previously mentioned, the Alfvén waves can be written as circularly polarized waves propagating parallel to $\boldsymbol{B}_0$ and the variation with $z$ and $t$ is of the form $\exp[i(kz-\omega t)]$. Moreover, the ion current can be written as function of the magnetic perturbation $\boldsymbol{B}_1$ as $\boldsymbol{J}_i = \nabla \times \boldsymbol{B}_1/(4\pi)$. Thus the two equations of motion become

$$\omega \boldsymbol{v}_n = -i\nu_{in}(\boldsymbol{v}_n - \boldsymbol{v}_i)\,, \tag{26}$$

$$\omega^2 \boldsymbol{v}_i = -i\omega\ \nu_{ni}(\boldsymbol{v}_i - \boldsymbol{v}_n) + k^2 v_A^2 \boldsymbol{v}_i\,. \tag{27}$$

To derive the second equation (ion equation of motion) we have used the fact that $\partial \boldsymbol{B}_1/\partial t = \nabla \times (\boldsymbol{J}_i \times \boldsymbol{B}_0)/(m_i n_i)$ which under a Fourier transformation becomes $\boldsymbol{B}_{1,k} = \boldsymbol{k} \times (\boldsymbol{J}_{i,k} \times \boldsymbol{B}_0)/(m_i n_i \omega)$. Thus, using the two relations $\boldsymbol{J}_{i,k} = -i\boldsymbol{k} \times \boldsymbol{B}_{1,k}/(4\pi)$ and $\boldsymbol{J}_i = m_i n_i \boldsymbol{v}_i$, one obtains the term $-ik^2 v_A^2 \boldsymbol{v}_i/\omega$. These two equations can be combined to obtain the following dispersion relation

$$\omega(\omega^2 - k^2 v_A^2) + i\nu_{ni}[(1+f_{in})\omega^2 - f_{in}k^2 v_A^2] = 0\,, \tag{28}$$

where $f_{in} \equiv m_i n_i/(m_n n_n)$. The wave-frequency is a complex variable so that $\omega = \omega_R - i\omega_I$ and the Eq. (28) can be separated into a real and an imaginary part as

$$\omega_R^2 = 3\omega_I^2 + v_A^2 k^2 + 2\nu_{ni}(1+f_{in})\omega_I\,, \tag{29}$$

$$\omega_R^2 = \frac{\omega_I[\omega_I^2 + v_A^2 k^2 + \omega_I \nu_{ni}(1+f_{in})] + f_{in}\nu_{ni}v_A^2 k^2}{3\omega_I + \nu_{ni}(1+f_{in})}\,. \tag{30}$$

The study of the dispersion relation (28) leads to identify four cases (see Ref. [28]) :

1. $f_{in} < 1/8$ and $4f_{in} < v_A^2 k^2/\nu_{ni}^2 < 1/4$ the waves do not propagate because the wave frequency is purely imaginary ;

2. $f_{in} \ll 1$ and $v_A^2 k^2/\nu_{ni}^2 \ll 4f_{in}$

$$\omega_R \approx \pm v_A k\sqrt{f_{in}}\,, \tag{31}$$

$$\omega_I \approx \frac{v_A^2 k^2}{2\nu_{ni}}\,, \tag{32}$$

   here the waves propagate with a phase velocity equals to $v_A\sqrt{f_{in}}$ which is lower than $v_A$ because the ion mass density is smaller than the neutral mass density;

3. $f_{in} \ll 1$ and $v_A^2 k^2/\nu_{ni}^2 \gg 1/4$

$$\omega_R \approx v_A k\,, \tag{33}$$

$$\omega_I \approx \frac{\nu_{ni}}{2}\,, \tag{34}$$

   here the waves propagate with a phase velocity equals to $v_A$, even though the ion mass density is smaller than the neutral mass density, because in this case the wave frequency is larger than the collision frequency;

4. $f_{in} \gg 1$

$$\omega_R \approx v_A k, \tag{35}$$

$$\omega_I \approx \frac{\nu_{ni}}{2} \frac{v_A^2 k^2}{v_A^2 k^2 + \nu_{ni}^2 f_{in}^2}, \tag{36}$$

as in the previous case the phase velocity is equal to $v_A$ but here the ion mass density is larger than the neutral mass density.

Comparing Eq. (31) and Eq. (33) we see that the effect of frequent collisions is to reduce the Alfvén speed to a value determined by the total mass rather than the ion mass only. This is due to the fact that ions and neutrals collide with a frequency smaller than the wave frequency.

**Table 1:** Physical parameters from Ref. [128] relative to the two different phases of the ISM occupying the largest fraction of the volume of the disk (where most of the SNs are expected to explode) and containing a percentage of the matter in the neutral state: the warm neutral medium (WNM) and the warm ionized medium (WIM). Most of the matter is expected to be composed by Hydrogen with a smaller fraction of Helium. T indicates the temperature, $n_H = n_n + n_i$ is the Hydrogen density, $n_i$ is the ion number density and $f_{in} = n_i/n_n$ ($m_i = m_n = m_p$).

| ISM phase | T[K] | $n_H[cm^{-3}]$ | $n_i[cm^{-3}]$ | $f_{in}$ |
|---|---|---|---|---|
| WIM | $8 \times 10^3$ | $0.2 - 0.5$ | $0.12 - 0.45$ | $1.5 - 9.0$ |
| WNM | $6 \times 10^3 - 10^4$ | $0.2 - 0.5$ | $0.0014 - 0.025$ | $0.007 - 0.05$ |

The importance of IN damping depends on the type of ISM where CRs propagate. In table 1 there are reported the physical parameters relative to the two different phases of the ISM that are: the warm neutral medium (WNM) and the warm ionized medium (WIM). These two phases occupy the largest fraction of the volume of the disk and, therefore, where most of the SNe are expected to explode. In the WNM most of the matter is in the neutral state ($f_{in} \ll 1$) and the efficiency of the IN damping is so high that the streaming instability can have a minor role in CR confinement around sources. The interesting phase is the WIM where most of the matter is in the ionized state ($f_{in} > 1$) and so the IN damping is less efficient in the dissipation of the turbulence energy. In this case the solutions to real and imaginary part are:

$$\omega_R \approx v_A k, \tag{37}$$

$$\omega_I \approx \frac{\nu_{ni}}{2} \frac{v_A^2 k^2}{v_A^2 k^2 + \nu_{ni}^2 f_{in}^2}. \tag{38}$$

Assuming for simplicity that the interstellar gas contains only Hydrogen as neutral component, so that $m_n = m_p = m_i$ and $f_{in} = n_i/n_n$. Thus, the damping rate for the energy spectrum is

$$\Gamma_{IN} = 2\omega_I = \frac{n_n}{n_i}\langle\sigma v\rangle n_i \frac{v_A^2 k^2}{v_A^2 k^2 + v_{ni}^2 f_{in}^2} = \frac{n_i\langle\sigma v\rangle}{f_{in}} \frac{v_A^2 k^2}{v_A^2 k^2 + v_{ni}^2 f_{in}^2}\,. \tag{39}$$

### 2.3.3 MHD cascade

A general feature of any kind of turbulence is the energy deposition from an initial scale, for instance the scale of the system, to smaller scales, a sort of "energy cascade". There isn't a unique explanation for this phenomenon, most of the time this energy transfer can be due to wave-wave interactions. In Ref. [122] the authors introduce a damping mechanism due to the collisions of Alfvén wave packets propagating in opposite directions. Their idea is based on the theory of non-linear interactions among shear Alfvén waves in an incompressible MHD fluid developed by [129, 130]. However, while in Ref. [129] the cascade is anisotropic because the energy deposition occurs preferentially perpendicular to the ordered magnetic field, [122] considers a cascade also in the parallel direction.

The situation depicted by [122] is characterized by a turbulence excited isotropically at an MHD scale $L_{MHD}$ with rms fluctuations of the fluid velocity $\delta v \sim v_A$ and of the magnetic field $\delta B \sim B_0$. The damping is due to collision of Alfvén waves with other waves from this pre-existing MHD cascade. To estimate the damping rate, three assumptions are made:

1. "critical balance", i.e. there is a balance between the inverse of the Alfvén time scale $v_A k_\parallel \sim v_A \Lambda_\parallel$, where $\Lambda_\parallel$ is the correlation length (i.e. $v_{\lambda_\perp} \sim v_{\Lambda_\parallel}$), and the inverse of non-linear time scale at which the energy is transferred to smaller scales $v_{\lambda_\perp}/\lambda_\perp$

$$\frac{v_A}{\Lambda_\parallel} \sim \frac{v_{\lambda_\perp}}{\lambda_\perp}\,; \tag{40}$$

2. "Kolmogorov hypothesis of the scale independence of $\epsilon$", i.e. the rate of energy dissipation per unit mass, $\epsilon$, is constant over the inertial range of the cascade identified as $l_{dissipation} \ll \lambda_\perp \ll L_{MHD}$ [4]. These eddies have energy per unit mass of order $v_{\lambda_\perp}^2$ and the time scale over which the energy is transferred

4 In the Kolmogorov' theory of turbulence a turbulent flow can be considered to consist of eddies of different sizes, where an "eddy" can be conceived to be a turbulent motion, localized over a region of a certain size, that is at least moderately coherent over this region. It is characterized by a length scale $\lambda_\perp$ and a velocity $v_{\lambda_\perp}$.

to smaller eddies is $t_{cascade} \sim \lambda_\perp / v_{\lambda_\perp}$ (see Ref. [131] and references therein). Thus, the constant rate of energy dissipation per unit mass can be estimated as

$$\epsilon \sim \frac{v_\perp^2}{t_{cascade}} \sim \frac{v_{\lambda_\perp}^3}{\lambda_\perp} \sim \frac{v_A^3}{L_{MHD}}\,; \tag{41}$$

3. the scaling of the amplitude of the magnetic fluctuations in the inertial scales is that obtained in the Iroshnikov-Kraichnan theory of MHD turbulence (see Ref. [130]), i.e.

$$\frac{\delta B}{B_0} \sim \left(\frac{\lambda_\parallel}{L_{MHD}}\right)^{1/4}\,. \tag{42}$$

From Eq. (41) an expression for the fluctuation amplitudes in the perpendicular scale $\lambda_\perp$ is obtained and reads

$$v_{\lambda_\perp} \sim v_A \left(\frac{\lambda_\perp}{L_{MHD}}\right)^{1/3}\,. \tag{43}$$

Substituting Eq. (43) into Eq. (40) the scale of the eddy shape is given as a function of the perpendicular scale $\lambda_\perp$

$$\Lambda_\parallel(\lambda_\perp) \sim L_{MHD}^{1/3} \lambda_\perp^{2/3}\,. \tag{44}$$

The damping rate can be estimated as the inverse of the cascade time and reads

$$\Gamma_{FG} \sim \frac{1}{t_{cascade}(\lambda_\perp)} \sim \frac{v_{\lambda_\perp}}{\lambda_\perp} \sim \frac{v_A}{L_{MHD}^{1/3} \lambda_\perp^{2/3}}\,. \tag{45}$$

This damping rate is a function of $\lambda_\perp$, but the purpose is to express it as a function of $\lambda_\parallel \sim r_L$. To do this one can consider the scaling of $\delta B/B_0$ expressed in Eq. (42) and use an independent condition that is $\delta B/B_0 \sim \lambda_\perp/\Lambda_\parallel$, which gives $\lambda_\perp \sim \lambda_\parallel^{3/4} L_{MHD}^{1/4}$. Thus, the final expression for the damping rate results

$$\Gamma_{FG} = \frac{v_A}{\sqrt{r_L L_{MHD}}}\,. \tag{46}$$

# 3 SELF-CONFINEMENT OF COSMIC RAYS AROUND GALACTIC SOURCES

Non linear effects play a crucial role in the transport of CRs. In this Chapter we focus on Galactic sources, here assumed to be supernova remnants (SNRs). In regions near sources one may expect that the CR density and the associated density gradient may be large enough to affect the environment in which accelerated particles propagate, through the excitation of electromagnetic instabilities (see Ref. [9–11, 117]). The electromagnetic instability which is assumed to play the leading role in the self-confinement is the *resonant streaming* instability [21–23], described in Sec. 2.2.2. When accelerated particles stream faster than the local Alfvén speed, hydromagnetic (Alfvén) waves with wavelengths comparable to particles Larmor radii become unstable. The initial small turbulence can be amplified by several orders of magnitude and, in turn, can reduce the diffusion coefficient that describes particle motion. As a consequence, CRs are forced to be confined in near-source regions for a time longer than naively expected so that particles can accumulate a non-negligible fraction of the Galactic grammage (introduced in Ch. 1 in Sec. 1.2.1). Thus, an important implication of the self-confinement is that this scenario makes the translation of the grammage, and so of the B/C ratio, to a confinement time in the Galaxy rather problematic (as discussed in Sec. 1.3).

The generation of resonant streaming instability by non-linear transport in the vicinity of Galactic sources has been recently investigated in Ref. [9–11]. In Ref. [9] the non-linear transport equation (derived in Ch. 2) is solved with a semi-analytical approach. The authors found a self-similar solution considering only the non-linear Landau damping (NLLD) [123] as the mechanism responsible for wave dissipation. In Ref. [10] the non-linear transport equation is solved analytically together with the time evolution of the self-generated turbulence assuming that the wave damping mechanism is the ion-neutral damping (IND) [27, 28]. In Ref. [11] a numerical approach is used to solve the non-linear system composed by the CR transport equation and the wave equation where both the NLLD and the IND are assumed responsible for wave dissipation. The authors focus on the impact of CR self-confinement regards the gamma-ray observations of molecular clouds located in the vicinity of SNRs.

In this Chapter we solve numerically the non-linear coupled equations discussed in Ch. 2, assuming three damping mechanisms: NLLD (see Sec. 2.3.1), IND (see Sec. 2.3.2) and a damping firstly proposed

by Farmer and Goldreich (FG) in Ref. [122] (see Sec. 2.3.3). In Sec. 3.4 we investigate the implications on the way information relative to CR Galactic transport is derived from the measurement of secondary to primary ratios. Then, in Sec. 3.5 we study one of the possible signatures of the self-confinement process which is the formation of an extended halo of $\gamma$-ray emission around sources. This radiation is due to the decay of $\pi^0$-mesons produced by the interaction between CRs and nuclei of the Interstellar Medium. We calculate the sum of these halos over the whole CR source population. In Sec. 3.5.4 we compare our predictions with the diffuse gamma-ray emission from the Galactic disc, measured by the *Fermi*-LAT telescope over 7 years of data acquisition and recently analyzed in Ref. [88, 89].

## 3.1 PHYSICAL FRAMEWORK

In this section we discuss the assumptions made to solve the non-linear coupled equations (8) and (14). The numerical recipe used to solve the system is explained in Appendix C. The scenario we have in mind is the escape of relativistic protons accelerated by the explosion of a SN located in the galactic disc. The ISM surrounding the parent star is characterized by a magnetic field with a mean value of about $B_0 \sim 3\,\mu G$. This background field can be assumed to have a well established direction over the coherence length $L_c$ being of the order of 100 pc [8]. In a near source region of dimension $\sim L_c$ escaping particles, propagating with superalfvénic speed, can excite resonant streaming modes (described in Sec. 2.2.2) so that the local magnetic field is amplified. This self-generated turbulence, in turn, confines energetic particles in such a region for a time longer than naively expected. As a consequence, CRs can accumulate a grammage which might be a non negligible fraction of the Galactic grammage (defined in Sec. 1.2.1). The geometry of the problem is in principle three dimensional but within a distance of $\sim L_c$ from the SNR it can be treated as one dimensional using the flux-tube approximation [9]. This approximation holds because high energy particles diffuse preferentially along the direction of the background magnetic field $\boldsymbol{B}_0 = B_0 \hat{z}$, after leaving the SN located at $z = 0$, as sketched in Fig. 5. The transverse dimension of the flux-tube coincides with the diameter of the source while the length is $2L_c$. In this approximation, all the quantities depend only on the spatial coordinate $z$.

The mathematical description of particle propagation in the source proximity consists of two coupled transport equations: one for CRs, equation (8), and the other for the turbulence, equation (14), both

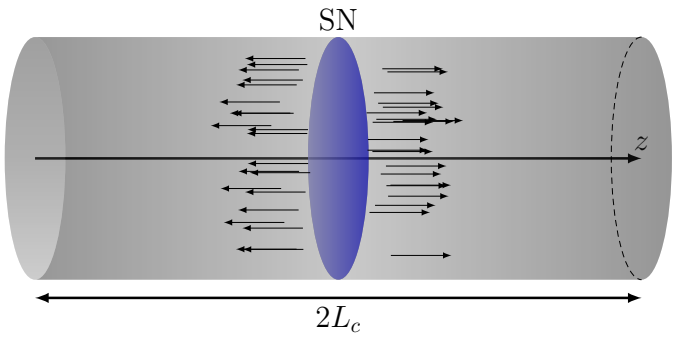


**Figure 5:** Sketch of the flux-tube model; the arrows represent the direction of escaping particles along the field lines parallel to the $z$-axis. The source located at the center of the tube is depicted as a disc with a dimension along $z$ negligible with respect to the length of the tube. The representation is not drawn to scale.

discussed in Chapter 2. The CR transport equation (8) in the flux-tube approximation can be written as

$$\frac{\partial f}{\partial t} + u\frac{\partial f}{\partial z} - \frac{\partial}{\partial z}\left[D(p,z,t)\frac{\partial f}{\partial z}\right] - \frac{du}{dz}\frac{p}{3}\frac{\partial f}{\partial p} = 0\,, \tag{47}$$

where the velocity characterizing the advection term reduces to $u = +v_A$ for $z > 0$ and $u = -v_A$ for $z < 0$. The reason of this expression for the advection term requires a brief discussion. In general the distribution of Alfvén waves includes waves propagating in both directions along the background field. However, as pointed out in Sec. 2.2.2, particles streaming with super-Alfvén bulk speed amplify the turbulence preferentially in the direction of the density gradient. Thus, while for $z > 0$ the escaping protons excite the waves with velocity $+v_A$, for $z < 0$ they excite the waves with velocity $-v_A$ and consequently the corresponding spatial derivative is equal to $du/dz = 2v_A\,\delta(z)$.

The transport equation (47) requires an initial condition to be solved that in this scenario translates into a suitable choice for particle injection. Particles' release into the source vicinity lasts until the acceleration has faded or operates at a much reduced efficiency. This implies that protons escape faster than they are replenished from their source, as pointed out in Ref. [10]. In both these scenarios, the escaping particles are decoupled from the acceleration region [10, 11]. Thus, at a zero-order approximation the emission of CRs with a given momentum $p$ can be described as an instantaneous injection at $t = 0$ added to the Galactic CR spectrum. The injection of all particles at $z = 0$ (where the source is located) introduces numerical problems for very low momenta because the associated density gradient needs an extremely small spatial resolution to be correctly resolved. Thus, we have adopted a different numerical recipe where particles

are spatially distributed following a narrow gaussian profile centered at $z = 0$, i.e.

$$f(p, z, t = 0) = q_0(p) \exp\left[-\left(\frac{z}{z_0}\right)^2\right] + f_g(p)\,, \tag{48}$$

as half width of half maximum $z_0$ equal to 1 pc, in order to have $z_0 \ll L_c$. We also checked that this choice of $z_0$ does non affect the final results provided it is small enough. Here $f_g(p)$ is the proton average Galactic CR spectrum. We take this flux from the latest measurement of the AMS02 [41] experiment

$$f_g(p) = 6.8 \times 10^{22} \left(\frac{p}{45 p_0}\right)^{-4.85} \times \left[1 + \left(\frac{p}{336 p_0}\right)^{5.54}\right]^{0.024} \left(\frac{\text{erg}}{c}\right)^{-3} \text{cm}^{-3}\,, \tag{49}$$

with $p_0 = m_p c$. The function $q_0(p) = A(p/p_0)^{-\alpha}$ represents the injection spectrum at a strong SNR shock which is assumed to be a power law with spectral index $\alpha$. In this work two different values for the spectral slope $\alpha = 4\,, 4.2$ will be considered. The normalization constant $A$ is calculated imposing that a fraction $\xi_{CR} = 20\%$ of the total kinetic energy of the SNR, assumed to be $E_{SN} = 10^{51}$ erg [1, 90], is released in the form of accelerated particles into the region $-L_c \leqslant z \leqslant L_c$

$$A = \frac{\xi_{CR} E_{SN}}{\pi R_{SN}^2 \mathcal{I}}\,. \tag{50}$$

Here, $\mathcal{I}$ is the integral of the kinetic energy over the whole particle distribution function, i.e.

$$\mathcal{I} \equiv \int_{-L_c}^{L_c} dz \exp\left[-\left(\frac{z}{z_0}\right)^2\right] \int_{p_0}^{p_{max}} dp 4\pi p^2 \left(\frac{p}{p_0}\right)^{-\alpha} \epsilon(p)\,, \tag{51}$$

with the upper limit of the particle distribution function $p_{max} \gg p_0$. The value of the radius of SNR has been chosen as the size of the slowly varying radius of a SNR during the Sedov-Taylor phase in the ISM, i.e. $R_{SN} \approx 20$pc [1, 90]. The problem is clearly symmetric with respect to $z = 0$, where the source is located, which leads to solve all the equations in half of the tube defined by $0 \leqslant z \leqslant L_c$. Eq. (47) is a second order partial differential equation and it requires two boundary conditions to find a particular solution. The first boundary condition comes from the integration of Eq. (47) around $z = 0$ which gives the following relation

$$D(p, z = 0, t) \left.\frac{\partial f}{\partial z}\right|_{z=0} = -\frac{v_A}{3} p \left.\frac{\partial f}{\partial p}\right|_{z=0}\,. \tag{52}$$

The second boundary condition corresponds to impose that the distribution function reduces to the Galactic one $f_g(p)$, expressed in Eq. (49), at the boundary of the box, i.e. $f(p, z = L_c, t) = f_g(p)$.

As mentioned before, the accelerated particles excite the resonant modes of the streaming instability, via the interaction with those Alfvén waves moving in the direction of the decreasing CR density and having their wavenumber $k = 1/r_L(p)$, where $r_L(p) = pc/(eB_0)$. In such a way the magnetic turbulence is amplified and the spatial diffusion coefficient decreases leading to a confinement into the near source region. It is reasonable to assume that the value of the enhanced turbulence $\delta B$ remains smaller than the background field during the whole confinement (we have checked at posteriori that this is always the case). In such a regime quasi-linear theory is valid and the expression for the spatial diffusion coefficient is the one discussed in Sec. 2.1, which reads

$$D(p, z, t) = \frac{1}{3} r_L(p) \frac{\nu(p)}{\mathcal{F}(k, z, t)|_{k=1/r_L(p)}} . \tag{53}$$

The quantity $\mathcal{F}(k, z, t)$ represents the self-generated magnetic energy density per unit logarithmic bandwidth of waves with wavenumber $k$, normalized to the initial energy density $B_0^2/(8\pi)$

$$\frac{\delta B^2(z, t)}{8\pi} = \frac{B_0^2}{8\pi} \int \mathcal{F}(k, z, t) d \ln k . \tag{54}$$

The equation for the evolution of the self-generated turbulence $\mathcal{F}(k, z, t)$ is described in Sec. 2.2 and its mathematical expression is

$$\frac{\partial \mathcal{F}}{\partial t} + u \frac{\partial \mathcal{F}}{\partial z} = (\Gamma_{CR} - \Gamma_D) \mathcal{F}(k, z, t) , \tag{55}$$

which, as for the transport equation (47), is solved in the box $0 \leqslant z \leqslant L_c$ with $u = v_A$. At $t = 0$ we assume that the magnetic turbulence is the one estimated from the Galactic diffusion coefficient, i.e.

$$\mathcal{F}(k, z, t = 0) = \mathcal{F}_g(k) \equiv \frac{1}{3} r_L(p) \left. \frac{\nu(p)}{D_g(p)} \right|_{r_L(p)=1/k} , \tag{56}$$

where $D_g(p)$ is the Galactic diffusion coefficient. As functional form for $D_g(p)$ we use the formula derived in Ref. [132] from a leaky-box fit to GALPROP (see http://galprop.stanford.edu) results for a Kolmogorov turbulence spectrum, i.e.

$$D_g(p) = 5.2 \times 10^{28} \beta^{-2} \left( \frac{p}{3 p_0} \right)^{1/3} \text{ cm}^2 \text{s}^{-1} , \tag{57}$$

where $\beta = v(p)/c$. As boundary condition we require that $\partial \mathcal{F}/\partial z = 0$ at $z = 0$.

In Sec. 2.2.2 we showed the calculation of the growth rate $\Gamma_{CR}$ of the resonant streaming instability (the final expression is reported

Eq. (16)). In this work we consider as energy range from 10 to $10^4$ GeV. In this range the fastest growing modes are those generated by particles with $E = 10\,\mathrm{GeV}$. Hence, to give an estimate of the magnitude of the growth rate we evaluate $\Gamma_{CR}$ at this energy. As parameters reference values we assume $B_0 = 3\,\mu\mathrm{G}$ and ISM number density $n_i = 0.45\,\mathrm{cm}^{-3}$. At the beginning of the escape the initial conditions impose $\mathcal{F}(10\mathrm{GeV}) \sim \mathcal{F}_g(10\mathrm{GeV}) \sim 10^{-6}$ while $|\partial f/\partial z| \sim |2q_0/z_0|$, which as an order of magnitude give $\Gamma_{CR}(10\mathrm{GeV}) \sim 2 \times 10^{-5}\mathrm{s}^{-1}$ for both injection slope $\alpha = 4$ and 4.2. This value has to be compared with the damping rates of the three damping mechanisms described in Sec. 2.3 to evaluate the importance of this instability.

### 3.1.1 Damping processes

We consider three damping mechanisms which can dissipate the energy of unstable resonant waves and, consequently, reduce the effect of magnetic field self-generation. These mechanisms are: non-linear Landau damping (NLLD), ion-neutral damping (IND) and a damping firstly proposed by Farmer and Goldreich (FG) in Ref. [122].

As discussed in Sec. 2.3.1, the NLLD is a non-linear process characterized by a cascade energy *a la* Kolmogorov due to wave-wave interactions. The dependence of $\Gamma_{NLLD}$ on the wavenumber can be translated into a dependence on particle energy through the resonance condition $k = 1/r_L$ which yields

$$\Gamma_{NLLD}(E,z,t) = 4.7 \times 10^{-9} \sqrt{\mathcal{F}(E,z,t)} \times \left(\frac{B_0}{3\mu\mathrm{G}}\right)^2 \times \left(\frac{E}{10\mathrm{GeV}}\right)^{-1} \left(\frac{n_i}{0.45\mathrm{cm}^{-3}}\right)^{-1/2} \mathrm{s}^{-1}. \quad (58)$$

From the above expression it is evident that at the beginning of the escape, where $\mathcal{F} \sim \mathcal{F}_g \sim 10^{-6}$, for particles with energy of 10 GeV $\Gamma_{NLLD}(10\mathrm{GeV}) \sim 4.7 \times 10^{-12}\mathrm{s}^{-1}$ is several order of magnitude smaller than $\Gamma_{CR}(10\mathrm{GeV})$.

The second damping mechanism is IND which occurs only in a partially ionized medium, as discussed in Sec. 2.3.2. Indeed, the physical process at the basis of wave energy dissipation is the viscosity effect produced by charge exchange between ions and neutral atoms. A difference with respect to the NLLD is the linearity of this process together with the fact that its damping rate does not depend on $\mathcal{F}$. The efficiency of this mechanism in quenching streaming instability depends on the ionization level of the near source region. The phases of ISM which occupy most of the disc volume are: the warm neutral medium (WNM), the warm ionized medium (WIM) and the hot fully ionized medium (HIM). Following Ref. [133], one could argue that the part of ISM which is most important in terms of particle propagation is a mixture of WIM and HIM. In the WNM, composed mostly by neu-

tral atoms, instead IND would severely inhibit wave growth, thereby suppressing diffusion. For this reason the WNM is not considered here. In table 1 in Sec. 2.3.2 we report the parameters characterizing the WIM, taken from Ref. [128]. Most of the gas is ionized with density that can be as high as $\sim 0.45\,\mathrm{cm}^{-3}$ but neutral gas is still present with density $\sim 0.05\,\mathrm{cm}^{-3}$. However, following Ref. [134], it is possible that the WIM, having temperature around 8000 K, is made of fully ionized hydrogen, while only helium would be partially ionized. This latter picture would have prominent consequences in terms of IND. Indeed, the cross section for charge exchange between H and He is about three orders of magnitude smaller [135] than for neutral and ionized H, so that the corresponding damping rate would be greatly diminished. For completeness we mention that there is another process which can contribute to the ambipolar diffusion responsible for IND, which is the elastic interaction between protons and neutral atoms [136]. In case of $p + He$ collisions this process is the dominant one in term of cross section. However, while the momentum transfer due to charge exchange interaction results almost the same over the angular velocity distribution in the energy range 1 - 10 eV (the typical range of energy of the background protons in the ISM we consider), in case of elastic collision this strongly depends on the angular velocity distribution. Comparing the charge exchange cross section for $p + H$ interaction with the momentum transfer cross section for $p + He$ interaction [135] we find that the last process is still negligible with respect to the first, so that in case of a medium with fully ionized hydrogen where only helium is partially ionized the effect of IND is effectively reduced with respect to the case of partially ionized hydrogen. Unfortunately, at present, there is no quantitative assessment of this phenomenon and one can only rely on a comparison between cross sections of charge exchange. On the other hand, it is also possible that a small fraction of neutral hydrogen is still present, in addition to neutral helium: as reported in Ref. [134], the density of neutral H can be $\lesssim 6 \times 10^{-2} n_i$, and for $n_i = 0.45\mathrm{cm}^{-3}$ this implies an upper limit to the neutral H density of $\sim 0.03\,\mathrm{cm}^{-3}$. For this kind of near source region, those waves excited by particles with energy $E = 10\,\mathrm{GeV}$ undergo a damping rate $\Gamma_{IND}(10\mathrm{GeV}) \sim 4.5 \times 10^{-10}\mathrm{s}^{-1}$, still smaller than the streaming growth rate.

The third mechanism taken into account is the wave-wave damping firstly proposed by Farmer and Goldreich in Ref. [122] and described in Sec. 2.3.3. They suggested that waves generated by the CR resonant streaming instability interact with oppositely directed turbulent wave packets characterizing a pre-existing MHD turbulence. As a consequence, wave energy dissipates due to a cascade from a large injection scale $L_{MHD}$, comparable with the background coherence scale $L_c$, to smaller scales. At $E = 10\mathrm{GeV}$ also this damping is negligible with respect to the growth of CR streaming instability.

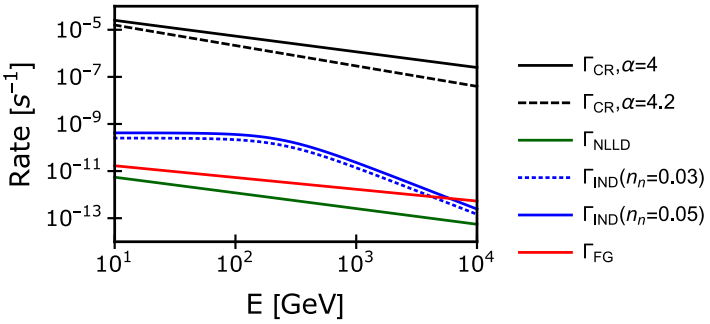


**Figure 6:** Growth rate of the streaming instability compared to the damping rates of the three processes as a function of particle energy $E$ at the beginning of particle propagation into the near source region. The solid black line represents the estimate of $\Gamma_{CR}(E) \propto 2q_0(E)/(z_0\mathcal{F}_g(k_{res}))$ for the injection slope $\alpha = 4$, while the dashed black line represents the same estimate of $\Gamma_{CR}$ for $\alpha = 4.2$. The solid green line corresponds to the evaluation of $\Gamma_{NLLD}$ at $\mathcal{F} = \mathcal{F}_g$. The blue lines correspond to the $\Gamma_{IND}$ for the case with neutral density $n_n = 0.03\,cm^{-3}$ (dotted line) and for the case with neutral density $n_n = 0.05\,cm^{-3}$ (solid line). Finally the solid red line represents the $\Gamma_{FG}$ where the MHD scale is equal to $L_c$.

In Fig. 6 the resonant growth rate together with damping rates are plotted as functions of particle energy $E$, calculated for the initial configuration $f(t = 0, z, p) = f(z, p)$ and $F(t = 0, z, k) = F_g(z, k)$. It is clear from the plot that the growth of the resonant streaming instability is faster than all the damping rates over the whole energy range and for both the two injection slopes.

## 3.2 NUMERICAL SOLUTIONS

The numerical procedure used to solve the coupled equations (47) and (55) is based on a finite difference method for the discretization of partial derivatives (both in space and time) and a backward integration in time for Eq. (47), as explained in Appendix C.

We consider four different types of ISM, which are listed in Table 2. Case A corresponds to the best scenario in terms of the importance of CR self-confinement process for the grammage accumulated in the source vicinity. In this case there is the assumption that hydrogen is fully ionized and the neutral component is made only by He atoms. In Cases B and C hydrogen is assumed to be partially ionized in order to estimate the effect of IND on reducing the self-confinement time and, consequently, the accumulated grammage. In particular, in case B the choice for $n_n$ derives from the assumption that the density of neutral H is $\leqslant 6 \times 10^{-2} n_i$ [134] which for $n_i = 0.45\,cm^{-3}$ gives an upper limit of $n_n = 0.03\,cm^{-3}$. Case D refers to a more rarefied medium

**Table 2:** Table of the four different types of ISM considered in this work. The parameter $n_i$ indicates the number density of ionized H while the parameter $n_n$ corresponds to the number density of neutral H. Both these densities are expressed in $cm^{-3}$. The choice for these values is based on the study of ISM performed in Ref. [128, 133, 134].

| Case | $n_i[cm^{-3}]$ | $n_n[cm^{-3}]$ |
|---|---|---|
| A | 0.45 | 0 |
| B | 0.45 | 0.03 |
| C | 0.45 | 0.05 |
| D | 0.01 | 0 |

than the one considered in case A. This case refers to the scenario of core collapse SNs expanding into low density bubbles generated by the wind of their progenitors. It is not well clear which is the configuration of the magnetic field in the bubble generated by the progenitor star. In this work we assume that the coherence scale is comparable with that of the magnetic field in the interstellar medium, hence 100 pc. In any case, if the bubble modifies the large magnetic field, the coherence length should correspond to the size of the bubble which is not that different from 100 pc (around $\sim$ 20 - 30 pc). Nevertheless, we warn the reader that the observational consequences of CRs propagation in this rarefied medium do not significantly modify the current interpretation of data regarding both the Galactic grammage and the diffuse gamma-ray emission.

In figure 7 the numerical solutions of Eq. (47), Eq. (154) and Eq. (55) as functions of $z$ are shown for four different times after particles release ($10^4, 5\times10^4, 10^5$ and $5\times10^5$ yr) and at one given energy $E = 10$ GeV. In the energy range considered in this work, i.e. 10 - $10^4$ GeV, the unstable modes excited by particles with $E = 10$ GeV are the most efficient in terms of self-confinement process. Thus, we choose this value as reference energy. These solutions are relative to case A where no neutrals are present, the ion density $n_i = 0.45\,cm^{-3}$ and the injection slope is $\alpha = 4$. Here we define the CR density $n_{CR}$ as $(4/3)\pi p^3 f$ and the Galactic density $n_g = (4/3)\pi p^3 f_g$. From the top panel of Fig. 7 it is evident that at $E = 10$ GeV the CR density $n_{CR}$ remains larger than the Galactic density $n_g$ (black dashed line) at least for $t \sim 10^5$ yr in a region of about few pc very close to the parent source. Even after $5\times10^5$ yr the particle density is still larger than the Galactic one for $z$ up to 50 pc. This behavior implies that the accelerated particles remain self-trapped into the near source region for at least $5\times10^5$ yr. This is a relevant time scale if compared to the standard diffusion time $\tau_d = L_c^2/D_g$ calculated at $E = 10$ GeV, which is of

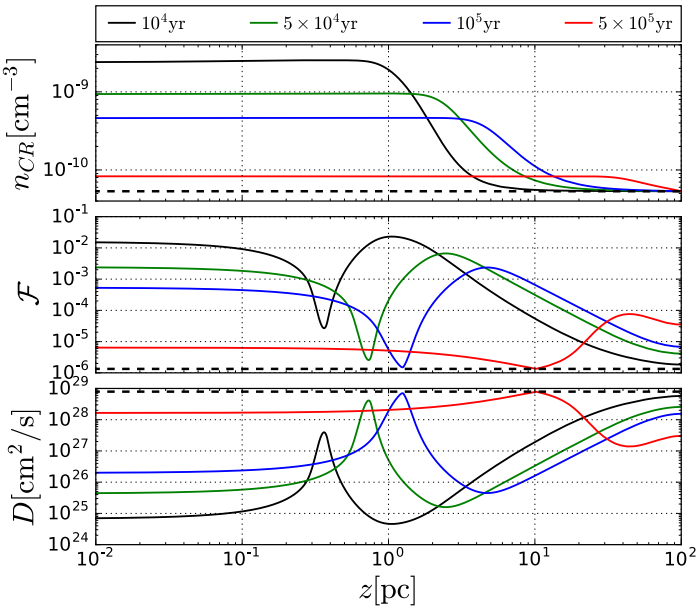


**Figure 7:** Numerical solutions of the particle density $n_{CR} = (4/3)\pi p^3 f$ (top panels), of the turbulence spectrum $\mathcal{F}$ (center panels) and of the spatial diffusion coefficient D (bottom panels) as functions of $z$ for different times as reported in the legend and at fixed particle energy $E = 10\,\mathrm{GeV}$. The black dashed lines correspond to $n_g = (4/3)\pi p^3 f_g$, $\mathcal{F}_g$ and $D_g$, in the associated panels. These results refer to the case of fully ionized ISM characterized by $n_i = 0.45\,\mathrm{cm}^{-3}$ and the value of the injection slope is $\alpha = 4$.

the order $\approx 4\times10^4\,\mathrm{yr}$. In the central panel the spatial profile of the magnetic turbulence $\mathcal{F}$ is reported. It is evident, for instance at $10^4$yr (solid black line), that in correspondence to the strong gradient of $n_{CR}$ around $z \sim 1$ - $2\,\mathrm{pc}$ $\mathcal{F}$ peaks at a value $\sim 3\times10^{-2}$. Thus, there is an enhancement of magnetic turbulence which is about four orders of magnitude higher than the background turbulence $\mathcal{F}_g$ (represented by a dashed black line). This means that particles effectively affect their own motion by self-generating unstable waves. We note that this value is still below the limit of validity of quasi-linear theory $\mathcal{F} \ll 1$. When the bulk of particles leaves the region the instability ceases to grow and the level of turbulence drops to $\mathcal{F}_g$. The behavior of $\mathcal{F}$ at small $z$ is a numerical feature due to the boundary condition (52) imposed at $z = 0$. Here, the advection is large enough to deprive the CR distribution at $z \sim 0$, and consequently to generate a gradient into f, which in turn enhances the turbulence amplification. Nearby $z \sim 0$ the CR gradient is such that the unstable waves propagate along the wrong direction, namely towards $z = 0$, so that the Alfvén velocity is reduced. In this scenario the advection limits a bit the effect of self-confinement, because particles escape faster from the near source region. As a result, the confinement time and therefore the grammage are slightly reduced. In Ref. [9–11] the authors

assume that advection plays a little role in CRs propagation around SNRs, so that it is neglected. Here, in order to check that this term does not affect in a relevant way the self-confinement process, we compared the grammage obtained with and without advection into the coupled equations (47) and (55). We found that the variation is present. We note also that at $z$ around $L_c$ $\mathcal{F}$ increases as time passes. This behavior is due to the free escape boundary condition imposed at $z = L_c$. Indeed, we impose that particle distribution $f$ must be equal to the mean Galactic distribution $f_g$ at $z = L_c$. This implies an abrupt change from a self-similar diffusion solution to a free escape one. In such a way we introduce an artificial density gradient and consequently an enhancement of turbulence. Nevertheless, we expect that this feature does not affect self-confinement, in particular the accumulated grammage. Hence, this artificial gradient produces an amplified turbulence which is always smaller than the one actually responsible for self-confinement. In the bottom panel we report the spatial diffusion coefficient $D$. It shows, clearly, a profile which is inverse of the turbulence $\mathcal{F}$ behavior, due to their mathematical relation (154). Thus, in correspondence to the maximum level of turbulence amplification $D$ reaches its minimum $\approx 5 \times 10^{24}\,\mathrm{cm}^2/\mathrm{s}$. This value is more than four orders of magnitude lower than $D_g$ (dashed black line). We recall that in the standard diffusive paradigm of CR Galactic propagation (see Sec. 1.2.1) the Galactic diffusion coefficient is usually assumed to be the same in the disc and the halo. However, at those energies where self-generation of magnetic turbulence can be very efficient in confining particles in near source regions, this assumption can be controversial, as we will show in Sec. 3.4.

In Fig. 8 there is the same plot of Fig. 7 but for $E = 10^3\,\mathrm{GeV}$. As described for the case $E = 10\,\mathrm{GeV}$, at time $10^4\,\mathrm{yr}$ particles are confined very close to the source, in a region of few pc. In correspondence with the density gradient, the turbulence reaches its maximum value of $2 \times 10^{-1}$. This implies that even at such high energy the interaction between CRs and the magnetized ISM is strong enough to amplify the Galactic turbulence by four order of magnitude. We note also that at $E = 10^3\,\mathrm{GeV}$ the level of maximum amplification is one order of magnitude larger than the one reached at $E = 10\,\mathrm{GeV}$. However, this is due to a higher value of $\mathcal{F}_g$ which is proportional to $E^{2/3}$. CR density, turbulence and diffusion coefficient start to be different with respect to those shown at $E = 10\,\mathrm{GeV}$ when $t \sim 5 \times 10^4\,\mathrm{yr}$. This difference becomes more evident at $10^5\,\mathrm{yr}$ where the strong density gradient has reached $\sim 30\,\mathrm{pc}$, which is one order of magnitude more distant than in the previous one. The reason is that the injected CR spectrum is a power-law in energy space (see Sec. 3.1), so that the instability is more efficient, or in other terms the self-confinement lasts longer, at low than at high energies. At $5 \times 10^5\,\mathrm{yr}$ the density is equal to the Galactic one which means that all the injected particles have left

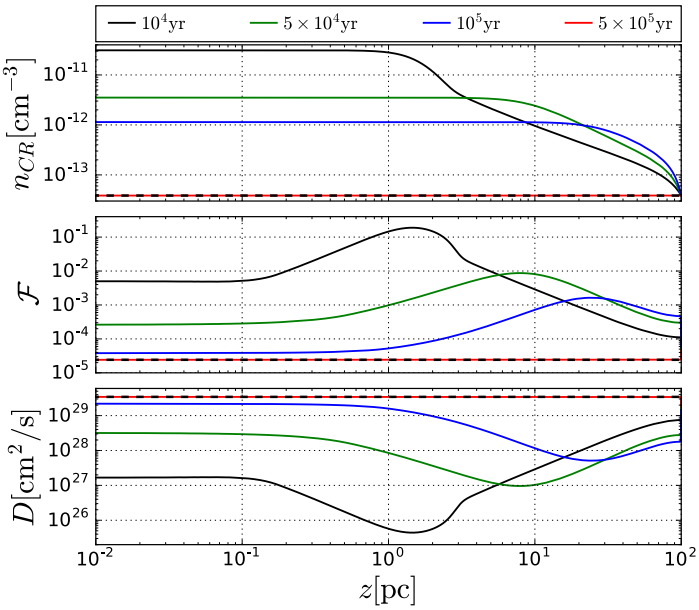


**Figure 8:** Same as Fig. 7, but for particle's energy $E = 10^3$ GeV.

the region, while in the other case particle density is still larger than Galactic density (for $z$ up to 50 pc, as previously mentioned). The second difference with respect to the case of Fig. 7 is the behavior at small $z$. This time the diffusion term dominates over advection and spreads out the distribution reducing the spatial gradient and, consequently, a smaller turbulence enhancement is observed.

When the injection slope is $\alpha = 4.2$ the efficiency of the resonant streaming instability is reduced at high energies with respect to the case with $\alpha = 4$. Indeed, while at $E = 10$ GeV the behavior of $n_{CR}$, $\mathcal{F}$ and D is basically the same as that shown in Fig. 7, for $E = 10^3$ GeV the situation is different and it is presented in Fig. 9. At time $10^5$ yr most of particles have left the region, differently to the previous case where at the same time the peak of the turbulence is at $z \approx 30$ pc (solid blue line, central panel of Fig. 8). Moreover, there is a reduction of the maximum level reached by the self-generated turbulence at each time.

To understand the effect of IND on particle self-confinement, we show the spatial profile of CR density at $E = 10$ GeV in Fig. 10 for the first three cases defined in Table 2. One can clearly see that for all three cases particle density remains more than one order of magnitude larger than the Galactic mean density (dashed black line) in a region around 1 - 2 pc from the source and on time scales of order $10^4$ years. We note that this time is comparable with the standard diffusion time $\tau_d = L_c^2/D_g$ calculated at the same energy. Thus, at this stage streaming instability grows faster than IND even in the case with the lowest level of ionization (i.e. case C bottom panel). Nevertheless, at later times the IND starts to be relevant. In fact, when

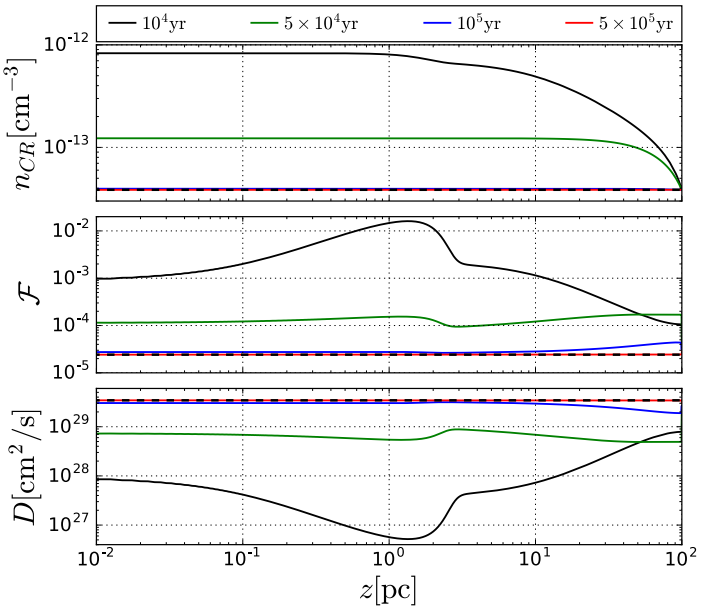


**Figure 9:** The caption is analogous of that describing Fig. 8, the only difference relies on the value of the injection slope which is $\alpha = 4.2$.

neutrals are present the density drops down to $n_g$ at $10^5$ yr, which means that particles have left the near source region. The turbulence spectrum for these cases is shown in Fig. 11. At $t = 10^4$ yr all cases show the same spatial profile for $z \geqslant 0.5$ pc, reaching the maximum value around 1pc where there is the strongest CR density gradient. However, the profiles differ at small $z$. Hence, when neutrals are present the diffusion term becomes dominant over the advection one at earlier times. This implies that the density gradient produced by the advection is less evident and consequently a lower level of turbulence is amplified. After $10^5$ yr the situation is changed. Indeed, while in case A particles are self-confined within $\simeq 5$ pc from the source, in case B they have reached $\simeq 7$ pc. In case C the effect is even more evident with a size of the confinement region about 50% larger than in case A. This demonstrates how IND effectively reduces the amplification of magnetic turbulence and hereupon limits the importance of self-confinement process.

The last of the four cases taken into account is that of rarefied totally ionized medium with ion density $n_i = 0.01\,\mathrm{cm}^{-3}$, which we identify as case D. This instance can be relevant when the SNR originates from a core collapse SN and expands into a low density bubble, which is generated by the wind of the SN progenitor. Here, the Alfvén speed is larger than in case A, which implies a faster growth of unstable modes. At the same time either NLLD and FG damping become faster, due to their proportionality to $v_A$. This would lead to the conclusion that these effects balance out the faster wave growth, so that the importance of particle confinement is the same as of case

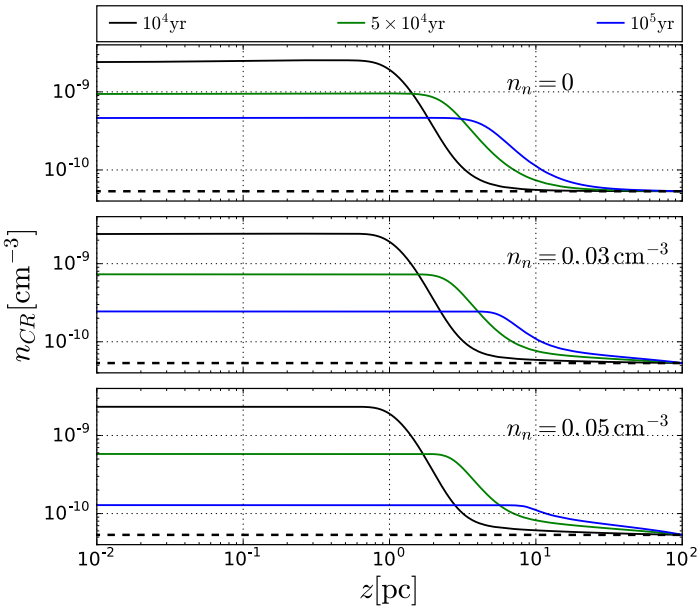


**Figure 10:** Particle density $n_{CR}$ for $E = 10\,\mathrm{GeV}$ as a function of distance from the source. The curves refer to times $10^4$, $5 \times 10^4$ and $10^5$ years, as labelled. In case A (*Top Panel*) the medium is fully ionized with $n_i = 0.45\,\mathrm{cm}^{-3}$ while in case B (*Central Panel*) and in case C (*Bottom Panel*) the medium is partially ionized, as listed in Table 2. In all the three panels the black dashed lines correspond to $n_g = (4/3)\pi p^3 f_g$.

A. The situation, however, is complicated by the fact that also advection becomes more important, which leads to an enhancement of particles escape. In Fig. 12 and Fig. 13 we show the spatial profile of CR density, of $\mathcal{F}$ and of D for $E = 10\,\mathrm{GeV}$ and $E = 10^3\,\mathrm{GeV}$, respectively. In both figures a strong density gradient is clearly visible near $z \sim 0$, which is induced by the advection term. We recall that this feature is probably a fake effect due to the boundary condition (52) imposed at $z = 0$. Comparing Fig. 12 with Fig. 7 we note that CR density of case D is smaller than that of case A for each time. This is a consequence of the advection which is more relevant in the rarefied medium. As a result, the effect of self-confinement is reduced at low energies with respect to case A. Comparing Fig. 13 with Fig. 8 we note, instead, that CR density has a similar value in both cases and for each time. Thus, at higher energies advection does not influence the effect of streaming instability.

In the next section we estimate the time spent by accelerated particles while they are confined in regions of dimension $\sim L_c$.

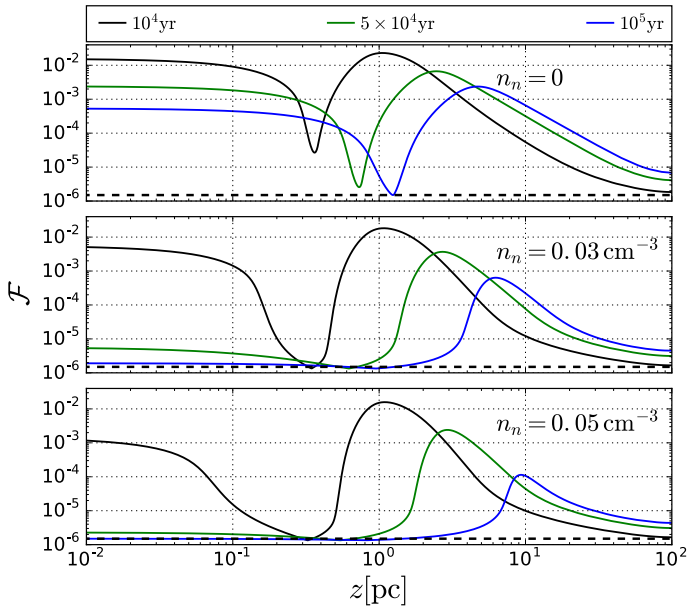


**Figure 11:** Turbulence spectrum $\mathcal{F}$ for $E = 10\,\mathrm{GeV}$ as a function of distance from the source for the same cases reported in Fig. 10. In all the three panels the black dashed lines correspond to the Galactic turbulence $\mathcal{F}_g$.

## 3.3 CONFINEMENT TIME IN THE NEAR SOURCE REGION

The calculation of the time spent by CRs near their parent sources is not straightforward due to the nonlinear processes involved. In case where a burst of particles is injected a $t = 0$ with a preassigned diffusion coefficient equal to $D_g(p)$, about 89% of the total injected amount $N_{CR}^{inj}$ leaves the box within the classical diffusion time $\tau_d = L_c^2/D_g$. We evaluate the total amount injected into a near source region as $N_{CR}^{inj}(p) = 2\pi L_c R_{SN}^2 q_0(p)$. The same idea has been used to estimate the escape time in the nonlinear case. More precisely, we calculate the number of accelerated particles inside the tube at time $t$ and at fixed momentum $p$, namely $N_{CR}(p,t)$, as the difference between the total amount of particles in the tube and the background term:

$$N_{CR}(p,t) = 2\pi R_{SN}^2 \int_0^{L_c} dz[f(p,z,t) - f_g(p)]\,. \tag{59}$$

The escape time $t_{esc}(p)$ corresponds to the time at which $N_{CR}(p, t_{esc}(p))$ is 11% of $N_{CR}^{inj}(p)$. This estimate is not valid when $t_{esc}(p)$ becomes smaller than the duration of the SN release phase which happens for $E > 10^4$ GeV.

The behavior of the escape time as a function of particle energy is plotted in Fig. 14. We show the results for all different types of ISM,

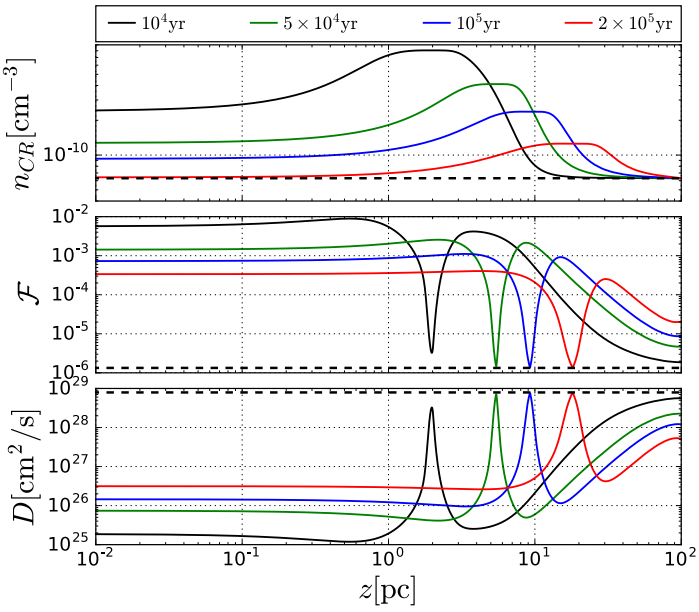


**Figure 12:** Same as Fig. 7 but for the case of full ionized diluted medium with $n_i = 0.01\,\mathrm{cm}^{-3}$ and $E = 10\,\mathrm{GeV}$.

as listed in Table 2, and for injection slope $\alpha = 4$. The grey dashed line represents the standard diffusion time $\tau_d = 8.3\times10^4 (E_{GeV})^{-1/3}$ yr.

In case A where no neutrals are present (solid black line), the escape time is about two orders of magnitude longer than the standard diffusion time $\tau_d$ for energies up to few TeV. For higher energies the efficiency of streaming instability decreases and $t_{esc}$ is severely reduced even if we still have $t_{esc} > \tau_d$. Hence, in such a medium the self-generated turbulence effectively affects particles motion, leading to a propagation that is not characterized by a constant diffusion coefficient. A similar conclusion can be deduced for case D, where the medium is fully ionized but more rarefied ($n_i = 0.01\,\mathrm{cm}^{-3}$, solid blue line). In particular, the escaping time is roughly the same as for case A for energies around 1 TeV. At lower energies the advection is non negligible and contributes to reduce $\tau_{esc}$. On the other hand, for energies $>$ few TeV the escaping time becomes larger with respect to case A. This is due to a faster growing of CR streaming instability in the rarefied medium, in fact $\Gamma_{CR} \propto 1/\sqrt{n_i}$, as we see from Eq. (16). At the same time the strength of damping mechanisms is reduced. On one hand the IND is absent, and, on the other hand, both NLLD and FG are less effective because their damping rate decreases with energy, namely $\Gamma_{NLLD} \propto E^{-1}$ and $\Gamma_{FG} \propto E^{-1/2}$. The importance of self-confinement is effectively reduced when neutrals are present in the medium (as showed by Ref. [11, 117]). The dashed black line and the dashed dotted black line represent the escape time for case B with $n_n = 0.03\,\mathrm{cm}^{-3}$ and C with $n_n = 0.05\,\mathrm{cm}^{-3}$, respectively. IND decreases the level of turbulence especially in the energy range [$10^2$ -

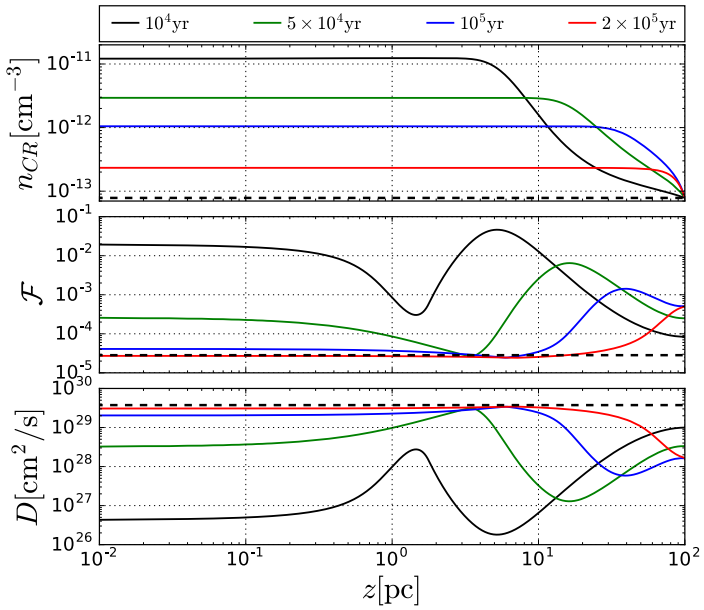


**Figure 13:** Same as Fig. 12 but for $E = 10^3$ GeV.

$10^3]$ GeV. However, the escape time remains larger that the diffusion time at all energies and in particular for $E \leqslant 50$ GeV and $E \sim$ few TeV. This because the damping rate of the IND remains roughly constant up to $E \approx 500$ GeV and then decreases as $\propto E^{-1}$ ($\Gamma_{IND}$ is plotted in Fig. 6 for both cases), so that the maximum destroying effect is reached in the energy range $[10^2$ - $10^3]$ GeV.

Fig. 15 shows the confinement time for all cases when the injection slope is $\alpha = 4.2$. At low energies the behavior is quite similar to the case with $\alpha = 4.0$ while at high energies the escape time is strongly reduced for all cases because the smaller energy density of CRs.

## 3.4 GRAMMAGE

As discussed in Sec. 1.2.1, an important quantity strictly related to the residence time of CRs in the Galaxy is the grammage, defined as the amount of matter traversed by CRs during their propagation. Such quantity is inferred from the measurement of the ratio of primary to secondary nuclei, as for instance the boron (B)/carbon (C) ratio [82]. Boron is mainly a secondary product of the nuclear collisions of Carbon (and other heavier) nuclei, while C is mainly primary, namely directly accelerated in the CR sources. The standard diffusive picture of the propagation of Galactic CRs is based on the fact that the Galactic transport is mainly diffusive [1, 6, 7], with a momentum dependent diffusion coefficient $D_g(p)$ over a magnetized halo of size $H \sim 3$kpc, where the gas density is negligible. In this simple picture the propagation time is dominated by diffusion in the halo,

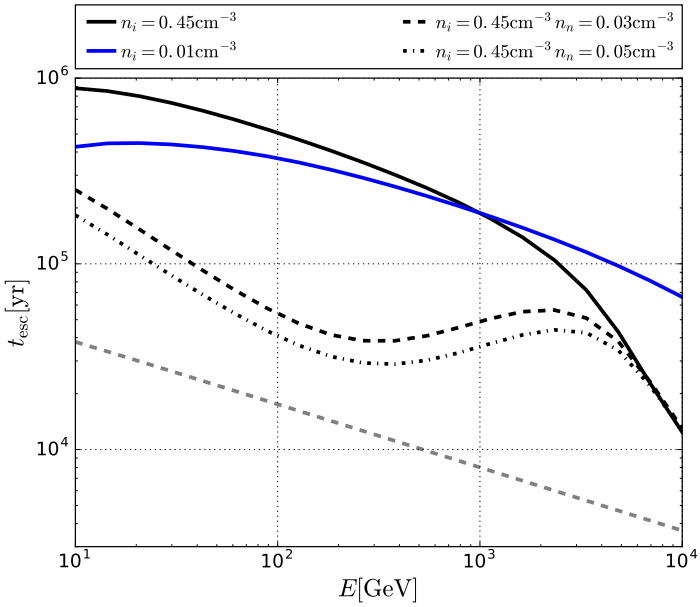


**Figure 14:** CR escape time $t_{esc}$ as a function of particle energy E[GeV] for the four different types of ISM listed in Table 2: case A (black solid line); case B (black dashed line); case C (black dotted dashed line); (4) case D (blue solid line). The grey dashed line represents the standard diffusion time $\tau_d = L_c^2/D_g = 8.3 \times 10^4 (E_{GeV})^{-1/3}$ yr. The injection slope is $\alpha = 4$.

$\tau_d(p) = H^2/D_g(p)$, but most of the grammage is accumulated when CRs traverse the disc, where the gas is located within a thin region of half-width $h \sim 150\,\mathrm{pc}$. The B/C ratio is proportional to $X_g$ and scales as $1/D_g(p)$, where it is assumed that the Galactic diffusion coefficient $D_g$ is the same throughout the disc and halo regions. Nevertheless, in the near-source regions where the propagation can be dominated by the non-linear process of self-confinement the accumulated grammage may become a non-negligible fraction of $X_g$. Moreover, another contribution might derive from the transport inside the source which has been estimated in Ref. [20]. These two phenomena can lead to important implications on the actual model of diffusive propagation in the Galaxy, in particular relying on the interpretation of the B/C ratio as the overall grammage from which the Galactic diffusion coefficient is inferred. Indeed, in the range of energy where the grammage is heavily affected by the self-confinement in the source vicinity or inside the accelerator the diffusion coefficient inferred from the B/C ratio is likely to reflect more a combination of Galactic propagation plus one of the two phenomena described above [117] rather than the pure diffusive transport on Galactic scales previously described.

In this work we estimate the grammage traversed by CRs while propagating in the region immediately outside the source as

$$X(p) = 1.4 m_p n_i v(p) t_{esc}(p)\,, \tag{60}$$

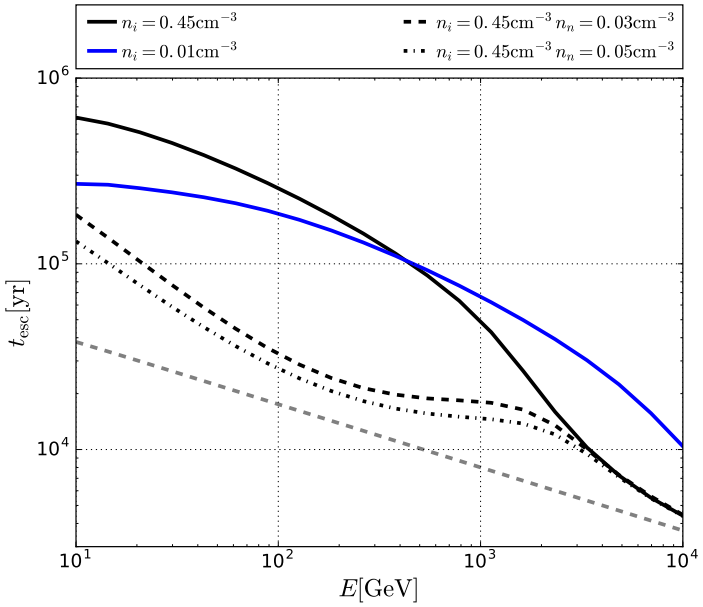


**Figure 15:** The caption is analogous of that describing Fig. 14, the only difference relies on the value of the injection slope which is $\alpha = 4.2$.

with the escape time $t_{esc}(p)$ defined in Sec. 3.3. The numerical factor 1.4 accounts for the fact that both protons and helium nuclei in the interstellar medium serve as target for the particle collisions that define $X(p)$.

The grammage $X$ as a function of particle energy is plotted in Fig. 16, with injection slope $\alpha = 4$. The thick dashed line shows the grammage estimated from the measured B/C ratio, assuming standard CR propagation in the Galaxy with turbulence described *a la* Kolmogorov [132]. The thick solid curve represents the grammage as calculated in the model of non-linear CR propagation of Ref. [19] (see also [46]). For comparison we also report (with thick dotted line) an estimate of the grammage traversed by CRs during the time they spent inside the SNR as calculated by Aloisio et al. [20]. Their estimate is valid for $E \geqslant$ few TeV under the assumption that all particles below such energy are released at the end of the Sedov-Taylor phase. Their estimate is adapted to our case using $n_i = 0.45\,\mathrm{cm}^{-3}$. In case A, in the energy region $E \lesssim$ few TeV, the grammage contributed by non-linear propagation in the near-source region is comparable (within a factor of $\sim$ few) with that accumulated throughout the Galaxy, if the standard diffusion coefficient is adopted. When neutral atoms are present, the IND severely limits the waves' growth: in cases B and C the grammage in the energy range below few hundreds GeV is about ten times smaller. However, since the importance of IND decreases with decreasing wavenumber $k$, particles at energies above $\sim 1$ TeV are again allowed to generate their own waves. Hence, the grammage in the near-source region increases, thereby becoming compara-

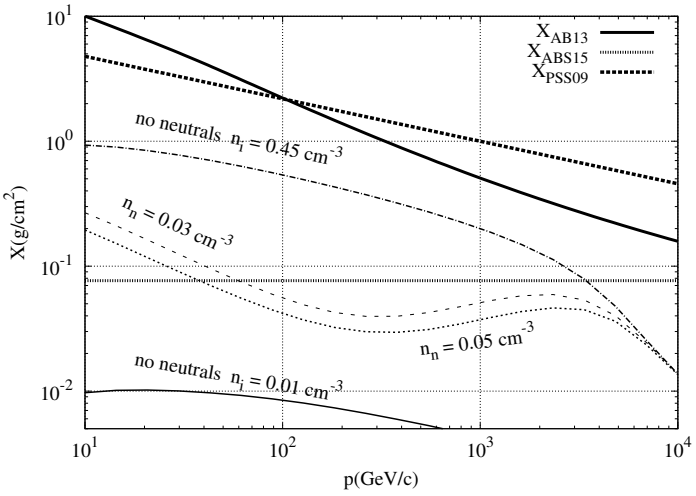


**Figure 16:** Grammage accumulated by CRs in the near-source region for $L_c = 100$ pc in the four cases listed in Table 2: case A (thin dotted-dashed black line); case B (thin dashed black line); case C (thin dotted black line); case D (thin solid black line), as labelled. The thick dashed line (labelled as $X_{PSS09}$) shows the grammage inferred from the measured B/C ratio [132], while the thick solid line (labelled as $X_{AB13}$) shows the grammage resulting from the non-linear propagation model of Ref. [19]. The horizontal (thick dotted) line (labelled as $X_{ABS15}$) is the grammage accumulated inside the SNR, as estimated in Ref. [20]. The value of the injection slope is $\alpha = 4$.

ble with the one accumulated inside the source. Case D corresponds to a small grammage due to the low gas density. Nevertheless, we note that Cases A and D correspond to roughly the same propagation time in the near-source region, in particular in the energy range $[10^2 - 10^3]$ GeV, as shown in Fig. 14. This might have important observational consequences in case where a dense target for pp collisions, such as a molecular cloud, is present in a region where the gas density (outside the cloud) is very low and IND is absent. In fact, in this situation the long escape times due to self-confinement can induce an enhancement of gamma-ray emission. This emission is due to the decay of $\pi^0$'s produced by the collisions between CRs and the dense target, which can be detected for instance studying the gamma-ray emission from molecular clouds located in the vicinity of SNRs. We refer to Ref. [10, 11] for the implications of the self-generation in terms of enhanced gamma ray emission from dense clouds in the near source region when also neutral atoms are present. It is interesting to notice that in cases where neutral atoms are absent, for particles with energies up to $\sim 1$ TeV, the grammage decreases with energy in roughly the same way as the observed grammage [132]. This behavior is a result of the dependence of NLLD rate on k. Fig. 17 shows the grammage calculated with injection slope $\alpha = 4.2$. The most

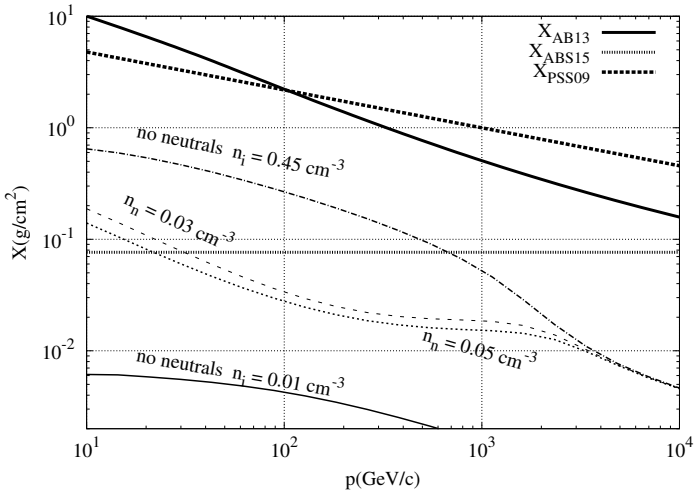


**Figure 17:** The caption is analogous of that of Fig. 16, the only difference relies on the value of the injection slope which is $\alpha = 4.2$.

important difference with respect to the previous case belongs to particles at energies above $\sim 1$ TeV. In such energy range the accumulated near source grammage remains below the one accumulated inside the source. This reflects the small density of particles at such energies, corresponding to a low growth rate of the instability and therefore to a small confinement time, as shown in Fig. 15.

The above results show that the grammage traversed by CRs with energies up to a few TeV is heavily affected by the self-induced confinement close to the sources, to an extent that depends on the number density of neutral hydrogen in the Galactic disc. At energies $\gtrsim 1$ TeV the grammage traversed by CRs can reasonably be expected to be heavily affected by the in-source contribution, due to the fact that CRs are trapped in the downstream region of the SN shock before escaping, as already proposed in Ref. [20] (where the confinement time is assumed to be $\sim 10^4$ years). The general picture that arises from these considerations is that at all energies the observed grammage is affected by either non-linear propagation in the near-source region or transport inside the source, thereby making the translation of the grammage (from B/C) to a confinement time in the Galaxy rather problematic. More specifically, both the normalization and the slope of the inferred diffusion coefficient are likely to reflect more a combination of Galactic propagation plus one of the two phenomena described above rather than the pure CR transport on Galactic scales.

The CR self-confinement near sources can induce an observational signature: the formation of extended halos of gamma ray emission from $\pi^0$ decay in such regions. Indeed, during CR propagation in near source regions, energetic protons can interact with the ambient gas via inelastic scattering and produced $\pi^0$-mesons. These mesons, in turn, decay into $\gamma$ photons with a typical energy $\sim 0.1$ times the en-

ergy of the parent proton (i.e. $p_{CR} + p_{ISM} \rightarrow \pi^0 \rightarrow 2\gamma$, see Ref. [137] and references therein). The self-confinement process can give rise to the formation of an halo of gamma radiation characterized by an extended shape along the direction of escaping particles (which in the flux-tube approximation coincides with the direction of magnetic field lines). An estimate of the gamma-ray emissivity within 100 pc from relatively young CRs sources has been performed by Aharonian and Atoyan in Ref. [138]. The authors assumed a diffusion coefficient two orders of magnitude smaller than the Galactic one and showed that CRs sources may significantly exceed the gamma-ray emission resulting from the average Galactic CR distribution, providing that the energy injected from SNRs or pulsar to relativistic particles is larger than few percents. Moreover, they argued that the presence of massive gas targets, as molecular clouds, near CRs sources may drive to the generation of detectable gamma-ray fluxes. In that paper, however, the value of such diffusion coefficient was only assumed and not motivated by some physical mechanism. In this thesis we do not estimate the emission from a single halo because is too faint to be detected with current gamma-ray telescopes. However, the sum of these halos over the whole CR source population produces a contribution to the diffuse gamma-ray radiation from the Galactic disc. The diffuse Galactic emission has been measured by the *Fermi*-LAT telescope over 7 years of data acquisition and recently analyzed in Ref. [88, 89]. Therefore, the predicted emission from the total halo's population can be compared with the available data. A clear understanding of the diffuse gamma-ray emission is essential to infer the correct CR distribution in the whole Galactic volume, hence it is important to disentangle the actual diffuse gamma ray emission from the one coming from the sources and the near-source regions. The purpose of this last part of the Chapter is to estimate such contribution comparing with the recent analysis performed in Ref. [88, 89].

## 3.5 DIFFUSE GAMMA-RAY EMISSION

In order to estimate the diffuse $\gamma$-ray emission from these self-confined CRs, the first step is to evaluate the emissivity of the $\gamma$ halo produced around a single SNR. Then, after a sampling of the SNR distribution into the Galactic disc, the diffusive emission, along a fixed direction is calculated summing over all halos located along that line of sight.

Using the numerical solutions of the coupled equations (47) and (55), we evaluate the time-dependent CR spectrum $J_p(E,t) \equiv dN_{CR}/dE$ over the flux tube with radius $R_{SN}$ and length $2L_c$ as:

$$J_p(E,t) = 2\pi R_{SN}^2 \int_0^{l_c} dz\, f(E,z,t)\,, \tag{61}$$

where the relation $4\pi p^2 f(p)dp = f(E)dE$ has been used. It is important to note that Eq. (47) does not contain CR energy losses due to the inelastic proton-proton interaction because the energy loss time is $\sim 7 \times 10^7$ yr, hence much larger than the maximum escape time.

### 3.5.1 Emission from a single source

The gamma-ray emissivity, $q_\gamma(E_\gamma, t)$, from a single source is connected to the integral of $\pi^0$ emissivity $q_\pi(E_\pi, t)$ over pion energy $E_\pi$

$$q_\gamma(E_\gamma, t) = 2\int_{E_{min}(E_\gamma)}^{\infty} \frac{q_\pi(E_\pi, t)}{\sqrt{E_\pi^2 - m_\pi^2 c^4}} dE_\pi \,, \tag{62}$$

where $E_{min} = E_\gamma + m_\pi^2 c^4/(4E_\gamma)$ with $m_\pi$ the $\pi^0$ rest mass. The factor 2 multiplying the integral in Eq. (62) comes from the fact that $\pi^0$ decays into 2 photons. We derive the emissivity $q_\pi(E_\pi, t)$ of $\pi^0$-mesons from the CR proton flux, $J_p$ defined in Eq. (61), using the $\delta$-function approximation as done in Ref. [137]

$$\begin{aligned} q_\pi(E_\pi, t) &= c n_i \int \delta(E_\pi - K_\pi E_{kin}) \sigma_{pp}(E) J_p(E, t) dE \\ &= c \frac{n_i}{K_\pi} \sigma_{pp}\left(m_p c^2 + \frac{E_\pi}{K_\pi}\right) J_p\left(m_p c^2 + \frac{E_\pi}{K_\pi}, t\right) . \end{aligned} \tag{63}$$

Here $E_\pi = K_\pi E_{kin}$ where $K_\pi$ is the mean fraction of proton kinetic energy $E_{kin} = E - m_p c^2$ transferred to $\pi^0$ per collision. The functional form used for the inelastic cross section $\sigma_{pp}(E)$ is taken from Ref. [139] and reads

$$\begin{aligned} \sigma_{pp}(E) = \Bigg[ & 34.3 + 1.88 \ln\left(\frac{E}{1\,\text{TeV}}\right) \\ & + 0.25 \ln\left(\frac{E}{1\,\text{TeV}}\right)^2 \Bigg] \times \left[1 - \left(\frac{E_{th}}{E}\right)^4\right]^2 \text{mb} \,, \end{aligned} \tag{64}$$

where $E_{th} = m_p c^2 + 2 m_\pi c^2 + m_\pi^2/(2m_p) c^2 = 1.22\,\text{GeV}$ is the threshold energy for $\pi^0$ production. The value chosen for the parameter $K_\pi$ is 0.17 over the whole range of proton energy $E = [10 \text{ - } 10^4]$ GeV, as in Ref. [137].

Fig. 18 reports the $\gamma$-ray emissivity multiplied by the square of the photon energy, shown at four different times in case of fully ionized medium and injection slope $\alpha = 4$ (case A of Table 2). At time $t = 10^4$ yr (solid black line) CRs with $E \leqslant 10^3$ GeV are still inside the box. This implies that for $E_\gamma \leqslant 10^2$ GeV one has $q_\gamma \simeq q_\gamma(t = 0) \propto E_\gamma^{-2}$, having the same slope of the CR distribution. The situation remains almost the same up to $t \sim 10^5$ yr (solid blue line). When $t \sim t_{esc}(10\,\text{GeV}) \sim 10^6$ yr also CRs with $E = 10$ GeV left the near source region. Thus, the distribution function reduces to the

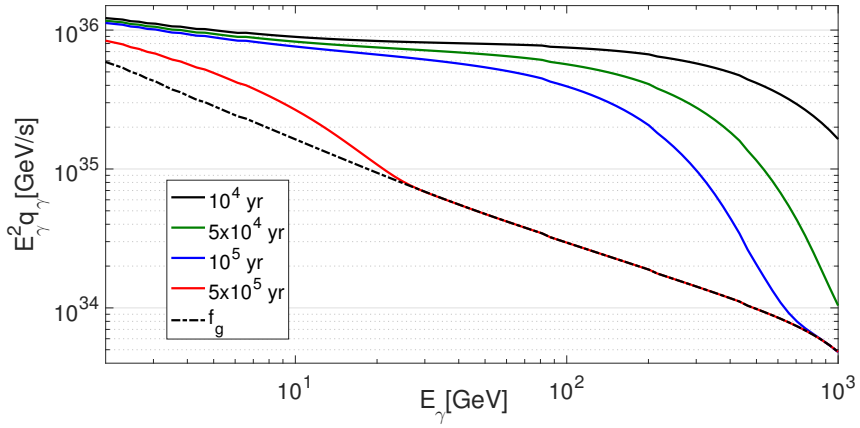


**Figure 18:** $\gamma$-ray emissivity multiplied by the square of the photon energy for case A of Table 2 of fully ionized medium with $n_i = 0.45\,\mathrm{cm}^{-3}$ and injection slope $\alpha = 4$ at four different times $10^4, 5\times10^4, 10^5$ and $5\times10^5$ yr, as labeled. The dotted dashed black line correspond to the Galactic emissivity $q_{\gamma,g}$ which is the emissivity calculated with $f = f_g$.

Galactic one and the emissivity becomes equal to the Galactic average $q_{\gamma,g} \propto E_\gamma^{-2.7}$ (represented by dotted dashed black line). The plot of the emissivity for the case D with rarefied fully ionized medium is not shown because it presents quite the same time evolution of case A. When neutrals are included, the escape time decreases, as shown in Fig. 14, hence the gamma-ray emissivity is accordingly reduced for $5\times10^4$ yr , as shown in Fig. 19. It is interesting to note that in case C (and case B) a bump in the emissivity appears around $E \sim 300$ GeV for $t = 5\times10^4$ yr, because at such energies IND is less important than at lower energies. This bump will persist, to some extent, in the total flux integrated over all remnants, producing a slope change around $\sim 100$ GeV, as we will show in Sec. 3.5.3.

### 3.5.2 Source distribution in the Galactic disc

To estimate the contribution of self-confined CRs to the diffuse $\gamma$-ray emission, the second step is to sample the distribution of SNRs located into the Galactic disc. We assume that the Galactic disc is characterized by a diameter of $\sim 30$ kpc and a thin width of $\sim 300$ pc. At zeroth order the disc can be described using a cylindrical symmetry, with a SNR distribution which is uniform in the azimuthal direction $\phi$ and depends only upon the galactocentric radius $R$. We use the functional form in $R$ derived by the recent work of Green in Ref. [140] who also assumed an uniform distribution in $\phi$ and inferred the ra-

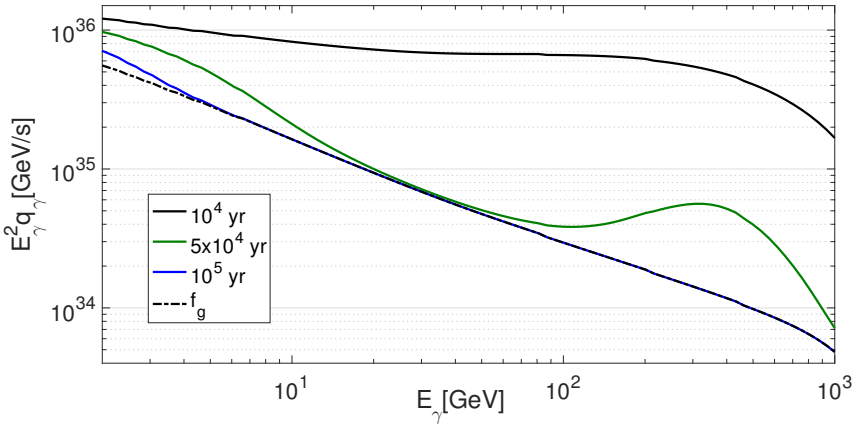


**Figure 19:** Same as Fig. 18 but for the case C with $n_i = 0.45\,\mathrm{cm}^{-3}$ and $n_n = 0.05\,\mathrm{cm}^{-3}$.

dial dependence analyzing a sub-sample of radio SNRs. The result is:

$$g_{SN,R}(R) \propto \left(\frac{R}{R_\odot}\right)^{\alpha} \exp\left(-\beta \frac{R - R_\odot}{R_\odot}\right), \tag{65}$$

where for the best-fitting Green [140] obtained $\alpha = 1.09$, $\beta = 3.87$ and the position of the sun $R_\odot$ is assumed as 8.5 kpc. First of all we notice that this distribution is peaked around $\sim 4$ kpc, half of the distance between the Sun and the Galactic center. In addition we mention that, as discussed by Green [140], the fit reported in Eq. (65) is not extremely well defined because there is some degeneracy between parameters $\alpha$ and $\beta$. Nevertheless such uncertainty does not have a significant impact on our results. In passing, we notice that the distribution in Eq. (65) has been used by Recchia et al. [141] to justify the peak of CRs inferred around $R \sim 4$ pc by the analysis of gamma-ray diffuse galactic emission of FermiLAT performed in Ref. [88, 89]. We also need to define the time distribution of SN explosions. Indeed, it is generally accepted that on average a SN explodes every 30 yr in our Galaxy [1, 90]. We assume that the time at which a SN explodes follows a Poisson distribution where the mean rate of explosions $\mathcal{R}_{SN} = 1/30\,\mathrm{yr}^{-1}$. The sources that contribute to the total $\gamma$-ray emission are those with an age that does not exceed the maximum confinement time, corresponding to that of CRs with $E = 10$ GeV in all the analyzed cases.

### 3.5.3 Gamma-ray emission from the Galactic disc

Here we compare the gamma-ray emission resulting from all $\gamma$-halos with data on the diffuse $\gamma$-ray emission of the Galactic disc. This emission has been detected by the *Fermi*-LAT telescope over 7 years of observations, in an energy range from 0.1 GeV to $\geqslant 100$ GeV and

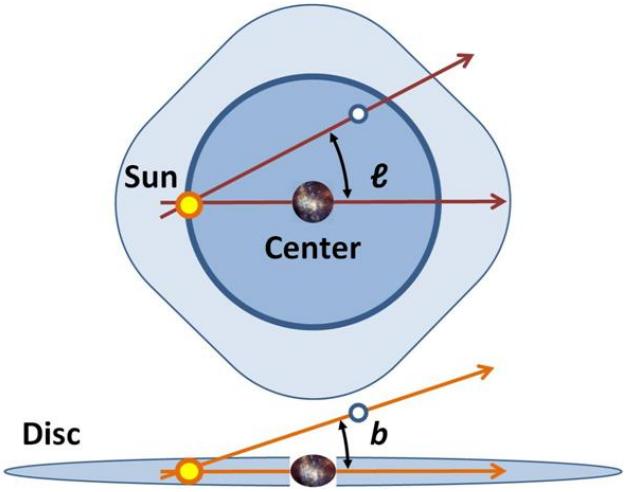


**Figure 20:** Sketch of the Galactic coordinate system where $l$ is the Galactic longitude and $b$ the galactic latitude (Wikimedia Commons).

with a very high flux sensitivity [142]. In 2016 Yang et al. [88] and Acero et al. [89] published two independent analyses of the *Fermi*-LAT data presenting their results in different ways. In Ref. [88] the authors show the spectral energy distribution $E_\gamma^2 dN/dE$ ($dN/dE$ is the gamma-ray flux per unit energy) of the $\gamma$-ray spectrum, as reported in Fig.(1) of the paper, considering three different regions of the Galactic disc: towards the direction of the Galactic center, towards the direction orthogonal to the Galactic center and towards the outside of the disc. In Ref. [89], instead, the *Fermi* collaboration shows the spectral energy distribution of the gamma-ray emissivity $E_\gamma^2 q_\gamma$ per hydrogen atom in nine Galactocentric annuli, as reported in Fig.(7) of the paper. However, this data representation is model dependent since it relies on the kind of ISM in which CRs propagate. On the contrary, the analysis performed in Ref. [88] is model independent and therefore the comparison with it is more suitable because. For completeness we show the comparison with both works.

We start describing the procedure used to calculate the spectral energy distribution of an angular sector in order to compare our results with those of Ref. [88]. It is necessary to change system of coordinates, passing from Galactocentric system to the Galactic coordinate system where the Sun is the center of the reference frame. Each source is represented by two new coordinates: $d$ is the distance of a SN from the Sun, $l$ is the Galactic longitude, i.e. the angular distance of a SN with primary direction from the Sun to the Galactic center, as sketched in Fig. 20. An angular sector corresponds to a cone with the principal vertex on the Sun and with angular aperture $\Delta l = l_2 - l_1$, where $l_1$ and $l_2$ are two arbitrary Galactic longitudes. In such a region of the

disc, the $\gamma$-ray flux emitted by self-confined CRs is estimated as the sum over all the fluxes emitted by SNe with $l_1 \leqslant l \leqslant l_2$:

$$\phi_{\Delta l}(E_\gamma, \Delta l) = \sum_{l_1 \leqslant l \leqslant l_2} \frac{q_\gamma(t_{age}, E_\gamma)}{4\pi d^2} \,. \tag{66}$$

Here we sum also over $t_{age}$ which is the time at which the SN explodes and injects the accelerated particles into the surrounding ISM. It is worth noticing that in this observable the most important contribution is provided by the nearest SNe to the Sun. The second procedure we describe is the one used to calculate the spectral energy distribution of a ring sector of the Galactic disc, in order to compare our results with those of Ref. [89]. In this case the Galactocentric system of coordinate $R, \phi$ is used. A ring sector corresponds to a portion of the disc with radial size $DR = R_2 - R_1$, centered with respect to the Galactic center. Thus, the total $\gamma$-ray emissivity per H atom is defined as:

$$\phi_{DR}(E_\gamma, DR) = \sum_{R_1 \leqslant R \leqslant R_2} \frac{q_\gamma(t_{age}, E_\gamma)}{4\pi n_i DV} \,, \tag{67}$$

where the sum is also over the age of the source, $DV = \pi h_d(R_2^2 - R_1^2)$ and $h_d = 300\,\mathrm{pc}$ is the height of the Galactic disc. The observable expressed in Eq. (67) provides some different information with respect to the one expressed in Eq. (66), because all the sources contribute with the same weight. Moreover, while the flux defined in Eq. (66) is model independent since directly measured by *Fermi*-LAT, the $\gamma$-ray emissivity per H atom depends on the gas distribution.

In Section 3.5.4 we compare the predictions obtained within the model of self-confinement with the data measured by *Fermi*-LAT and analyzed in two works, Ref. [88] (see Fig.1 in the cited reference) and Ref. [89] (see Fig.7 in the cited reference), recalling that the comparison with the results presented by the *Fermi* collaboration is less reliable due to the model dependence from the gas distribution in the Galaxy.

### 3.5.4 Results

In order to take into account the statistical fluctuations in the spatial and temporal SNR distribution, the SNR sampling in the disc has been repeated for 100 times. For each sampling the total $\gamma$-ray emission has been calculated in both ways defined by equations (66) and (67). The spectral energy distribution of the total $\gamma$-ray emission for all the realizations has been plotted in Fig. 21 for the angular sector $5^\circ \leqslant l \leqslant 15^\circ$ calculated for case A of Table 2. The fluctuations in the gamma-ray flux are mainly due to SNRs located in the vicinity of the Sun.

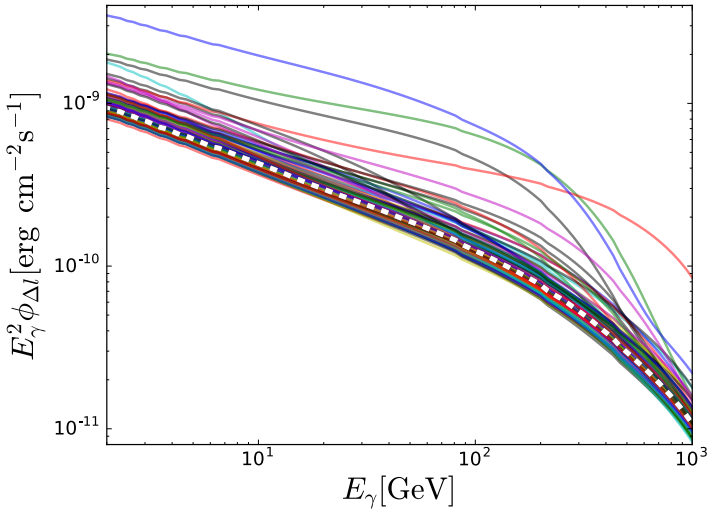


**Figure 21:** Spectral energy distribution of the total $\gamma$-ray emission $E_\gamma^2 \times \phi_{Dl}$ as a function of photon energy for all the 100 samplings for case A of fully ionized medium and injection slope $\alpha = 4$ in the angular sector $5° \leqslant l \leqslant 15°$, corresponding to looking towards the Galactic center. The white thick dashed line corresponds to the mean value. In each panel the green curve represents our estimate of the diffuse gamma-ray emission.

In order to represent the result in a more suitable way, we consider the mean value over the whole samplings with an uncertainty band calculated at the 68th percentile. In Figure 22 we compare our predictions on the spectral energy distribution of the total $\gamma$-ray emission with *Fermi*-LAT data analyzed Ref. [88]. We consider the case of fully ionized medium with $n_i = 0.45\,\mathrm{cm}^{-3}$. From top to bottom we show three different sectors with $l \in 5°$ - $15°$, $85°$ - $95°$ and $175°$ - $185°$ which correspond to looking towards the Galactic Center, a direction orthogonal to the Galactic Center and towards the anti-center, respectively. The mean number of SNRs is maximum in the first sector, i.e. $\sim 700$. This quantity decreases moving away from the Galactic Center, being $\sim 350$ and $\sim 15$ in the sectors $85°$ - $95°$ and $175°$ - $185°$, respectively. Correspondingly, the statistical error increases for the more external sectors. In all cases our predictions are very close to the data. This implies that the streaming instability can provide a non-negligible contribution to the diffuse emissivity, in particular towards the Galactic center where the majority of sources is located. Indeed, at $E_\gamma = 2\,\mathrm{GeV}$ the predicted mean flux is about 60% of the observed flux. The fact that the predicted flux almost saturates the observed one has to be taken with caution. In fact in this case a totally ionized plasma has been considered, which cannot be a realistic assumption for all SNRs. As a consequence the resulting flux has to be taken as un upper limit. In addition we notice that in all the three sectors the slope of the predicted flux is close to the slope which can be inferred

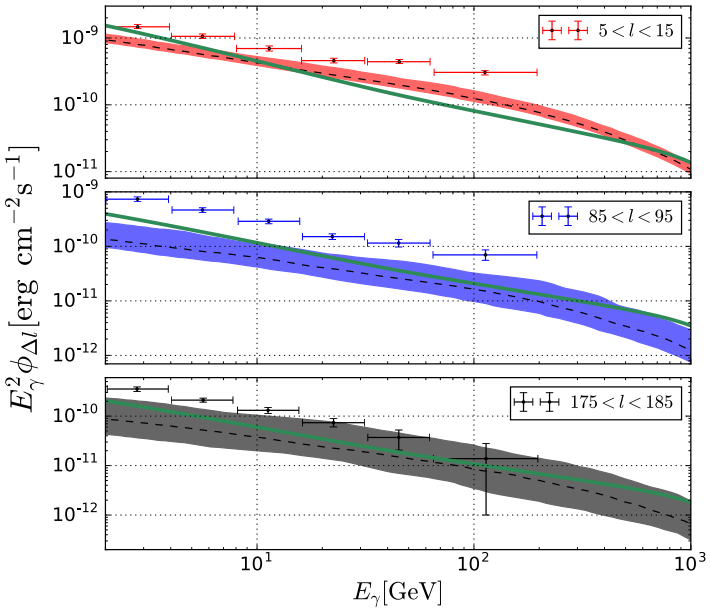


**Figure 22:** Parameters : $n_i = 0.45\mathrm{cm}^{-3}$ and $n_n = 0\mathrm{cm}^{-3}$ and injection slope $\alpha = 4$. The spectral energy distribution of the total $\gamma$-ray emission $E_\gamma^2 \times \phi_{Dl}$ is reported in three different angular sectors, i.e. on top $5° \leqslant l \leqslant 15°$, on center $85° \leqslant l \leqslant 95°$ and on bottom $175° \leqslant l \leqslant 185°$. The black dashed line corresponds to the mean value, while the band corresponds to a confidence level of 64%. The analyzed data (from Ref. [88]) are plotted with their error-bars.

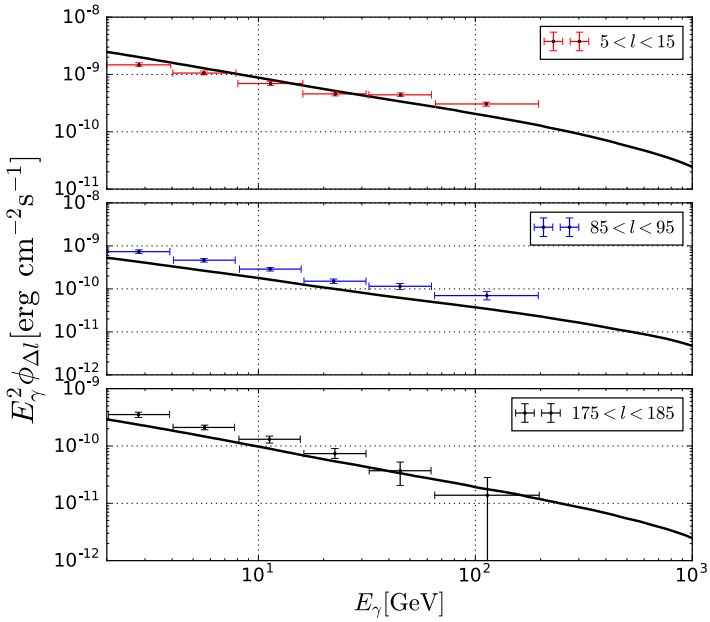


**Figure 23:** Comparison between the sum of the diffuse gamma-ray emission with the mean value gamma-ray emission produced by the self-confinement process (corresponding to the black dashed line in Fig. 22) and data from Ref. [88].

from the data, especially at lower energies. In each panel the green curve represents the estimate of the spectral energy distribution of the diffuse gamma-ray emission due to the average Galactic CR spectrum. To evaluate this quantity we have assumed that the average CR energy spectrum $f_{CR}$ depends from the Galactocentric radius in the same way as the SNRs distribution. Moreover, we assume that at the Sun position $f_{CR}$ has to be equal to the one measured by AMS02 [41] (expressed in Eq. (49)). The distribution of the gas, assumed to be made by H and He atoms, is the one used in the GALPROP code (see galprop.stanford). In all panels our model of the diffuse gamma-ray emission underestimates the data, which probably depends on our choice for the gas distribution. In particular in sector 5° - 15° the difference is more pronounced for energies $\geqslant 10\,\mathrm{GeV}$, while in the other two sectors this difference is present in all energy range measured by *Fermi*-LAT. When we add this diffuse emission to the one produced by the self-confinement process, as reported in Fig. 23, the difference with respect to data is reduced. This fact implies that the gamma-ray emission produced by the self-confined accelerated particles might be a non-negligible contribution to the diffuse gamma-ray emission in the Galactic disc.

In Fig. 24 we report the spectral energy distribution of the total $\gamma$-ray emissivity per H atom in six different ring sectors compared with data taken from Acero et al. [89]. In each sector the mean number of SNRs is quite large, namely around $10^3$ - $2 \times 10^3$. This explains

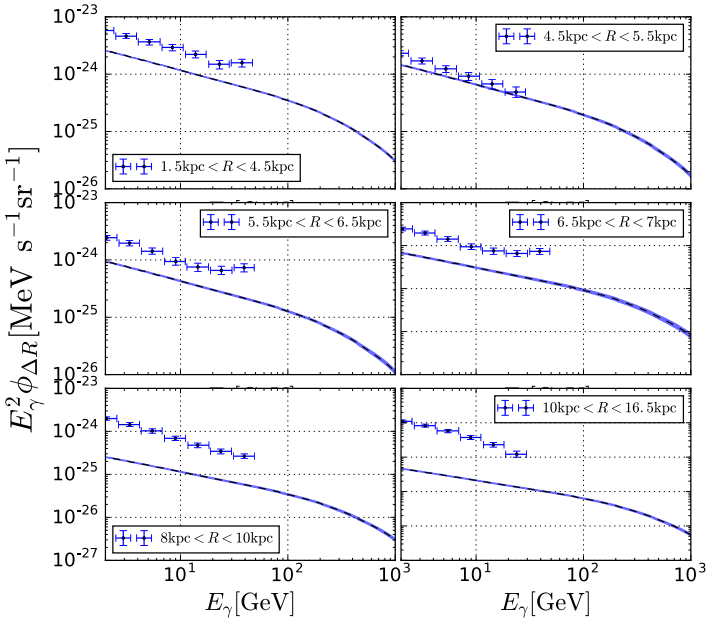


**Figure 24:** Parameters : $n_i = 0.45\mathrm{cm}^{-3}$ and $n_n = 0\mathrm{cm}^{-3}$ and injection slope $\alpha = 4$. The spectral energy distribution of the total $\gamma$-ray emission per H atom $E_\gamma^2 \times \phi_{DR}$ is reported in six different ring sectors (see labels). The black dashed line corresponds to the mean value, while the band corresponds to a confidence level of 64%. The analyzed data (from Ref. [89]) are plotted with their error-bars.

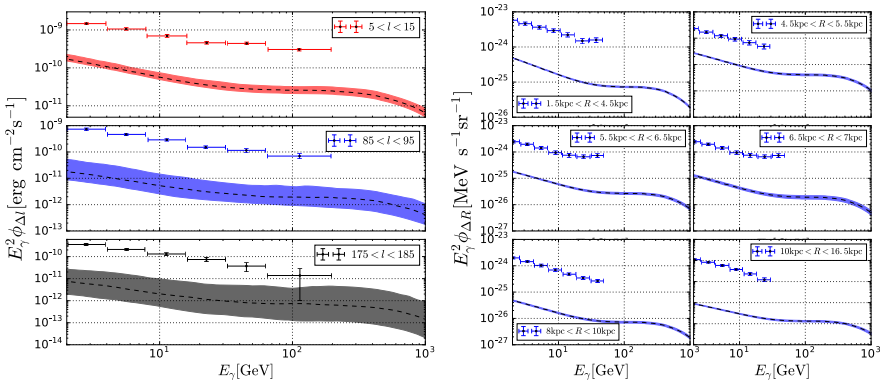


**Figure 25:** *Left panel*: same as Fig. 22; *Right panel*: same as Fig. 24. For both panels $n_i = 0.45\text{cm}^{-3}$ and $n_n = 0.05\text{cm}^{-3}$.

why the width of the uncertainty band is so small with respect to the angular sectors. Moreover, compared to the left panel, the data in the right panels do not include any information about the distance of the sources in Ref. [89]. This is the reason why in the first case the error-bars are so large with respect to the second case. Therefore, while the comparison with the results presented in Ref. [88] is more appropriate, because these refer directly to the observed data without any model dependent assumption, in Ref. [89] the comparison is useful only to analyze the behavior of the slope of the spectral distribution. In the two panels on the top, the distance from the Galactic center is $\leqslant 5.5\,\text{kpc}$ and the predictions have roughly the same slope of the analyzed data. In the two panels on the center the change in the slope present in the analyzed data at $E_\gamma \approx 30\,\text{GeV}$ is not predicted by the model. In the last two panels on the bottom there is not a good agreement between the results and the analyzed data.

In Fig. 25 and Fig. 26, where partially ionized media have been considered, IND reduces the CR contribution to diffuse $\gamma$-ray emission. Of course, this effect is less evident in Fig. 26 due to the decreasing neutral density. What is interesting to notice is that at $E_\gamma \geqslant 10^2\,\text{GeV}$, which corresponds basically to CRs with $E \geqslant 10^3\,\text{GeV}$, there is a change of slope in both the $\gamma$-ray flux and the $\gamma$-ray emissivity per H atom. This is due to the fact that CR streaming instability is more efficient to confine particles at such energies, as it can be seen from the escape time plotted in Fig. 14. In Fig. 27 we consider the case of fully ionized medium with ion density $n_i = 0.01\text{cm}^{-3}$. On the left panels, the spectral energy density is about two order of magnitude smaller than the data, because it scales as $n_i$. On the right panels, the behavior is quite similar to the case A though the smaller confinement time reduces the $\gamma$-ray emission. When the injection slope is equal to $\alpha = 4.2$ the confinement time is significantly reduced at high energies and as a consequence also the predicted diffuse $\gamma$-ray emission becomes lower, as it is shown in Fig. 28 for case with no neutrals and

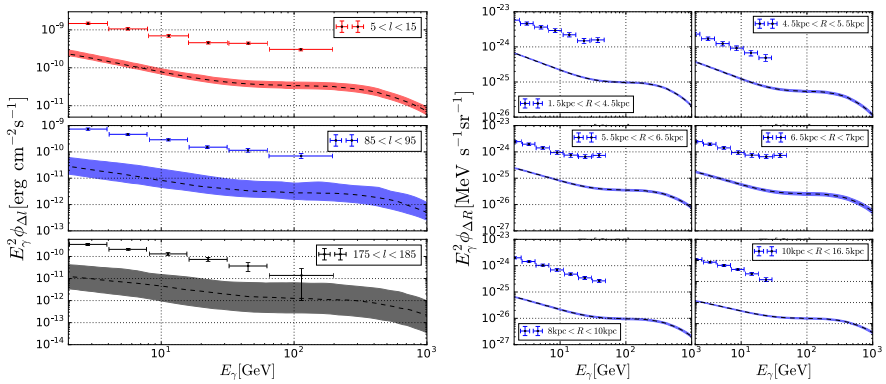


**Figure 26:** *Left panel*: same as Fig. 22; *Right panel*: same as Fig. 24. For both panels $n_i = 0.45\text{cm}^{-3}$ and $n_n = 0.03\text{cm}^{-3}$.

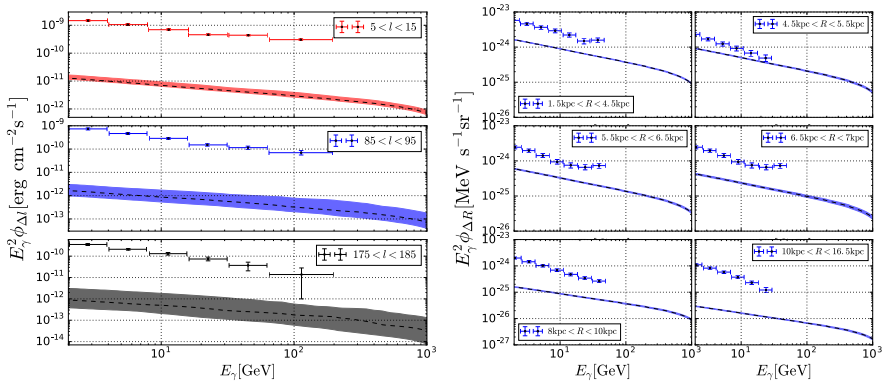


**Figure 27:** *Left panel*: same as Fig. 22; *Right panel*: same as Fig. 24. For both panels $n_i = 0.01\text{cm}^{-3}$ and no neutrals.

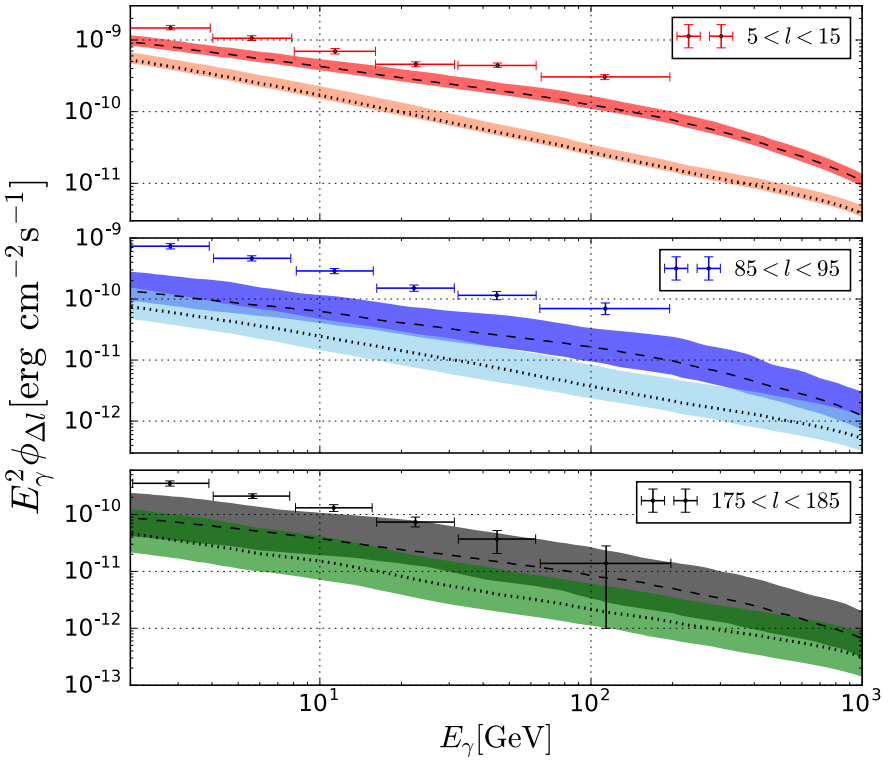


**Figure 28:** Comparison of the spectral energy distribution in the angular sector obtained using two different injection slope $\alpha = 4$ and $\alpha = 4.2$ for case A with no neutrals and $n_i = 0.45\,\mathrm{cm}^{-3}$. For all the three panels the black dashed line indicates the mean value for $\alpha = 4$ while the dotted black line indicates the one for $\alpha = 4.2$. *Top panel*: the red band corresponds to $\alpha = 4$ while the coral band corresponds to $\alpha = 4.2$. *Central panel*: the blue band corresponds to $\alpha = 4$ while the cyano band corresponds to $\alpha = 4.2$. *Bottom panel*: the grey band corresponds to $\alpha = 4$ while the green band corresponds to $\alpha = 4.2$.

$n_i = 0.45\,\mathrm{cm}^{-3}$ and in Fig. 29 where neutrals are present. In particular in Fig. 29 when $\alpha = 4.2$ the change in the slope at $E_\gamma = 10^2\,\mathrm{GeV}$ disappears.

A clear understanding of the diffuse gamma-ray emission is essential to infer the correct CR distribution in the whole Galactic volume, hence it is important to disentangle the actual diffuse gamma ray emission from the one coming from the sources and the near-source regions. The above results show that in case of fully ionized medium the resulting $\gamma$-ray emission saturates the observed one leaving little room for other diffuse components. This result is not surprising because we do not expect all SNRs to explode in a fully ionized ISM. In the partially ionized medium, on the contrary, ion-neutral damping reduces the CR confinement time and the $\gamma$-ray emission contribute to roughly 1% of the observed one, a contribution which increases for energies $E_\gamma \sim 100\,\mathrm{GeV}$.

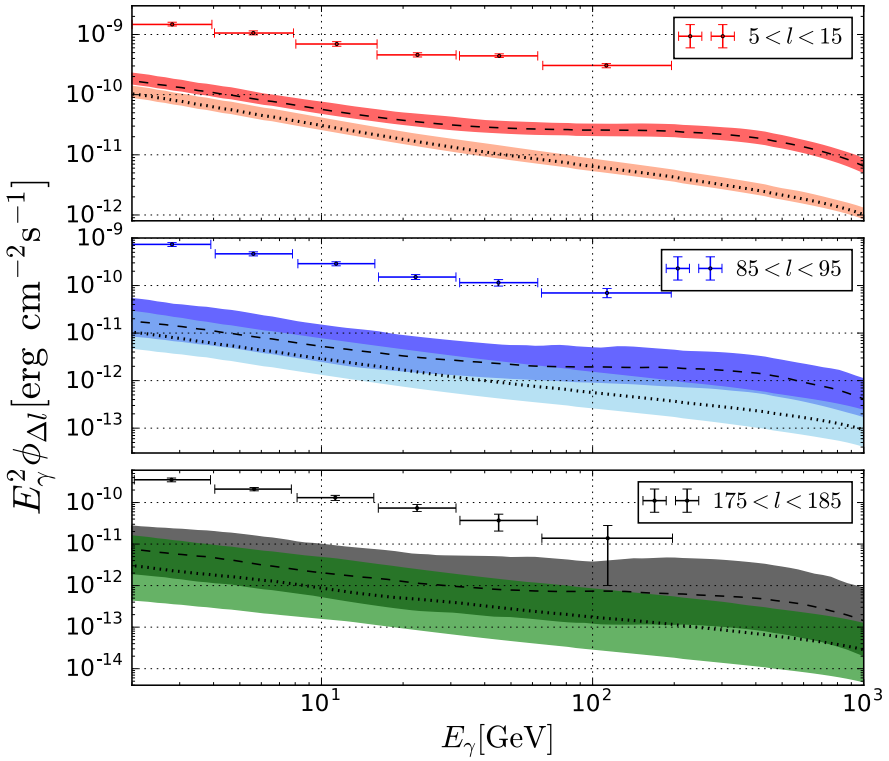


**Figure 29:** Same as Fig. 28 but for case B, i.e. $n_i = 0.45\,\mathrm{cm}^{-3}$ and $n_n = 0.05\mathrm{cm}^{-3}$.

## 3.6 CONCLUSIONS

In this Chapter we solved numerically the non-linear CR transport equation (47) together with the self-generated wave equation (55) in a region of 100 pc around the source. We assumed the accelerator to be a typical SNR with a total energy of $10^{51}$erg and a CR acceleration efficiency of 20%. Moreover, we considered that the coherence scale of the Galactic magnetic field $L_c$ is about $\sim$ 100 pc and we assumed that as far as this distance from the source the problem can be modeled as one dimensional. At larger distances diffusion becomes three dimensional and the density of CRs contributed by the individual source quickly drops below the Galactic average (assumed to be the one observed at the Earth). The CR density gradient in the near source region is responsible for generation of Alfvén waves that in turn scatter the particles. As a consequence, CRs residence time in the near source region is increased.

This phenomenon was previously analyzed in Ref. [9], where the authors studied the consequences of an impulsive release of CRs by a source embedded in a fully ionized medium without analyzing the effect of neutral atoms. In order to obtain a self-consistent analytical expression for the spatial diffusion coefficient, the authors considered a steady state solution for the self-generated turbulence, differently

with respect to our approach where we solve numerically the time dependent wave equation. There are two more recent papers [10, 11] which solve the non-linear coupled equations in connection with the problem of the interaction of CRs with molecular clouds in the near source region. In Ref. [11], in particular, the authors solve numerically the non-linear system of differential equations as done in this work, but focusing mainly on the ion-neutral damping induced by the presence of neutral particles in the ISM and for this reason taking into account the warm ionized phase and the warm neutral phase of the ISM. The main outcome of such paper is that the streaming instability may affect CRs propagation over a region of few tens of pc around the SNR, inducing a suppression of the diffusion coefficient by more than a factor of two with respect to the average Galactic one. Furthermore, the authors discuss the important observational consequence of the gamma-ray emission due to the interaction of the escaping CRs with a molecular cloud near the source.

Here, we consider two phases of the ISM, namely the hot fully ionized medium and the warm partially ionized medium. In the first case the relevant process assumed to damp the resonant streaming instability is the non-linear Landau damping (discussed in Sec. 2.3.1), while in the second case is the ion-neutral damping (discussed in Sec. 2.3.2). In both cases we study the non-linear evolution of CR propagation near the source calculating the escape time, as defined in Sec. 3.3, and most importantly the grammage (this quantity has not been estimated in Ref. [9–11]), as defined in Sec. 3.4. In the absence of neutrals and with gas density of $\sim 0.45\,\mathrm{cm}^{-3}$, we showed that the grammage accumulated in the near source region is comparable (within a factor of few) with the one that is usually inferred from the measured B/C ratio. On the other hand, when neutrals are present, as expected for the standard ISM, the accumulated grammage becomes negligible. Nevertheless, it is worth noticing that the strength of ion-neutral damping, could be different from what we have assumed, because in the warm-hot ISM most of the neutral gas is expected to be in the form of He atoms and not only due to Hydrogen atoms, as we assumed. The cross section for H-He charge exchange is much smaller than for H-H [135], therefore it could be that most damping is actually due to a residual fraction of neutral H and we made an attempt to bracket the importance of this process as due to all these uncertainties. In particular, we found that at all energies the observed grammage might be affected by either non-linear propagation in the near-source region, which depends on the level of ionization of the ambient medium, or transport inside the source, Thus, we argued that both the normalization and the slope of the diffusion coefficient inferred from B/C ratio could reflect more a combination of Galactic propagation plus the two phenomena de-

scribed above rather than being the result of the Galactic transport only.

We studied a possible observational signature of this process which derives from the formation of extended halos of gamma ray emission from $\pi^0$ decay in a region of size $\sim L_c$ around CR sources. The gamma-ray halo formed within 100 pc around a Galactic CR source has been studied in Ref. [138]. In this paper, the authors assumed a diffusion coefficient two orders of magnitude smaller than the average Galactic one and showed that the gamma-ray emissivity induced by escaping CRs may significantly exceed the one produced by the "sea" of Galactic CRs. Moreover, they argued that the energy injected from SNRs or pulsar to relativistic particles can be larger than few percents. Nevertheless, this study was performed without a physical mechanism responsible for the reduction of the diffusion coefficient. In our work we analyzed the sum of these halos over the whole CR source population because it can produce a non negligible contribution to the diffuse gamma-ray emissivity from the Galactic disc. We calculated the $\gamma$-ray emission of these halos for energy $E_\gamma$ in the range $[1 - 10^3]$ GeV, and we compared our results with the diffuse Galactic $\gamma$-ray emission detected by *Fermi*-LAT, which has been analyzed in Ref. [88, 89]. We found that in case of fully ionized medium the resulting $\gamma$-ray emission saturates the observed one. Nevertheless, this contradictory result is not surprising because here we have assumed that all SNRs explode in a fully ionized medium, which we expect to be an approximation too optimistic. Thus, this estimate is an upper limit of the real self-confined CRs contribution. In the opposite, lower limit case, where partially ionized medium is considered, ion-neutral damping reduces the CR confinement time and the $\gamma$-ray emission contribute to roughly 1% of the observed one. This contribution increases for energies $E_\gamma \sim 100$ GeV.

We conclude warning the reader that in case one considers smaller acceleration efficiency ($\leqslant$ 10%) and/or softer spectra steeper than -4, the non-linear effects on both the grammage and the gamma-ray emission are expected to be negligible with respect to the Galactic observed quantities.

# 4 SELF-CONFINEMENT OF COSMIC RAYS CLOSE TO EXTRAGALACTIC SOURCES

The aim of this Chapter is to study the propagation of ultra-high energy CRs (UHECRs) while leaving the parent galaxy. In extra-galactic environments the interaction between CRs and the ambient medium can give rise, under certain conditions, to the non-resonant streaming instability, first proposed by Bell [25, 26] and described in Ch. 2 in Sec. 2.2.3. When the accelerated particles stream away from their source, they produce an electric current and the background plasma reacts generating a return current. This return current can generate unstable modes. The growth of such instabilities leads to large turbulent magnetic fields and to enhanced particles' scattering. As a result, CRs can become self-confined near the source regions, in analogy with the Galactic case. This can have important implications on Extra-Galactic CR propagation. In particular, if particles remain self-confined for times exceeding the age of the Universe, they cannot propagate to the Earth. Thus, the self-confinement process can introduce a critical energy below which CRs cannot reach the Earth, giving rise to a low energy cutoff in the extragalactic CR component., as we will discuss in Sec. 4.4.

In the next section we describe the physical framework discussing the relevant model parameters, such as the mean value and coherence scale of the Extra-Galactic magnetic field and the injection CR spectrum. In Sec. 4.2 and Sec. 4.3 we calculate the amplified magnetic field in three dimensional and one dimensional regimes of propagation, respectively. Finally, in Sec. 4.4 we discuss the confinement energy in this two different regimes.

## 4.1 PHYSICAL FRAMEWORK

In this work we do not make any particular assumption about the nature of the nature of Extra-Galactic sources producing UHECRs. We just assume that the source, whatever it is, is located in its parent galaxy. We further assume that the spectrum of particles leaving the source is a power law with injection slope 4 in the momentum domain, i.e. $q(p) \propto p^{-4}$ up to some maximum momentum $p_{max}$.

The distribution function of CRs streaming out of such sources at a distance $r$ from it can be written as

$$f(p,r) = \frac{dN_{CR}}{dV d^3p} = q(p)\,A(r) \\ = A(r)\frac{1}{4\pi p_0^3}\left(\frac{p}{p_0}\right)^{-4}\Theta(p_{max}-p)\Theta(p-p_0)\,. \tag{68}$$

We calculate $A(r)$ by imposing that the source luminosity in CR, $L_{CR}$, divided by the surface $S = 4\pi r^2$, namely

$$P_s = \frac{F_s}{S} \sim \frac{L_{CR}/c}{4\pi r^2}\,, \tag{69}$$

equals the CR pressure at the same distance $r$, defined as

$$P_{CR} = \frac{4\pi}{3}\int_{p_0}^{p_{max}} dp\, p^3 v(p) f(p,r) \simeq A(r)\frac{cp_0}{3}\ln\left(p_{max}/p_0\right), \tag{70}$$

where we have considered only relativistic CRs. By equating equations. (69) and (70) and considering the fact that in the relativistic regime $4\pi p^2 f(p)dp = f(E)dE$, in the energy domain one has

$$f(E,r) = \frac{L_{CR}}{\Lambda}\frac{E^{-2}}{4\pi r^2 c} \\ \approx 1.7\times 10^{-14} L_{44}\, E_{GeV}^{-2}\, r_{Mpc}^{-2}\ cm^{-3}GeV^{-1}\,, \tag{71}$$

where $\Lambda = \ln(E_{max}/E_0)/3 \approx 25$ with $E_{max} = cp_{max} \gg E_0 = cp_0$ and $L_{CR} = 10^{44} L_{44}$erg/s (energies are in GeV and distances in Mpc). It is reasonable to suppose that the parent galaxy is located in a region of the intergalactic medium (IGM) where the density of baryonic gas is $n_b = \Omega_b \rho_{cr}/m_p \approx 2.5\times 10^{-7}\,cm^{-3}$, with $\rho_{cr}$ being the critical mass density of the Universe and $\Omega_b = \rho_b/\rho_{cr} \simeq 0.022$ the ratio of the baryon density $\rho_b$ with respect to the critical one. We assume that a cosmological magnetic field permeates the IGM surrounding the source with a strength $B_0 = 10^{-13} B_{-13}$G and a correlation scale $\lambda_B \sim 10\,$Mpc [30, 31]. As in the galactic environment, on scales smaller than $\lambda_B$, the field can be considered as oriented along a given $\hat{z}$ direction and the associated Alfvén speed is $v_A = B_0/\sqrt{4\pi\Omega_b\rho_{cr}} \approx 44\, B_{-13}\,cm\,s^{-1}$. After the acceleration has taken place, the positively charged particles (assumed to be protons) propagate into the IGM surrounding the source. In this scenario, the electric current formed by the escaping CRs can induces the motion of the background plasma in the form of a return current in order to ensure local charge and current neutrality. As explained in Sec. 2.2.3, this situation is known to give rise to the non-resonant streaming instability that is potentially very important for CR transport [25, 143]. The purpose here is to study under which conditions the instability

takes place in the IGM close to the source and what are the consequences on CR propagation [121].

In the next sections we analyze the condition for the development of non-resonant modes of the streaming instability assuming a ballistic CRs propagation. We consider two possible scenarios: the first case in which the background magnetic field is extremely small so that we can assume three dimensional propagation (discussed in section 4.2) and the second case in which the background magnetic field is strong enough to imply a propagation one dimensional (discussed in section 4.3).

## 4.2 THREE DIMENSIONAL PROPAGATION

In the case where the background field is zero, or if the Larmor radius of the particles is $r_L \gg \lambda_B$ the situation can be described as a ballistic regime in a three-dimensional space. The current associated with CRs streaming away from their sources in the IGM is easily written as a function of the minimum energy $E$ of particles producing the current as

$$J_{CR} = ec \int_E^{E_{max}} dE' f(E', r) = \frac{eL_{CR} E^{-1}}{4\pi \Lambda r^2}\,, \tag{72}$$

where in the first equality we used the fact that particles are relativistic so that their streaming velocity is well approximated by the speed of light and in the last equality Eq. (71) has been used together with the condition $E \ll E_{max}$.

A current propagating in a plasma can give rise to instabilities of different types. To be in the CR current-driven regime which gives rise to the non-resonant streaming modes, the condition (149) has to be satisfied, which can be rewritten as

$$J_{CR} E > \frac{ceB_0^2}{4\pi}\,. \tag{73}$$

This condition, which is the standard one for the development of non-resonant modes of the streaming instability, as derived in Ref. [25], is equivalent to the requirement that the energy density of CRs is locally larger than the energy density in the form of pre-existing magnetic field, $B_0^2/4\pi$. It is important to note that for an injection spectrum $\propto E^{-2}$, this requirement becomes independent of $E$ and, using Eq. (72), it can be formulated as

$$r < r_{inst} = 3.7 \times 10^4 \frac{L_{44}^{1/2}}{B_{-13}} \mathrm{Mpc}\,, \tag{74}$$

therefore, obtaining a condition on the maximum distance from the source at which non resonant modes can be excited. When Eq. (74)

is satisfied unstable modes with a wavelength much smaller then the particles Larmor radius, grow with a rate given by Eq. (19). In particular, the fastest growing mode has a wavenumber

$$k_{max} = \frac{\xi}{r_{L,0}} = \frac{B_0 J_{CR}}{m_p n_p v_A^2}\,, \tag{75}$$

that reflects the equilibrium between magnetic tension and $J_{CR} \times \delta B$ force on the plasma, namely $k_{max} B_0 = \frac{4\pi}{c} J_{CR}$, being $\delta B$ the amplified magnetic field. The associated growth rate is derived from Eq. (19) with the substitution of the expression for $k_{max}$ and it reads

$$\gamma_{max} = k_{max} v_A = \sqrt{\frac{4\pi}{n_b m_p}} \frac{J_{CR}}{c}\,, \tag{76}$$

independent of the initial value of the local magnetic field $B_0$. The fact that the scale of the fastest growing modes $k_{max}^{-1}$ is much smaller than the Larmor radius of the particles dominating the current implies that these unstable modes have no direct influence on particle scattering but they contribute to the magnetic field amplification. This conclusion is however changed by the non-linear evolution of the modes which leads the amplification to reach a saturation level affecting particles' escape. To estimate this saturation level, a simple reasoning is followed. As long as the unstable modes develop on small scales, the current cannot be affected by the instability, hence one could treat the two as evolving separately. In this scenario, the force acting on a fluid element composing the background plasma is basically $\sim J_{CR}\delta B/c$. Thus, the equation for momentum conservation describing the motion of the fluid element is

$$\rho \frac{dv}{dt} \simeq \frac{1}{c} J_{CR} \delta B \exp\left(\gamma_{max} t\right)\,, \tag{77}$$

where in the last passage we have assumed that the amplification follows an exponential growth, i.e. $\delta B(t) = \delta B \exp\left(\gamma_{max} t\right)$. From the above equation one can approximate the velocity of the fluid element as $v \sim (\delta B(t) J_{CR})/(c\rho\gamma_{max})$, which upon integration, leads to an estimate of the mean fluid displacement as

$$\Delta x \sim \frac{\delta B(t) J_{CR}}{c\rho\gamma_{max}^2}\,. \tag{78}$$

The saturation of the instability happens if the displacement equals the Larmor radius of particles in the current as calculated in the amplified magnetic field, i.e. $\Delta x = E/(e\delta B)$. When this condition is fulfilled, the consequence is that scattering becomes efficient and the current is destroyed. This simple criterion returns a sort of equipartition between the magnetic energy density and the initial energy density carried by the CR current, or in mathematical terms

$$\frac{\delta B^2}{4\pi} \approx \frac{J_{CR} E}{ce} = \frac{L_{CR}}{4\pi \Lambda r^2 c}. \tag{79}$$

It is worth to stressing that in the case considered here we have $J_{CR} \propto E^{-1}$, hence the magnetic field saturates to a value which is independent of the energy of particles producing the current. In Ref.[144] the authors inferred a somewhat lower value of the saturation from their numerical simulations, as due to the non-linear increase of the wavelength of the fastest growing modes. Following such a prescription the saturation level of the magnetic field would be $\sim 10$ times smaller. The condition of equipartition expressed by Eq. (79) has been often assumed in the literature without justification, while here arises as a result of the physics of magnetic amplification itself.

Using Eq. (79) the strength of the saturated field can be written in terms of the distance $r$ from the source

$$\delta B(r) = 3.7 \times 10^{-9} L_{44}^{1/2} r_{\rm Mpc}^{-1} G\,, \tag{80}$$

expressing the rather strong amplification with respect to the background field.

Nevertheless, the previous estimation is valid only if the growth is fast enough so as to reach saturation in a fraction of the age of the universe, $t_0$. Numerical simulations of the instability, as done in Ref. [25] show that saturation can occur when $\gamma_{max}\tau \sim 5-10$. This latter condition reads $\gamma_{max} t_0 \gtrsim 5$ and translates into a second condition on the maximum distance from the source at which the instability can reach the saturation level, which is:

$$r < r_{growth} = 1.2 \times 10^4 L_{44}^{1/2} E_{\rm GeV}^{-1/2}\ {\rm Mpc}\,. \tag{81}$$

In the regions where both the two conditions expressed by Eqs. (74) and (81) are fulfilled, the magnetic field reaches the saturation level and can be estimated as in Eq. (80). Moreover, when this happens $\delta B \gg B_0$ and there is roughly equal power at all scales. In other words being $\delta B$ in Eq. (79) independent of energy $E$, it is reasonable to assume that particle propagation can be described as diffusive, with a diffusion coefficient corresponding to Bohm diffusion in the magnetic field $\delta B$.

Two important comments are in order. Bohm diffusion regime is generally found in the quasi-linear theory of wave particle interactions when $\delta B/B_0 < 1$ and $\delta B^2$ is roughly independent on the scale (see Ref. [15]). In the particular case of turbulence generated by Bell's instability, with $\delta B/B_0 \gg 1$ and scale invariant power spectrum, there is additional evidence that transport is governed by Bohm diffusion, as discussed in Ref. [145] and Ref. [143]). Thus, in the Bohm regime the particle diffusion coefficient can be written as:

$$D(E, r) = \frac{c\, r_L}{3} = 9 \times 10^{24} E_{\rm GeV}\ r_{\rm Mpc}\ L_{44}^{-1/2}\ {\rm cm^2 s^{-1}}\,, \tag{82}$$

where particle Larmor radius is calculated in the amplified magnetic field $\delta B$ expressed in Eq. (80).

An important conclusion about the effect of the non-resonant instability on particle motion during the escape from the source is that if the initial propagation is in the ballistic regime the accelerated particles can produce enough turbulence to make their motion diffusive. The diffusion time over a distance $r$ from the source can be estimated as

$$\tau_d(E, r) = \frac{r^2}{D(E, r)} \approx 3.3 \times 10^{16} r_{\rm Mpc}\, E_{\rm GeV}^{-1}\, L_{44}^{1/2}\, {\rm yr}\,, \tag{83}$$

from which follows that particles can be confined within a distance $r$ from the source for a time exceeding the age of the Universe if their energy fulfills the required condition:

$$E \lesssim E_{conf} = 2.6 \times 10^6\ r_{\rm Mpc}\, L_{44}^{1/2}\ {\rm GeV}\,. \tag{84}$$

A bit of attention needs to be paid on the assumption of ballistic regime, because when the motion becomes diffusive the initial assumption is no longer valid. However, what really matters is the electric current which is responsible for the excitation of the magnetic fluctuations. Indeed, such current remains the same in the diffusive regime, as we will show in the following.

For particles with energy $E > E_{conf}$ in Eq. (84), and assuming that energy losses are negligible, quasi-stationary diffusion can be described by the transport equation (8) where only the diffusion term is retained, which in spherical coordinates reads

$$\frac{1}{r^2}\frac{\partial}{\partial r}\left[r^2 D(p, r)\frac{\partial f}{\partial r}\right] = \frac{q(p)}{4\pi r^2}\delta(r), \tag{85}$$

where $q(p)$ is the injection rate of particles with momentum $p$ at $r = 0$. Here the advection term has been neglected since there is no bulk motion of the background plasma and the Alfvén speed is very small. The above equation can be integrated in $r$ and the solution for the differential density of CRs at distance $r$ from the source in the energy domain is

$$f(E, r) \approx \frac{L_{CR} E^{-2}}{8\pi r D(E, r)\Lambda}. \tag{86}$$

By exploiting the definition of diffusive regime, it is clear that the density of particles returned by Eq. (86) is larger than the density in the ballistic regime, Eq. (71). However, the current in the diffusive regime is calculated as

$$J_{CR}^{\rm diff} = -eED(E, r)\frac{\partial f}{\partial r} = e\frac{L_{CR} E^{-1}}{4\pi r^2 \Lambda}\,, \tag{87}$$

which is exactly the same current used in the case of ballistic CR propagation and reported in Eq. (72).

This is a very important and general result: the magnetic field, expressed in Eq. (80), is generated outside a CR source independently of the propagation mode of CRs, since it is only determined by the current and not by the absolute value of the CR density. Clearly the particles that are confined within a distance $r$ around the source do not contribute to the CR current at larger distances.

## 4.3 ONE DIMENSIONAL PROPAGATION

As mentioned before, the assumption of initial ballistic regime in a three-dimensional space is valid if the Larmor radius in the pre-existing magnetic field is much larger than the assumed coherence scale of the field, namely

$$E \gg 10^6 \mathrm{GeV}\, B_{-13} \lambda_{10}\,, \tag{88}$$

where $\lambda_{10} = \lambda_B/(10\,\mathrm{Mpc})$. However, when the background field is relatively strong, then the propagation of CRs from the source becomes intrinsically one dimensional, which implies that the differential number of particles in the energy domain can be written as

$$f(E,r) = \frac{Q(E)t}{\pi r_L^2 v t} = \frac{2Q(E)}{\pi R_c(E)^2 c}\,, \tag{89}$$

where $Q(E) = L_{CR} E^{-2}/\Lambda$ with $\Lambda$ defined in Sec. 4.1. In the above relation we used the fact that the mean velocity of the particles is $v = c/2$ for a distribution that is isotropic on a half plane and that particles spread in the direction perpendicular to the background field by a distance equal to $R_c(E) = \max(r_L(E), R_s)$ with $R_s$ the source size and $r_L(E)$ the Larmor radius of particles of given energy $E$. For a given source of size $R_s$ the particles with $r_L > R_s$ have $E_{\mathrm{GeV}} \gtrsim 9 \times 10^6 B_{-10}(R_s/100\mathrm{kpc})$. For energies larger than this the expression for the distribution function becomes

$$f(E,r) \approx 47 L_{44} E_{\mathrm{GeV}}^{-4} B_{-10}^2 \mathrm{cm}^{-3}\mathrm{GeV}^{-1}\,. \tag{90}$$

Like in the three dimensional regime, the electric current associated to those particles with energy $> E$ able to reach a given location is

$$J_{CR} \approx e\frac{c}{2}\int_E^{E_{max}} dE' f(E',r) = e\frac{EQ(E)}{\pi r_L^2(E)}\,, \tag{91}$$

for which the condition (73) translates into an energy condition

$$E < E_{inst} = 3.5 \times 10^9 L_{44}^{1/2}\,\mathrm{GeV}\,, \tag{92}$$

being independent of $B_0$. The value reached by the amplified magnetic field in the saturation phase is estimated from the equipartition

between the amplified magnetic energy density and the energy density carried by CRs as

$$\delta B \approx 0.7\, E_{GeV}^{-1}\, L_{44}^{1/2}\, B_{-10}\, G\,. \tag{93}$$

This apparently huge value of the magnetic field reflects the very large density of particles at low energies in the proximity of the source. Nevertheless, it is important to note that this value is normalized to the density of GeV particles, which only live in the proximity of the source, generating small scale fields to which high energy particles are almost insensitive. At Mpc scales instead, where only high energy particles can arrive, the field strength is much lower and the reason is shown below. The effect on particle motion by the excitement of the non-resonant streaming modes is to make the propagation diffusive and a reasonable estimate of the diffusion coefficient is still the Bohm approximation. Thus, one can write the Bohm-like diffusion coefficient as

$$D(E, r) = 4.8 \times 10^{16}\, E_{GeV}^{2}\, L_{44}^{-1/2} B_{-10}^{-1}\, cm^2 s^{-1}, \tag{94}$$

which leads to an estimate of the diffusion time:

$$\tau_{diff} = 6.2 \times 10^{24}\, E_{GeV}^{-2}\, L_{44}^{1/2}\, B_{-10}\, r_{Mpc}^{2}\, yr\,. \tag{95}$$

To reach a given distance $r$ from the source the diffusion time has to be shorter than the age of the universe, obtaining a condition on the maximum distance achievable from the escaping particles

$$r_{conf} \approx 0.5 \left(\frac{E}{10^7\, GeV}\right) L_{44}^{-1/4}\, B_{-10}^{-1/2}\, Mpc. \tag{96}$$

Following the usual procedure, one can use Eq. (76) in order to calculate the growth rate of the fastest modes

$$\gamma_{max} = 1.9 \times 10^{18} L_{44} B_{-10}^{2} E_{GeV}^{-3}\, s^{-1}, \tag{97}$$

and imposing the condition that $\gamma_{max} t_0 > 5$ another condition on particle energy is obtained

$$E \lesssim E_{growth} \approx 5.3 \times 10^{11}\, L_{44}^{1/3} B_{-10}^{2/3}\, GeV. \tag{98}$$

It is currently not known if the particles' escape occurs in one or in the other regime since only limits exist on the cosmological magnetic field, as for instance those obtained from Faraday rotation measures [29] where the limits are of the order of $\leqslant$ nG and are model dependent. There are also numerical simulations of large scale structure formation in the presence of a background magnetic field that find value in voids typically of the order of $10^{-13}$ G [146]. Independently of what kind of propagation regime sets up, the electric current formed by the escaping CRs in the proximity of their source is

able to give rise to the non-resonant streaming instability and one of the most important effect of particle propagation is their confinement in the near-source region, as happen for CRs in Galactic sources. For both the two regimes there are particles which are not able to escape from the near-source region in a time smaller than the age of the Universe. In the next section we will estimate this confinement energy.

## 4.4 CONFINEMENT ENERGY

We start discussing the confinement energy $E_{cut}$ in the three dimensional regime. In this regime the confinement energy found in Eq. (84) is somewhat ambiguous since it depends on the distance $r$. In order to find the highest energy up to which CRs are confined to the source vicinity, all the following three conditions need to be satisfied simultaneously: (1) the existence of fast growing modes Eq. (74), (2) the growth rate faster than the expansion rate of the universe Eq. (81) and (3) the diffusion time over a distance $r$ from the source larger than the Age of the universe Eq. (84). The first condition yields a limit on the distance from the source easy to satisfy (unless the ballistic regime holds) while the other two conditions lead to the constraint

$$E_{cut} \approx 10^7 L_{44}^{2/3}\,\mathrm{GeV}\,. \tag{99}$$

The particles with energies less than $E_{cut}$ are confined within a distance from the source equal to

$$r_{conf} \approx 3.8 L_{44}^{1/6}\,\mathrm{Mpc}. \tag{100}$$

Within such a distance the magnetic field is given by Eq. (80) and larger than $\delta B(r_{conf}) \approx 9.6 \times 10^{-10} L_{44}^{1/3}\,\mathrm{G}$. It is noteworthy that both the size of the confinement region and the magnetic field depend weakly upon the CR luminosity of the source, respectively as $L_{CR}^{1/6}$ and $L_{CR}^{1/3}$.

In the case of three one dimensional regime the intersection of all the three conditions listed above leads to conclude that particles with energies

$$E < E_{cut} = 2.2 \times 10^8 L_{44}^{1/4} B_{-10}^{1/2} \lambda_{10}\,\mathrm{GeV} \tag{101}$$

can be confined within a distance from the source

$$r_{conf} \approx 10\,\lambda_{10}\,\mathrm{Mpc}\,. \tag{102}$$

In this scenario the amplified magnetic field at such distance can be estimated using the equipartition argument and substituting the expression for $E_{cut}$ into Eq. (93) one finds

$$\delta B \approx 3 \times 10^{-9} L_{44}^{1/4}\, B_{-10}^{1/2}\, \lambda_{10}^{-1}\mathrm{G}\,. \tag{103}$$

Both the results illustrated in the two different regimes are only sensitive to the CR current, and hence insensitive to whether particle propagation is ballistic or diffusive. Hence one can conclude that magnetic fields at the level of 0.1 - 1 nG must be present in regions of a few Mpc around the sources of UHECRs. The physical prescription adopted here leads to estimating the strength of the self-generated magnetic field $\delta B$ at the level of equipartition with the energy in the form of escaping cosmic rays, independent of the value of the pre-existing field $B_0$. A weak dependence on $B_0$ was instead found for the saturation level in [144], which in our case would lead to $\delta B$ about $\sim 10$ times smaller for small values of $B_0$, thereby reducing the energy below which CRs are confined in the source proximity. Understanding the dynamics of the magnetic field amplification and saturation is clearly very important. One could test the amplification mechanism in the case of supernova remnant shocks: in this case the saturation criterion used here translates to $\delta B \approx \sqrt{4\pi w_{CR} v_s/c}$, with $v_s$ the velocity of the supernova blast wave and $w_{CR}$ is the energy density in accelerated particles. Applying this criterion, we obtain an estimate of the magnetic field which is in good agreement with that measured in young galactic SNRs [17]. On the other hand, due to the relatively small value of $\delta B/B_0$, the saturation provided by [144] would return a value of $\delta B$ only a factor $\sim 2$ smaller, too small a difference to discriminate between the two estimates. The testing is then left to numerical experiments studying the propagation of a current of energetic particles in a low density, low magnetic field plasma: hybrid simulations with this aim are currently ongoing. It is currently not known whether the confinement phenomenon occurs in one or the other regime since only limits exist on cosmological magnetic fields: upper limits can be obtained from Faraday rotation measures [29] but these limits are rather weak ($\lesssim$ nG) and model dependent. A lower limit can be found from gamma ray observations of distant TeV sources [147, 148] and these limits are typically at the level $B_0 \gtrsim 10^{-17}$ G. Numerical simulations of large scale structure formation in the presence of background magnetic fields typically find $\sim 10^{-13}$ Gauss magnetic fields in voids [146] (although see Ref. [149] for different conclusions). One of the consequences is that the spectrum of CRs leaving these sources and eventually reaching the Earth must have a low energy cutoff at an energy $E_{cut}$. It is important to note that this kind of cut-off has been often postulated in the literature in order to avoid some phenomenological complications that affect models for the origin of UHECRs, as discussed in Ch. 1 in Sec. 1.4.1. For instance, in the dip model [33, 34] a low energy cutoff is required to describe in an appropriate way the transition from Galactic to extragalactic CRs. In general this feature is usually explained as due to the existence of a magnetic horizon if the propagation of UHECRs is diffusive in the lower energy part of the spectrum, as done in Ref. [36]. A similar

low energy suppression of the CR flux is required by models with a mixed composition [35]. In the calculations illustrated above, the presence of nuclei is readily accounted for, provided the current is still produced by protons (assumed to be the most abundant specie). In this case, the value of $E_{cut}$ is simply shifted to $Z$ times higher energy for a nucleus of charge $Z$.

## 4.5 CONCLUSIONS

In this Chapter we studied under what conditions the electric current carrying by the escaping CRs gives rise to the non-resonant streaming instability, which leads to particle self-confinement around Extra-Galactic sources. The details of this process depend on the strength of the pre-existing magnetic field $B_0$. In case of $B_0 \lesssim 10^{-10}\,\mathrm{G}$ and in the absence of non-linear phenomena we assumed that CRs propagate in approximately straight lines. In this scenario we found that the development of a Bell-like instability induces particles with energy $\lesssim 10^7 L_{44}^{2/3}$GeV to be confined inside a distance of $\approx 3.8 L_{44}^{1/6}$ Mpc from the source for times exceeding the age of the Universe, thereby introducing a low-energy cutoff at such energy in the spectrum of CRs reaching the Earth. In case of larger $B_0$ the gyration radius of the particles can be smaller than the coherence scale of the field, and in this case CR propagation develops in basically one spatial dimension. For a coherence scale of 10 Mpc we found that CRs are confined in the source proximity for energies $E \lesssim 2 \times 10^8 L_{44}^{1/4} B_{-10}^{1/2}\ \lambda_{10}$GeV. It is worth noticing that the phenomenon of CR confinement might have profound implications for the description of the transition region between Galactic and Extra-Galactic CRs [33–35]. It is rather remarkable that the cutoff obtained here as due to self-trapping is in the same range of values that have been invoked in the literature based upon phenomenological considerations.

# 5 CONCLUSIONS

In this work, we investigate the self-confinement due to the generation of plasma instabilities when non-linear effects in the CR propagation around their sources are taken into account. This study has been pursued in both galactic and extra-galactic environments. The phenomenon of self-generation of magnetic waves is extremely important in CR physics, as demonstrated by the non-linear DSA theory where such effect can allow particles to reach the extreme energy of $\sim$ PeV. Such conclusion is also accompanied by observational consequences [1, 5], such as spatially thin rims of enhanced X-ray synchrotron emission [17]. Near CR sources one may expect that the density gradient of particles may be large enough to affect the environment in which CRs propagate. In fact, within a distance from the parent source of the order of the coherence scale of the background magnetic field, CR propagation is dominated by non-linear effects if the presence of neutral particles is negligible. A magnetic turbulence is self-generated by the interaction of energetic particles with magnetized ISM, via the excitation of CR streaming instability. Such phenomena can in turn affect CR transport, in general forcing their confinement in near-source regions to be longer than naively expected assuming the average galactic magnetic turbulence.

In Ch. 3, we considered particle self-confinement around Galactic sources. We solved numerically the non-linear CR transport equation together with the self-generated wave equation in a region immediately outside the source, assumed to be a typical SNR with a total energy of $10^{51}$erg and a CR acceleration efficiency of 20%. On scales of order the coherence scale of the Galactic magnetic field, i.e. $L_c \sim 100\,\mathrm{pc}$, the problem can be considered as one dimensional. At larger distances diffusion becomes three dimensional and the density of CRs contributed by the individual source quickly drops below the Galactic average (assumed to be the one observed at the Earth). The gradient in the spatial distribution of CRs in the near source region is responsible for generation of Alfvén waves that in turn scatter the particles, thereby increasing their residence time in the near source region. This phenomenon was previously studied in Ref. [10, 11] in connection with the problem of the interaction of CRs with molecular clouds in the near source region, and in Ref. [9], who studied the consequences of impulsive release of CRs by a source embedded in a fully ionized medium. We showed that in this scenario, the grammage traversed by CRs with energies up to a few TeV might be affected by the self-induced confinement close to the sources, to an

extent that depends on the number density of neutral hydrogen in the Galactic disc. In the absence of neutrals and with gas density of $\sim 0.45\,\mathrm{cm}^{-3}$, the grammage accumulated in the near source region is comparable (within a factor of few) with the one that is usually inferred from the measured B/C ratio. In spite of such conclusion the time spent by CRs in the near source region is still negligible compared with the total escaping time from the Galaxy, the reason being the fact that the density near the sources is much larger than the average density felt by CRs while diffusing in the Halo/disc system. The fact that the residence time in the near source region remains relatively short compared with the overall residence time in the Galaxy implies that the use of radioactive isotopes present in CRs to determine the residence time in the Galaxy is not affected by the propagation around the sources. A possible exception could be the short living isotopes, like 14C (Carbonio 14) whose half-life is only 5700 yr. On the other hand, when neutrals are present, as expected for the standard interstellar medium, the grammage accumulated in the source vicinity becomes negligible. Nevertheless, it is worth noticing that the strength of ion-neutral friction, responsible for the wave damping could be different from what we have assumed. This mainly because in the warm-hot interstellar medium most of the neutral gas is expected to be in the form of He atoms, while we assumed that the neutral density is only due to Hydrogen atoms. The cross section for H-He charge exchange is much smaller than for H-H, therefore it seems plausible to assume that most damping is actually due to a residual fraction of neutral H that may be left. Here we made an attempt to bracket the importance of IND as due to all these uncertainties.

At energies $\gtrsim 1\,\mathrm{TeV}$ the grammage traversed by CRs can reasonably be expected to be heavily affected by the in-source contribution, due to the fact that CRs are trapped in the downstream region of the SN shock before escaping, as already proposed in Ref. [20] (where the confinement time is assumed to be $\sim 10^4$ years). This is probably not the case at very high energies, around the knee, since such CRs are expected to escape from the source through the upstream region at earlier times [150]. The general picture that arises from these considerations is that at all energies the observed grammage might be affected by either non-linear propagation in the near-source region, which depends on the level of ionization of the ambient medium, or transport inside the source, thereby making the translation of the grammage (from B/C) to a confinement time in the Galaxy more complex than what it is usually assumed. More specifically, both the normalization and the slope of the diffusion coefficient inferred from B/C ratio could reflect more a combination of Galactic propagation plus the two phenomena described above rather than being the result

of the Galactic transport only. These results have been published in *Physical Review D* in 2016, see Ref. [117].

There is at least one possible signature which relates the CR residence time in the near source region with experimental data: the formation of extended halos of gamma ray emission from $\pi^0$ decay in a region of size $\sim L_c$ around CR sources. The emission from a single halo is too faint to be detected with the current gamma-ray telescopes. However, the sum of these halos over the whole CR source population can produce a non negligible contribution to the diffuse gamma-ray emissivity from the Galactic disc. We calculated the $\gamma$-ray emission of these halos for energy $E_\gamma$ in the range $[1 - 10^3]$ GeV, and considering two types of ISM: fully ionized medium and partially ionized medium with neutral fraction $\sim 0.1$. We compared our results with the diffuse Galactic $\gamma$-ray emission detected by *Fermi*-LAT and analyzed in Ref. [88, 89]. We found that in case of fully ionized medium the resulting $\gamma$-ray emission saturates the observed one leaving little room for other diffuse components. This contradictory result is not surprising because we do not expect all SNRs to explode in a fully ionized ISM. In the partially ionized medium, on the contrary, ion-neutral damping reduces the CR confinement time and the $\gamma$-ray emission contribute to roughly 1% of the observed one, a contribution which increases for energies $E_\gamma \sim 100$ GeV. We warn the reader that in case one considers smaller acceleration efficiency ($\leqslant 10\%$) and/or softer spectra steeper than -4, the non-linear effects on both the grammage and the gamma-ray emission are expected to be negligible.

One of the future developments of this work can be to improve the model to provide a better prediction on the $\gamma$-ray emission in the energy range observed by *Fermi*-LAT, but also to estimate the same emission in the range of the future Cherenkov Telescope Array. Another possible signature of the self-confinement process is the production of enhanced inverse Compton scattering and Synchrotron emission from electrons propagating in the protons self-generated turbulence. Hence, the calculation of this radiation can also provide new pieces of information.

In Ch. 4, we considered particle self-confinement around Extra-Galactic sources. The escaping CRs form an electric current to which the background plasma reacts, by generating a return current that in turn leads to the development of small scale instabilities. The growth of such instabilities leads to large turbulent magnetic fields and to enhanced particles' scattering. The details of this process depend on the strength of the pre-existing magnetic field $B_0$: if it is very weak (say $\lesssim 10^{-10}$ G) then, in the absence of non-linear phenomena, CRs will try to propagate in approximately straight lines. The resulting electric current leads to the development of a Bell-like instability, that modifies the propagation of particles to be diffusive:

particles with energy $\lesssim 10^7 L_{44}^{2/3}$GeV are confined inside a distance of $\approx 3.8 L_{44}^{1/6}$ Mpc from the source for times exceeding the age of the Universe, thereby introducing a low-energy cutoff at such energy in the spectrum of CRs reaching the Earth. Since the confinement distance is weakly dependent on the source luminosity, we conclude that a region with $\sim$ nG fields should be present around any sufficiently powerful CR source. If larger background magnetic fields are present around the source, the gyration radius of the particles can be smaller than the coherence scale of the field, and in this case CR propagation develops in basically one spatial dimension. For a coherence scale of 10 Mpc, CRs are confined in the source proximity for energies $E \lesssim 2 \times 10^8 L_{44}^{1/4} B_{-10}^{1/2} \lambda_{10}$GeV. The phenomenon of CR confinement illustrated here has profound implications for the description of the transition region between Galactic and Extra-Galactic CRs [33–35]. It is rather remarkable that the cutoff obtained here as due to self-trapping is in the same range of values that have been invoked in the literature based upon phenomenological considerations. This last result has been also published in *Physical Review Letter* in 2015, see Ref. [121].

# A DERIVATION OF THE COSMIC RAY TRANSPORT EQUATION

In this Appendix we will describe the procedure to obtain the CR transport equation, in particular following the treatment given in Ref. [104, 105].

The magnetic irregularities, here assumed to be made by Alfvén waves, define a frame of reference, which for convenience it is called the wave frame and denoted with $'$, propagating at the local Alfvén speed which is $\ll c$. In this frame the pitch angle scattering is elastic, therefore there is conservation of particle energy and momentum. However, this frame is in general non-inertial because the local Alfvén speed can vary with space and time and it is no trivial to write an equation of conservation for the distribution function $f(\boldsymbol{x}, \boldsymbol{p}, t)$.

The starting point is to write the time evolution of the distribution function $f(\boldsymbol{x}, \boldsymbol{p}, t)$ in the inertial rest frame which coincides with the observer's (Earth) frame, i.e.

$$\frac{\partial f}{\partial t} + \boldsymbol{v} \cdot \nabla_{\boldsymbol{x}} f + \frac{d\boldsymbol{p}}{dt} \cdot \nabla_{\boldsymbol{p}} f = 0 \tag{104}$$

where $d\boldsymbol{p}/dt$ is the force acting on particles which in this case is the Lorentz force $q(\boldsymbol{E} + \boldsymbol{v} \times \boldsymbol{B}/c)$. The equation (104) is the collisionless Vlasov equation and expresses the conservation of particle number in the six-dimensional phase space $(\boldsymbol{x}, \boldsymbol{p})$, i.e. $df(\boldsymbol{x}, \boldsymbol{p}, t)/dt = 0$ which is nothing more than the Liouville's theorem. Since CRs are mainly composed by protons $f$ is taken as referring to the accelerated proton distribution.

The rest frame presents a problem because there is no conservation of particle energy as instead it is the case in the wave frame. Thus, it is more convenient to introduce a set of mixed coordinates defined as follow: the time and the spatial coordinates are measured in the inertial rest frame, while the momentum coordinate is measured in the wave (primed) frame, i.e. $(\boldsymbol{x}, \boldsymbol{p}', t)$.

The passage from the rest to the mixed frame is determined by the Lorentz transformation of particle momentum $\boldsymbol{p}'$. The velocity of the wave frame with respect to the rest frame is indicated with $\boldsymbol{u}$. As mentioned before, the local Alfvén speed can vary with space and time but in the following it is assumed that $\boldsymbol{u}$ can vary only with space. Moreover, it holds that $|\boldsymbol{u}| = u \ll c$, so all the quantities are approximated to first order in $u/c$.

In the non-relativistic limit the Lorentz transformation of the momentum is

$$\boldsymbol{p}' = \boldsymbol{p} - m_p \gamma' \boldsymbol{u}\,, \tag{105}$$

where $\gamma' = 1/\sqrt{1-(v'/c)^2}$ is the particle Lorentz factor in the wave frame and $m_p$ is the proton rest mass.

The next step in deriving the CR transport equation is to transform the Vlasov equation (104) from the inertial rest frame to the mixed coordinate frame. Taking advantage of the fact that $f$ is a Lorentz invariant, in these mixed coordinates the distribution function becomes

$$\begin{aligned} f(\boldsymbol{x}, \boldsymbol{p}, t) &= f'(\boldsymbol{x}, \boldsymbol{p}', t) \\ &= f'(\boldsymbol{x}, \boldsymbol{p}' = \boldsymbol{p}, t) - m_p \gamma' \boldsymbol{u} \cdot \nabla_{\boldsymbol{p}'} f'(\boldsymbol{x}, \boldsymbol{p}' = \boldsymbol{p}, t)\,. \end{aligned} \tag{106}$$

The other transformation regards the partial derivatives. For the time partial derivative $\partial/\partial t$ one obtains

$$\begin{aligned} \frac{\partial}{\partial t} &\longrightarrow \frac{\partial}{\partial t} + \sum_{i=x,y,z} \frac{\partial p_i'}{\partial t} \frac{\partial}{\partial p_i'} \\ &= \frac{\partial}{\partial t} + \sum_{i=x,y,z} \frac{\partial (p_i - m_p \gamma' u_i)}{\partial t} \frac{\partial}{\partial p_i'} = \frac{\partial}{\partial t}\,, \end{aligned} \tag{107}$$

where it has been used the assumption that the velocity of scattering centers $\boldsymbol{u}$ depends only on space and that $\boldsymbol{p}$ is a time independent variable. The method adopted to evaluate the spatial and momentum derivatives is the same and their expressions are listed below

$$\frac{\partial}{\partial x_i} \longrightarrow \frac{\partial}{\partial x_i} - m_p \gamma' \frac{\partial u_j}{\partial x_i} \frac{\partial}{\partial p_j'}\,, \tag{108}$$

$$\frac{\partial}{\partial p_i} \longrightarrow \delta_{ij} \frac{\partial}{\partial p_i'} - m_p u_j \frac{\partial \gamma}{\partial p_i} \frac{\partial}{\partial p_j'}\,, \tag{109}$$

where $\delta_{ij}$ is the Kronecker delta.

At this point it is possible to substitute the expression for $f$ given in Eq. (106) in term of $f'$ into the Vlasov equation (104) neglecting those terms of the order $\mathcal{O}(u^2/c^2)$. As a result, the transformed Vlasov equation is

$$\frac{\partial f'}{\partial t} + (\boldsymbol{v}' + \boldsymbol{u}) \cdot \nabla_{\boldsymbol{x}} f' - (\boldsymbol{p}' \cdot \nabla_{\boldsymbol{x}}) \boldsymbol{u} \cdot \nabla_{\boldsymbol{p}'} f' = -\nabla_{\boldsymbol{p}'} \cdot \left[ f' \boldsymbol{F}' \right]\,, \tag{110}$$

where $\boldsymbol{F}' = e(\boldsymbol{E}' + \boldsymbol{v}' \times \boldsymbol{B}'/c)$ is the Lorentz force acting on particles written in the wave frame and $e$ is the electric charge of a proton. Assuming that in the rest frame the plasma is a perfect conductor, a reasonable statement for an astrophysical plasma, which means that the Ohm's law is $\boldsymbol{E} = -\boldsymbol{u} \times \boldsymbol{B}/c$ and considering the non-relativistic limit, the transformed electromagnetic fields are

$$\boldsymbol{E}' \simeq \boldsymbol{E} + \frac{\boldsymbol{u} \times \boldsymbol{B}}{c} = 0\,, \tag{111}$$

$$\boldsymbol{B}' \simeq \boldsymbol{B} - \frac{\boldsymbol{u} \times \boldsymbol{E}}{c} = \boldsymbol{B} + \frac{\boldsymbol{u} \times (\boldsymbol{u} \times \boldsymbol{B})}{c^2} \simeq \boldsymbol{B}\,. \tag{112}$$

The fact that the electric field vanishes demonstrates the conservation of particle energy in the wave frame. Moreover, the magnetic field is the same of that in the inertial rest frame $\boldsymbol{B} = \boldsymbol{B}_0 + \delta\boldsymbol{B}$ at first order in $u/c$. Hence, the dominant term of the force $\boldsymbol{F}'$ is $\boldsymbol{v}' \times \boldsymbol{B}_0/c$ and particle motion in the plane transverse to $\boldsymbol{B}_0$ is a uniform circular motion with the associated Larmor radius being $r_L = pc/(eB_0)$. For typical values of $B_0$ presumed both in the galactic case ($\sim \mu G$) and in the extra-galactic case ($\leqslant$ nG), it can be assumed that $r_L(p)$ is smaller than all the typical length scales relevant for particle diffusion. This ensures that $f'$ is nearly independent on the gyration phase $\phi$ while depends only on $\boldsymbol{x}, \mu', p', t$ where $\mu' = \cos\theta'$ is the cosine of the pitch angle defined in the wave frame. Thus, the modified Vlasov Equation (110) can be averaged on $\phi'$.

The detailed calculation regarding on how to obtain the averaging of each term of Eq. (110) is performed in Ref. [90, 105]. Here we report the result of the averaged modified Vlasov equation

$$\begin{aligned}
&\frac{\partial f'}{\partial t} + (\mu' v' \boldsymbol{n} + \boldsymbol{u}) \cdot \nabla_{\boldsymbol{x}} f' + \\
&\quad - \left\{ \frac{1-\mu'^2}{2} (\nabla_{\boldsymbol{x}} \cdot \boldsymbol{u}) + \frac{3\mu'^2 - 1}{2} (\boldsymbol{n} \cdot \nabla_{\boldsymbol{x}})(\boldsymbol{n} \cdot \boldsymbol{u}) \right\} p' \frac{\partial f'}{\partial p'} \\
&\quad + \frac{1-\mu'^2}{2} v' (\nabla_{\boldsymbol{x}} \cdot \boldsymbol{n}) \frac{\partial f'}{\partial \mu'} = \frac{\partial}{\partial \mu'} \left\{ \frac{1-\mu'^2}{2} \nu'_{res} \frac{\partial f'}{\partial \mu'} \right\} ,
\end{aligned} \tag{113}$$

where it has been introduced a unit vector $\boldsymbol{n} = \boldsymbol{n}(\boldsymbol{x})$, directed along the local magnetic field. The term on the rhs of the equation derives from averaging over $\phi'$ of the term $\langle -\nabla_{\boldsymbol{p}'} \cdot [f' \boldsymbol{F}'] \rangle_{\phi'}$. Indeed, the dominant term of the Lorentz force vanishes $\langle \boldsymbol{v}' \times \boldsymbol{B}_0/c \rangle_{\phi'} = 0$, while the only term that remains is the pitch angle scattering off Alfvén waves. The scattering frequency $\nu'_{res} = \nu'_{res}(p', \mu')$ has been calculated in Sec. 2.1 where it is reported in Eq. (9).

In the wave frame it is reasonable to expect that the scattering process is sufficiently strong to make the distribution function almost isotropic on spatial scales larger than the mean free path $v'/\nu'_{res}$. Thus, $f'$ can be expanded in power of the ratio of the mean free path $v'/\nu'_{res}$ to the scale length as

$$f'(\boldsymbol{x}, p', \mu', t) = f'_0 + f'_1 + f'_2 , \tag{114}$$

where

$$f'_n = \mathcal{O}\left( \frac{v'}{\nu'_{res}} \left| \frac{\partial}{\partial \boldsymbol{x}} \right| \right)^n f'_0 . \tag{115}$$

These terms represent growing orders of anisotropy, for instance the zero order term $f'_0$ is the isotropic part of $f'$, being independent on $\mu'$. It is important to remember that this assumption holds in the wave frame where the scattering is elastic, as mentioned before. A this point the approximated $f'$ can be inserted into Eq. (113) obtaining an

equation for each order. The zeroth order term satisfies the condition

$$\frac{\partial}{\partial\mu'}\left\{\frac{1-\mu'^2}{2}\nu'_{res}\frac{\partial f'_0}{\partial\mu'}\right\}=0\,, \tag{116}$$

which confirms that $f'_0$ is isotropic, after requiring that it is not singular at $\mu'=\pm1$. At first order the equation for $f'_1$ shows a dependence from $f'_0$ which is

$$\mu'\nu'(\boldsymbol{n}\cdot\nabla_{\boldsymbol{x}})f'_0=\frac{\partial}{\partial\mu'}\left\{\frac{1-\mu'^2}{2}\nu'_{res}\frac{\partial f'_1}{\partial\mu'}\right\}\,. \tag{117}$$

This equation can be integrated over $\mu'$ and one gets

$$\frac{\partial f'_1}{\partial\mu'}=-\frac{\nu'}{\nu'_{res}}(\boldsymbol{n}\cdot\nabla_{\boldsymbol{x}})f'_0\,. \tag{118}$$

Finally, the second and last order is

$$\begin{aligned}&\frac{\partial f'_0}{\partial t}+(\boldsymbol{u}\cdot\nabla_{\boldsymbol{x}})f'_0+\mu'\nu'(\boldsymbol{n}\cdot\nabla_{\boldsymbol{x}})f'_1+\\&\quad-\left\{\frac{1-\mu'^2}{2}\nabla_{\boldsymbol{x}}\cdot\boldsymbol{u}+\frac{3\mu'^2-1}{2}(\boldsymbol{n}\cdot\nabla_{\boldsymbol{x}})(\boldsymbol{n}\cdot\boldsymbol{u})\right\}p'\frac{\partial f'_0}{\partial p'}+\\&\quad+\frac{1-\mu'^2}{2}\nu'(\nabla_{\boldsymbol{x}}\cdot\boldsymbol{n})\frac{\partial f'_1}{\partial\mu'}=\frac{\partial}{\partial\mu'}\left\{\frac{1-\mu'^2}{2}\nu'_{res}\frac{\partial f'_2}{\partial\mu'}\right\}\,,\end{aligned} \tag{119}$$

where it appears a dependence of $f'_2$ from $f'_1$ and $f'_0$.
An average over $\mu'$ allows to eliminate the dependence from $f'_2$ of the above equation and the solution is

$$\frac{\partial f'_0}{\partial t}+(\boldsymbol{u}\cdot\nabla_{\boldsymbol{x}})f'_0-\nabla_{\boldsymbol{x}}\cdot[\boldsymbol{n}D_{\parallel}(\boldsymbol{n}\cdot\nabla_{\boldsymbol{x}})f'_0]=\frac{1}{3}(\nabla_{\boldsymbol{x}}\cdot\boldsymbol{u})p'\frac{\partial f'_0}{\partial p'}\,. \tag{120}$$

In obtaining Eq. (120) it has been used the following relation

$$\nu'\langle\mu'(\boldsymbol{n}\cdot\nabla_{\boldsymbol{x}})f'_1\rangle_{\mu'}=\nu'\left\langle\frac{1-\mu'^2}{2}\frac{\partial f'_1}{\partial\mu'}\right\rangle_{\mu'}=-D_{\parallel}(\boldsymbol{n}\cdot\nabla_{\boldsymbol{x}})f'_0\,, \tag{121}$$

where the spatial diffusion coefficient is defined as

$$D_{\parallel}(\boldsymbol{x},p',t)=\frac{\nu'^2}{2}\left\langle\frac{1-\mu'^2}{\nu'_{res}}\right\rangle_{\mu'} \tag{122}$$

and the subscript $\parallel$ indicates the direction parallel to the ordered magnetic field. Eq.(120) is the CR transport equation, also referred to as convection-diffusion equation.

# B DERIVATION OF THE GROWTH RATE FOR THE STREAMING INSTABILITY

The standard approach to calculate the growth rate of unstable modes in plasma physics (see for a detailed discussion Ref. [126]) is to linearized the Vlasvov equation together with the Maxwell's equations for the electromagnetic field, which is also referred to as the kinetic linear theory of plasma instabilities. At the end of this procedure a dispersion relation is obtained where a relation between the wave frequency $\omega$ and the wave vector $\boldsymbol{k}$ is established. The wave frequency has in general a complex value, so that we can write $\omega = \omega_R + i\omega_I$. The unstable modes correspond to those waves which have $\omega_I < 0$. In Ref. [151] the authors calculate the growth rate of the streaming instability in the upstream region of a shock generated by the blast wave of a SNR using this kinetic approach, and we refer to that paper for a detailed discussion of the method. Here we apply the same procedure considering accelerated particles which stream along the background field $\boldsymbol{B}_0$ during their propagation in the source vicinity.

The general dispersion relation of electromagnetic waves with $\boldsymbol{k} \parallel \boldsymbol{B}_0$ (circularly polarized) is of the form

$$\frac{c^2 k^2}{\omega^2} = 1 + \sum_\alpha \chi_\alpha \,, \tag{123}$$

where the susceptivity $\chi_\alpha$ is defined as

$$\chi_\alpha = \frac{4\pi^2 e^2}{\omega} \int dp\, p^2 \int_{-1}^{1} d\mu\, \nu(p)\, \frac{1-\mu^2}{\omega - k\nu\mu \pm \Omega_\alpha} \times \left\{ \frac{\partial f_\alpha}{\partial p} + \left( \frac{k\nu}{\omega} - \mu \right) \frac{1}{p} \frac{\partial f_\alpha}{\partial \mu} \right\} . \tag{124}$$

The index $\alpha$ indicates the particle species composing the plasma which are protons ($\alpha = p$) and electrons ($\alpha = e$) of the ISM, also defined as the background plasma, and CR protons ($\alpha = CR$). For the background plasma $\Omega_\alpha \approx \Omega^*_\alpha$ the non-relativistic cyclotron frequency $q_\alpha B_0/(m_\alpha c)$.

Let $n_p$ and $n_e$ be the number density of protons and electrons in the background plasma. Let us assume that CRs (protons) propagate as a beam-like in the background plasma following a power-law distribution in momentum space. The divergence of CR beam is neglected and as well as CRs escape from the source along the direction of $\boldsymbol{B}_0$. Another important assumption is that CRs are diluted with

respect to background plasma, which means $n_{CR} \ll n_p$. At the same time, the plasma reacts against the CR electric current via the generation of a return current. Imposing quasi-neutrality and no net current, one obtains the following conditions:

- quasi-neutrality $\longrightarrow n_p + n_{CR} = n_e \longrightarrow n_e \approx n_p$,
- zero total current $\longrightarrow J_{CR} + J_p + J_e = 0 \rightarrow n_p v_p + n_{CR} c = n_e v_e$. Due to the larger inertia of the background protons with respect to the background electrons it is reasonable to assume that the return current is made by electrons, therefore $n_{CR} c \approx n_e v_e \approx n_p v_e$.

The initial distribution functions for the background plasma are:

$$f_p^0(p) = \frac{n_p}{4\pi p^2}\delta(p)\,, \tag{125}$$

$$f_e^0(p,\mu) = \frac{n_e}{2\pi p^2}\delta(p - m_e v_e)\delta(\mu - 1)\,, \tag{126}$$

assuming an initial temperature $T = 0$. For the accelerated protons one has

$$f_{CR}^0(p,\mu) = \frac{n_{CR}}{2\pi} g(p)\delta(\mu - 1)\,, \tag{127}$$

where $g(p)$ is a power-law distribution with the condition that the normalization is $\int_0^\infty dp\, p^2\, g(p) = 1$.

The proton susceptivity $\chi_p$ requires to know $\partial f_p^0/\partial p$ and $\partial f_p^0/\partial \mu$:

$$\frac{\partial f_p^0}{\partial p} = \frac{n_p}{4\pi p^2}\left(-\frac{2}{p}\delta(p) + \frac{d\delta(p)}{dp}\right)\,, \tag{128}$$

$$\frac{\partial f_p^0}{\partial \mu} = 0\,. \tag{129}$$

Before proceeding into the calculation one has to remember the a property of the delta function is $\int f(x)\,\delta'(x)\,dx = -\int f'(x)\,\delta(x)\,dx = -f'(0)$. After some algebraic passages the solution turns out to be

$$\chi_p = -\frac{4\pi e^2 n_p}{m_p}\frac{1}{\omega(\omega \pm \Omega_p^*)}\,. \tag{130}$$

The regime under investigation is the low-frequency approximation, which means $\omega \ll \Omega_p^* \ll |\Omega_e^*|$ where the susceptivity becomes

$$\chi_p \simeq \mp\frac{4\pi e^2 n_p}{\omega m_p}\frac{1}{\Omega_p^*}\left(1 \mp \frac{\omega}{\Omega_p^*}\right) = \mp\left(\frac{c}{v_A}\right)^2 \frac{\Omega_p^*}{\omega}\left(1 \mp \frac{\omega}{\Omega_p^*}\right)\,. \tag{131}$$

For the background electrons the procedure is the same and the susceptivity due to left-handed polarized waves reads

$$\chi_e = -\frac{4\pi e^2 n_e}{\omega^2 m_e}\frac{\omega - k v_e}{\omega - k v_e \pm \Omega_e^*}\,, \tag{132}$$

which in the low frequency limit becomes

$$\chi_e \simeq \mp \frac{4\pi e^2 n_e}{\omega^2 m_e} \frac{\omega - k v_e}{\Omega_e^*} \left(1 \mp \frac{\omega - k v_e}{\Omega_e^*}\right) \simeq \pm \left(\frac{c}{v_A}\right)^2 \frac{\Omega_p^*}{\omega} \left(1 \mp \frac{n_{CR}}{n_p} \frac{kc}{\omega}\right) . \quad (133)$$

In the second passage of Eq. (133) we have used the fact that $n_e \simeq n_p$ and $k v_e \simeq (n_{CR}/n_p) kc$.

The last term is the CR contribution. A power-law spectrum is assumed in momentum space with slope $-4$, as

$$g(p) = \frac{1}{p_0^3} \left(\frac{p}{p_0}\right)^{-4} \Theta(p_{max} - p) \Theta(p - p_0) , \quad (134)$$

where $\Theta$ is the step function and accounts for the limited range of momenta spanned by CRs with $p_0$ the minimum momentum of the accelerated particles able to reach the location where the calculation is performed and $p_{max} \gg p_0$ the maximum momentum. Then, the CR susceptivity is

$$\chi_{CR} = \frac{4\pi e^2 n_{CR} p_0}{\omega} \int_{p_0}^{p_{max}} dp\, p^{-3} v(p) \frac{1}{\omega - k v \pm \Omega_{CR}} \left(\frac{k v}{\omega} - 1\right) . \quad (135)$$

Remembering that the calculation is performed in the low-frequency regime $\omega \ll \Omega_p^*$ and that CRs are relativistic particles so that $\Omega_{CR} = \Omega_p^*/\gamma$ and $k v \sim kc \gg \omega$, Eq. (135) can be rewritten as

$$\chi_{CR} \simeq -\frac{4\pi e^2 n_{CR} p_0}{m_p \omega^2} \frac{kc}{\Omega_p^*} \int_{p_0}^{p_{max}} dp\, p^{-2} \frac{1}{k v \gamma / \Omega_p^* \mp 1} . \quad (136)$$

## B.1 RESONANT BRANCH

The resonant branch is the one corresponding to the upper sign in the dispersion relation (124), which in other terms means that only right-handed polarized waves are considered. The reason is that the accelerated protons can resonate only with right-handed polarized Alfvén waves.

The expression for $\chi_{CR}$ in Eq. (136) presents a pole at $k v \gamma = \Omega_p^*$. We define $p_{res}(k) = \Omega_p^* m_p / k$, which corresponds to the minimum momentum of particle distribution that can resonate with waves with

wavenumber k, and we rewrite the CR susceptivity for right-handed polarized waves using the the Plemelj formula [1] as

$$\chi_{CR} \simeq -\frac{4\pi e^2 n_{CR} p_0 c}{\omega^2}\left\{\mathcal{P}\int_{p_0}^{p_{max}} dp\, p^{-2}\frac{1}{p-p_{res}(k)} -i\pi\frac{k}{\Omega_p^* m_p}\int_{p_0}^{p_{max}} dp p^{-2}\delta(p-p_{res}(k))\right\} \tag{138}$$

The term proportional to $-i\pi$ is different from zero only when $p_{res}(k) \geqslant p_0$.

When $p_{res}(k) < p_0$, or in other terms when $k > \Omega_p^* m_p/p_0$, the solution of the dispersion relation (136) gives no unstable modes, therefore we concentrate to solve Eq. (136) for those waves with $k \leqslant \Omega_p^* m_p/p_0$.

After some algebraic passage the CR susceptivity for $p_{res}(k) \geqslant p_0$ becomes

$$\chi_{CR} = \frac{4\pi e^2 n_{CR} c}{\omega^2}\frac{p_0}{p_{res}(k)}\frac{k}{\Omega_p^* m_p}[\mathcal{I}_r(k) - i\pi] \tag{139}$$

where we have introduced

$$\begin{aligned}\mathcal{I}_r(k) &= \lim_{\epsilon\to 0}\left\{\int_{kr_{L,0}}^{1-\epsilon} ds\,\frac{s^{-2}}{1-s} - \int_{1+\epsilon}^{\infty} ds\,\frac{s^{-2}}{1-s}\right\} \\ &= \frac{1}{kr_{L,0}} + \ln\left(\frac{1-kr_{L,0}}{kr_{L,0}}\right),\end{aligned} \tag{140}$$

with the variable of integration s defined as $p/p_{res}(k)$ and we have used the fact that $p_0/p_{res}(k) = kr_{L,0}$ and $r_{L,0} = p_0/(m_p\Omega_p^*)$.

We note that the total number of particles able to resonate with a k-mode, namely $N(p > p_{res}(k))$, is

$$\begin{aligned}N(p > p_{res}(k)) &= \int_{p_{res}(k)}^{\infty} dp\int_{-1}^{1} d\mu 2\pi p^2\, f_{CR}^0(p,\mu) \\ &= n_{CR}\frac{p_0}{p_{res}(k)},\end{aligned} \tag{141}$$

so that Eq. (139) can be rewritten as

$$\chi_{CR} = \left(\frac{c}{v_A}\right)^2 \frac{N(p > p_{res}(k))}{n_p}\frac{kc\Omega_p^*}{m_p}[\mathcal{I}_r(k) - i\pi]\,. \tag{142}$$

Finally we can write the dispersion relation for these unstable resonant modes which reads

$$\omega^2 = \frac{n_{CR}}{n_p}\Omega_p^* kc - \frac{N(p > p_{res}(k))}{n_p}\Omega_p^* kc[1 - \mathcal{I}_{nr}(k)] + v_A^2 k^2\,. \tag{143}$$

1 The Plemelj formula [152] states that the integral of a complex-valued function f defined and continuous on the real line between a and b divided by a pole of the first order can be solved as

$$\lim_{\epsilon\to 0}\int_a^b dx\frac{f(x)}{x \pm i\epsilon} = \mp i\pi\int_a^b dx f(x)\delta(x) + \mathcal{P}\int_a^b dx\frac{f(x)}{x} \tag{137}$$

where $\mathcal{P}$ denotes the Cauchy principal value.

We consider the generation of unstable resonant modes in regions near SNRs where we can assume that $n_{CR}/n_p \ll v_A^2/c^2$ [1], so that the solutions to Eq. (143) for the real and the imaginary part of the wave-frequency are

$$\omega_R = k v_A \tag{144}$$

$$\omega_I = \frac{\pi}{2}\Omega_p^* \frac{c}{v_A}\frac{N(p > p_{res}(k))}{n_p}\,. \tag{145}$$

These are Alfvén waves whose growth rate $\omega_I$ is the standard one, already known for the case of shocks, where c has to be replaced with the shock velocity $V_{sh}$ (see Ref. [22, 23]).

## B.2 NON-RESONANT BRANCH

The non-resonant branch is the one corresponding to the lower sign in the dispersion relation (124), which in other terms means that only left-handed polarized waves are considered. Indeed, the return current is composed mainly by background electrons which can resonate only with this type of waves.

In this regime the integral in Eq. (136) does not present any pole so that it can be rewritten as

$$\chi_{CR} = -\left(\frac{c}{v_A}\right)^2 \frac{n_{CR}}{n_p}\frac{kc\Omega_p^*}{\omega^2}\mathcal{I}_{nr}(k)\,, \tag{146}$$

where it has been introduced the function $\mathcal{I}(k)$ defined as

$$\begin{aligned}\mathcal{I}_{nr}(k) &= k r_{L,0}\int_{k r_{L,0}}^{(p_{max}/p_0)k r_{L,0}} ds\,\frac{s^{-2}}{1+s} \\ &\simeq 1 - k r_{L,0}\ln\left[\frac{1+k r_{L,0}}{k r_{L,0}}\right]\end{aligned} \tag{147}$$

with $r_{L,0} = p_0/(m_p\Omega_p^*)$. Putting all terms together, the dispersion relation of the non-resonant streaming modes in the low-frequency approximation turns out to be

$$\omega^2 = -\frac{n_{CR}}{n_p}\Omega_p^* kc[1 - \mathcal{I}_{nr}(k)] + v_A^2 k^2\,. \tag{148}$$

This dispersion relation gives unstable modes if the condition

$$\frac{n_{CR}}{n_p}\Omega_p^* kc[1 - \mathcal{I}_{nr}(k)] > v_A^2 k^2 \tag{149}$$

is satisfied. Under this condition the unstable modes are purely growing waves and their growth rate is

$$\omega_I = \sqrt{\frac{n_{CR}}{n_p}\Omega_p^* kc[1 - \mathcal{I}_{nr}(k)] - v_A^2 k^2}\,. \tag{150}$$

# C NUMERICAL TREATMENT FOR WAVE AND TRANSPORT EQUATIONS

## C.1 DISCRETIZATION OF WAVE AND TRANSPORT EQUATIONS

For the Alfvén speed we use the following expression:

$$v_A(z) = \begin{cases} +v_A & z > 0 \\ 0 & z = 0 \\ -v_A & z < 0 \end{cases}$$

where $v_A = B_0/\sqrt{4\pi n_d m_p}$ and therefore the spatial gradient is

$$\frac{dv_A}{dz} = 2v_A\delta(z)\,. \tag{151}$$

The 1D CR transport equation

$$\frac{\partial f}{\partial t} + v_A\frac{\partial f}{\partial z} - \frac{\partial}{\partial z}\left[D(p,z,t)\frac{\partial f}{\partial z}\right] - \frac{1}{3}\frac{dv_A}{dz}p\frac{\partial f}{\partial p} = 0\,, \tag{152}$$

while the wave equation is

$$\frac{\partial \mathcal{F}}{\partial t} + v_A\frac{\partial \mathcal{F}}{\partial z} = (\Gamma_{CR} - \Gamma_D)\mathcal{F}(k,z,t)\,, \tag{153}$$

and in the quasi-linear theory the spatial diffusion coefficient is calculated as

$$D = \frac{1}{3}r_L(p)\frac{v(p)}{\mathcal{F}(k_{res}(p))} \tag{154}$$

We pass to describe the numerical method used to solve the system formed by equation (152) and by equation (153).
Partial derivatives are discretized using a finite difference scheme in which linear grids are used, with a spatial resolution $Dz$ and a temporal resolution $Dt$. The evaluation of the spatial derivative is per-

formed with respect to the edges of the cell on a linear grid of $N_z + 1$ points ($0 \leqslant z \leqslant L_c$) as following [153]

$$\left.\frac{\partial f}{\partial z}\right|_z = \frac{f[z+Dz] - f[z-Dz]}{2Dz} \quad i_z = 1, \ldots, N_z - 1\,, \tag{155}$$

$$\left.\frac{\partial f}{\partial z}\right|_{z=0} = \frac{f[z+Dz] - f[z]}{Dz} \quad i_z = 0\,, \tag{156}$$

$$\left.\frac{\partial f}{\partial z}\right|_{z=L_c} = \frac{f[z] - f[z-Dz]}{Dz} \quad i_z = N_z\,. \tag{157}$$

$$\left.\frac{\partial^2 f}{\partial z^2}\right|_z = \frac{f[z+Dz] - 2f[z] + f[z-Dz]}{Dz^2} \quad i_z = 1, \ldots, N_z - 1\,. \tag{158}$$

### C.1.1 Initial conditions

At $t = 0$ I impose the following initial conditions:

$$f[t = 0, z, p] = A'(p) \exp[-(z/z_0)^2] + f_g(p) \tag{159}$$

$$D[t = 0, z, p] = D_g(p) \tag{160}$$

$$\mathcal{F}[t = 0, z, p] = \mathcal{F}_g(p) \tag{161}$$

where $A'(p)$ is a normalization constant defined as

$$A'(p) = \frac{q_0(p) T_{SN}}{\int_{-L_c}^{L_c} dz \exp[-(z/z_0)^2]} \tag{162}$$

and $q_0(p) = (p/p_0)^{-4} \times \xi E_{SN}/(T_{SN} \pi R_{SN}^2 I)$, $L_c = 100\,\mathrm{pc}$ and $z_0 = 4\,\mathrm{pc}$.
The analytic expression for $f_g$ and $D_g$ are:

$$f_g(p) = 5.7 \times 10^{30} \left(\frac{p}{p_0}\right)^{-4.7} \left(\frac{\mathrm{erg}}{c}\right)^{-3} \mathrm{cm}^{-3}\,, \tag{163}$$

$$D_g(p) = 3.6 \times 10^{28} \left(\frac{p}{p_0}\right)^{1/3} \mathrm{cm}^2 \mathrm{s}^{-1}\,. \tag{164}$$

### C.1.2 Boundary conditions

The transport equation (152) is a second-order partial differential equation, therefore it need two boundary conditions. I impose a first condition on the distribution function at $z = L_c$, i.e.

$$f[t, z = L_c, p] = f_g(p)\,. \tag{165}$$

The second boundary condition comes from the integration of Eq. (152) between $z = 0^+$ and $z = 0^-$

$$\int_{0^-}^{0^+} dz \left\{ \frac{\partial f}{\partial t} + v_A \frac{\partial f}{\partial z} - \frac{\partial}{\partial z}\left[ D(p, z, t) \frac{\partial f}{\partial z} \right] - \frac{1}{3} \frac{dv_A}{dz} p \frac{\partial f}{\partial p} \right\} = 0 \tag{166}$$

We analyze each of the four terms into the integral:

1. $\int_{0^-}^{0^+} \frac{\partial f}{\partial t}\, dz = 0$ because the distribution function is a continuos function;
2. $\int_{0^-}^{0^+} v_A \frac{\partial f}{\partial z}\, dz = v_A f|_{0^-}^{0^+} - \int_{0^-}^{0^+} f \frac{dv_A}{dz}\, dz = 0$. Indeed, the first term $v_A f|_{0^-}^{0^+} = v_A f(0^+) + v_A f(0^-) = 2v_A f(0)$ due to the symmetry property of $f$ with respect to $z = 0$. The second term is $-\int_{0^-}^{0^+} f \frac{dv_A}{dz}\, dz = -\int_{0^-}^{0^+} f 2v_A \delta(z)\, dz = -2v_A f(0)$. Thus, also the total expression is zero;
3. $-\int_{0^-}^{0^+} \frac{\partial}{\partial z}\left[D(p,z,t)\frac{\partial f}{\partial z}\right]\, dz = -D\frac{\partial f}{\partial z}\big|_{0^-}^{0^+} = -2D(z=0)\frac{\partial f}{\partial z}\big|_{z=0}$, because $D$ is symmetric around $z = 0$ while $\frac{\partial f}{\partial z}$ is antisymmetric;
4. $-\int_{0^-}^{0^+} \frac{1}{3}\frac{dv_A}{dz} p \frac{\partial f}{\partial p}\, dz = -\int_{0^-}^{0^+} \frac{1}{3} 2v_A \delta(z) p \frac{\partial f}{\partial p} = -\frac{2}{3} v_A p \frac{\partial f}{\partial p}\Big|_{z=0}$.

Therefore the boundary condition on the spatial derivative is

$$-2D(z=0)\frac{\partial f}{\partial z}\Big|_{z=0} - \frac{2}{3} v_A p \frac{\partial f}{\partial p}\Big|_{z=0} = 0\,, \tag{167}$$

using the discretization this expression becomes

$$f(0) = f(Dz) + \frac{v_A}{3} p\, \frac{\partial f}{\partial p}\Big|_{z=0} \frac{Dz}{D(z=0)}\,. \tag{168}$$

The wave equation is a first order partial differential equation, so it need only one boundary condition. I assume that in $z = 0$

$$\frac{\partial \mathcal{F}}{\partial z}\Big|_{z=0} = 0\,, \tag{169}$$

which means that $\mathcal{F}(0) = \mathcal{F}(Dz)$.

## C.2 NUMERICAL ALGORITHM

At $t > 0$ the procedure I implemented to solve equation (152) and equation (153) is:

1. calculate the growth rate of the streaming $\Gamma_{CR}$ using the quantities $f$ and $\mathcal{F}$ known at $t - Dt$

$$\Gamma_{CR}[t - Dt, z] = \frac{16\pi^2 v_A}{3\mathcal{F}[t - Dt, z] B_0^2} p^4 \nu(p)\, \frac{\partial f[t - Dt]}{\partial z}\Big|_z \tag{170}$$

   where the partial derivate is discretized as reported in Eq. (158);

2. calculate the non-linear damping $\Gamma_{NLD}$ using the quantity $\mathcal{F}$ known at $t - Dt$

$$\Gamma_{NLD}[t - Dt, z] = (2c_k)^{-3/2} k\, v_A \sqrt{\mathcal{F}[t - Dt, z]} \tag{171}$$

3. calculate $\mathcal{F}[t,z]$ discretizing Eq. (153) in the following way: for $i_z = 1,\dots,N_z-1$

$$\begin{aligned}\mathcal{F}[t,z] =& \mathcal{F}[t-Dt,z] - Dt\ v_A \frac{\mathcal{F}[t-Dt,z+Dz]-\mathcal{F}[t-Dt,z-Dz]}{2Dz}\\ &+ Dt\ \Gamma_{CR}[t-Dt,z]\mathcal{F}[t-Dt,z]\\ &- Dt\ (\Gamma_{NLD}[t-Dt,z]+\Gamma_{IN}+\Gamma_{FG})\mathcal{F}[t-Dt,z]\\ &+ Dt\ (\Gamma_{NLD,g}+\Gamma_{IN}+\Gamma_{FG})\mathcal{F}_g \end{aligned} \tag{172}$$

where $\Gamma_{NLD,g} = (2c_k)^{-3/2} k\, v_A \sqrt{\mathcal{F}_g}$.
For $i_z = N_z$

$$\begin{aligned}\mathcal{F}[t,N_z] =& \mathcal{F}[t-Dt,N_z] - Dt\ v_A \frac{\mathcal{F}[t-Dt,N_z]-\mathcal{F}[t-Dt,N_z-1]}{Dz}\\ &+ Dt\ \Gamma_{CR}[t-Dt,N_z]\mathcal{F}[t-Dt,N_z]\\ &- Dt\ (\Gamma_{NLD}[t-Dt,N_z]+\Gamma_{IN}+\Gamma_{FG})\mathcal{F}[t-Dt,N_z]\\ &+ Dt\ (\Gamma_{NLD,g}+\Gamma_{IN}+\Gamma_{FG})\mathcal{F}_g \end{aligned} \tag{173}$$

The last term $+Dt\ (\Gamma_{NLD,g}+\Gamma_{IN}+\Gamma_{FG})\mathcal{F}_g$ has been introduced to solve the numerical problem of $\mathcal{F}[t,z] < 0$ at $z \sim 0$. The boundary condition I use at $z = 0$ is

$$\left.\frac{\partial \mathcal{F}}{\partial z}\right|_{z=0} = 0\,. \tag{174}$$

4. calculate the diffusion coefficient using the quasi-linear approximation as

$$D[t,z] = \frac{1}{3} r_L(p) \frac{v(p)}{\mathcal{F}[t,z]}\,. \tag{175}$$

5. solve the CR transport equation (152) using the following discretization for $z = 1,\dots,N_z-1$

$$\begin{aligned}&f[t,z] + Dt\, v_A \frac{f[t,z+Dz]-f[t,z-Dz]}{2Dz}\\ &- DtD[t,z]\left\{\frac{f[t,z+Dz]-2f[t,z]+f[t,z-Dz]}{Dz^2}\right\}\\ &- Dt\left[\frac{D[t,z+Dz]-D[z-Dz]}{2Dz}\right]\frac{f[t,z+Dz]-f[t,z-Dz]}{2Dz}\\ &= f[t-Dt,z]\,. \end{aligned} \tag{176}$$

Here the two boundary conditions I implement are

$$f[t,0] = f[t,Dz] + \frac{v_A}{3} p\ \left.\frac{\partial f[t-Dt]}{\partial p}\right|_{z=0}, \tag{177}$$

$$f[t,z=L_c] = f_g(p)\,. \tag{178}$$

Eq. (176) represents a tridiagonal matrix

$$a_j x_{j-1} + b_j x_j + c_j x_{j+1} = d_j \tag{179}$$

where $j = 1, \dots N_z - 1$. We define two auxiliary variables $x_a$ and $x_c$ as

$$x_a = -\nu_A(1)\frac{Dt}{2Dz} - \frac{Dt}{Dz^2}D[t,1] + Dt\frac{D[t,2]-D[t,0]}{4Dz^2}, \quad (180)$$

$$x_c = \nu_A(N_z-1)\frac{Dt}{2Dz} - \frac{Dt}{Dz^2}D[t,N_z-1] + Dt\frac{D[t,N_z]-D[t,N_z-2]}{4Dz^2}. \quad (181)$$

We can write the coefficients of the tridiagonal matrix as

$$a_j = \begin{cases} 0 & j = 1 \\ -\nu_A(j)\frac{Dt}{2Dz} - \frac{Dt}{Dz^2}D[t,j] + Dt\frac{D[t,j+1]-D[t,j-1]}{4Dz^2} & j = 2,\dots,N_z-1 \end{cases}$$

$$b_j = \begin{cases} 1 + 2D[t,j]\frac{Dt}{Dz^2} + x_a & j = 1 \\ 1 + 2D[t,j]\frac{Dt}{Dz^2} & j = 2,\dots,N_z-1 \end{cases}$$

$$c_j = \begin{cases} \nu_A(j)\frac{Dt}{2Dz} - \frac{Dt}{Dz^2}D[t,j] - Dt\frac{D[t,j+1]-D[t,j-1]}{4Dz^2} & j = 1,\dots,N_z-2 \\ 0 & j = N_z-1 \end{cases}$$

$$d_j = \begin{cases} f[t-Dt,j] - x_a\frac{\nu_A}{3}p\left.\frac{\partial f[t-Dt]}{\partial p}\right|_{z=0} & j = 1 \\ f[t-Dt,j] & j = 2,\dots,N_z-2 \\ f[t-Dt,j] - f_g x_c & j = N_z-1 \end{cases}$$

The recipe to solve the tridiagonal system is the following:

1. define two auxiliary coefficients $c_j^{'}$ and $d_j^{'}$ in such a way that

$$c_1^{'} = \frac{c_1}{b_1} \quad \text{for} \quad j = 1 \quad (182)$$

$$d_1^{'} = \frac{d_1}{b_1} \quad \text{for} \quad j = 1 \quad (183)$$

$$c_j^{'} = \frac{c_j}{b_j - c_{j-1}^{'}a_j} \quad \text{for} \quad j = 2\dots N_z-1 \quad (184)$$

$$d_j^{'} = \frac{d_j - d_{j-1}^{'}a_j}{b_j - c_{j-1}^{'}a_j} \quad \text{for} \quad j = 2\dots N_z-1 \quad (185)$$

2. then the solution for $f[t,z]$ is

$$f[t, z = L_c] = f_g(p) \quad \text{for} \quad j = N_z \quad (186)$$

$$f[t, N_z - Dz] = d_{N_z-1}^{'} \quad \text{for} \quad j = N_z-1 \quad (187)$$

$$f[t,z_j] = d_j^{'} - c_j^{'}f[t,z_{j+1}] \quad \text{for} \quad j = N_z-1,\dots,1 \quad (188)$$

$$f[t, z = 0] = f[t,z_1] + \frac{\nu_A}{3}p\left.\frac{\partial f[t-Dt]}{\partial p}\right|_{z=0} \quad \text{for} \quad j = 0 \quad (189)$$

# BIBLIOGRAPHY


[1] Blasi, P., "The origin of galactic cosmic rays," The Astronomy and Astrophysics Review **21**, 1–73 (2013) (cit. on pp. 1, 7, 10–13, 24, 25, 40, 53, 61, 87, 99).

[2] T. K. Gaisser et al., "Cosmic ray energy spectrum from measurements of air showers," Frontiers of Physics **8**, 748–758 (2013) (cit. on pp. 1, 7, 9).

[3] J. R. Hörandel et al., "Results from the KASCADE, KASCADE-Grande, and LOPES experiments," in Journal of physics conference series, Vol. 39, edited by A. Bottino et al., Journal of Physics Conference Series (May 2006), pp. 463–470 (cit. on pp. 1, 7).

[4] T. K. Gaisser, "The Cosmic-ray Spectrum: from the knee to the ankle," Journal of Physics: Conference Series **47**, 15 (2006) (cit. on pp. 1, 7).

[5] E. Amato, "The origin of galactic cosmic rays," International Journal of Modern Physics D **23**, 1430013 (2014) (cit. on pp. 1, 10, 11, 87).

[6] I. V. M. A. W. Strong and V. Ptuskin, "Cosmic-ray propagation and interactions in the galaxy," Annual Review of Nuclear and Particle Science **57**, 285–327 (2007) (cit. on pp. 1, 12, 13, 23, 53).

[7] J. H. B. I. A. Grenier and A. W. Strong, "The nine lives of cosmic rays in galaxies," Annual Review of Astronomy and Astrophysics **53**, 199–246 (2015) (cit. on pp. 1, 12, 13, 53).

[8] M. C. Beck et al., "New constraints on modelling the random magnetic field of the MW," Journal of Cosmology and Astroparticle Physics **2016**, 056 (2016) (cit. on pp. 1, 3, 38).

[9] V. Ptuskin et al., "Non-linear diffusion of cosmic rays," Advances in Space Research **42**, 486–490 (2008) (cit. on pp. 2, 15, 26, 37, 38, 46, 71, 72, 87).

[10] M. A. Malkov et al., "Analytic solution for self-regulated collective escape of cosmic rays from their acceleration sites," The Astrophysical Journal **768**, 73 (2013) (cit. on pp. 2, 15, 26, 37, 39, 46, 56, 72, 87).

[11] L. Nava et al., "Non-linear diffusion of cosmic rays escaping from supernova remnants – i. the effect of neutrals," Monthly Notices of the Royal Astronomical Society **461**, 3552–3562 (2016) (cit. on pp. 2, 15, 26, 37, 39, 46, 52, 56, 72, 87).

[12] A. R. Bell, "The acceleration of cosmic rays in shock fronts. I," Monthly Notices of the Royal Astronomical Society **182**, 147–156 (1978) (cit. on pp. 2, 11, 25–27).

[13] A. R. Bell, "The acceleration of cosmic rays in shock fronts. II," Monthly Notices of the Royal Astronomical Society **182**, 443–455 (1978) (cit. on pp. 2, 11, 25).

[14] P. O. Lagage and C. J. Cesarsky, "Cosmic-ray shock acceleration in the presence of self-excited waves," Astronomy and Astrophysics **118**, 223–228 (1983) (cit. on pp. 2, 11, 25).

[15] P. O. Lagage and C. J. Cesarsky, "The maximum energy of cosmic rays accelerated by supernova shocks," Astronomy and Astrophysics **125**, 249–257 (1983) (cit. on pp. 2, 11, 25, 79).

[16] Bykov, A. M. et al., "Microphysics of Cosmic Ray Driven Plasma Instabilities," Space Science Reviews **178**, 201–232 (2013) (cit. on pp. 2, 11, 25, 26).

[17] J. Vink, "Supernova remnants: the x-ray perspective," The Astronomy and Astrophysics Review **20**, 49 (2011) (cit. on pp. 2, 3, 11, 25, 27, 84, 87).

[18] K. A. Eriksen et al., "Evidence for Particle Acceleration to the Knee of the Cosmic Ray Spectrum in Tycho's Supernova Remnant," The Astrophysical Journal Letters **728**, L28 (2011) (cit. on pp. 2, 11).

[19] R. Aloisio and P. Blasi, "Propagation of galactic cosmic rays in the presence of self-generated turbulence," Journal of Cosmology and Astroparticle Physics **2013**, 001 (2013) (cit. on pp. 2, 9, 55, 56).

[20] Aloisio, R. et al., "Nonlinear cosmic ray galactic transport in the light of ams-02 and voyager data," Astronomy and Astrophysics **583**, A95 (2015) (cit. on pp. 2, 54–57, 88).

[21] J. Skilling, "Cosmic ray streaming. II - Effect of particles on Alfven waves," Monthly Notices of the Royal Astronomical Society **173**, 245–254 (1975) (cit. on pp. 2, 14, 27, 37).

[22] Zweibel, E. G., "Energetic particle trapping by Alfven wave instabilities," AIP Conference Proceedings **56**, 319–328 (1979) (cit. on pp. 2, 14, 26, 37, 99).

[23] Achterberg, A., "Modification of scattering waves and its importance for shock acceleration," Astronomy and Astrophysics **119**, 274–278 (1983) (cit. on pp. 2, 14, 26, 37, 99).

[24] C. J. Cesarsky, "Cosmic-ray confinement in the galaxy," Annual Review of Astronomy and Astrophysics **18**, 289–319 (1980) (cit. on pp. 2, 26).

[25] A. R. Bell, "Turbulent amplification of magnetic field and diffusive shock acceleration of cosmic rays," Monthly Notices of the Royal Astronomical Society **353**, 550–558 (2004) (cit. on pp. 2, 21, 27, 29, 30, 75–77, 79).

[26] Bell, A. R., "The interaction of cosmic rays and magnetized plasma," Monthly Notices of the Royal Astronomical Society **358**, 181 (2005) (cit. on pp. 2, 21, 75).

[27] R. Kulsrud and W. P. Pearce, "The Effect of Wave-Particle Interactions on the Propagation of Cosmic Rays," Astrophysical Journal **156**, 445 (1969) (cit. on pp. 3, 31, 37).

[28] E. G. Zweibel and J. M. Shull, "Confinement of cosmic rays in molecular clouds," Astrophysical Journal **259**, 859–868 (1982) (cit. on pp. 3, 32, 37).

[29] P. Blasi et al., "Cosmological magnetic field limits in an inhomogeneous universe," The Astrophysical Journal Letters **514**, L79 (1999) (cit. on pp. 3, 82, 84).

[30] A. M. Hillas, "The Origin of Ultra-High-Energy Cosmic Rays," Annual review of astronomy and astrophysics **22**, 425–444 (1984) (cit. on pp. 3, 17, 76).

[31] Blasi, Pasquale, "Theoretical challenges in acceleration and transport of ultra high energy cosmic rays: A review," EPJ Web of Conferences **53**, 01002 (2013) (cit. on pp. 3, 9, 17, 19, 76).

[32] E. Waxman, "Extra galactic sources of high energy neutrinos," Physica Scripta **2005**, 147 (2005) (cit. on pp. 3, 17, 18).

[33] R. Aloisio et al., "A dip in the UHECR spectrum and the transition from galactic to extragalactic cosmic rays," Astroparticle Physics **27**, 76–91 (2007) (cit. on pp. 4, 18, 20, 21, 84, 85, 90).

[34] V. Berezinsky et al., "On astrophysical solution to ultrahigh energy cosmic rays," Physical Review D **74**, 043005, 043005 (2006) (cit. on pp. 4, 18, 20, 21, 84, 85, 90).

[35] R. Aloisio et al., "Ultra high energy cosmic rays: implications of auger data for source spectra and chemical composition," Journal of Cosmology and Astroparticle Physics **2014**, 020 (2014) (cit. on pp. 4, 18, 21, 85, 90).

[36] R. Aloisio and V. S. Berezinsky, "Anti-gzk effect in ultra-high-energy cosmic ray diffusive propagation," The Astrophysical Journal **625**, 249 (2005) (cit. on pp. 4, 20, 21, 84).

[37] M. Potgieter, "Very Local Interstellar Spectra for Galactic Electrons, Protons and Helium," Brazilian Journal of Physics **44**, 581–588 (2014) (cit. on p. 7).

[38] D. Caprioli et al., "Non-linear diffusive acceleration of heavy nuclei in supernova remnant shocks," Astroparticle Physics **34**, 447–456 (2011) (cit. on pp. 7, 9).

[39] P. Blasi and E. Amato, "Diffusive propagation of cosmic rays from supernova remnants in the Galaxy. I: spectrum and chemical composition," Journal of Cosmology and Astroparticle Physics **2012**, 010 (2012) (cit. on p. 9).

[40] O. Adriani et al., "PAMELA Measurements of Cosmic-Ray Proton and Helium Spectra," Science **332**, 69–72 (2011) (cit. on p. 9).

[41] M. Aguilar et al., "Precision Measurement of the Proton Flux in Primary Cosmic Rays from Rigidity 1 GV to 1.8 TV with the Alpha Magnetic Spectrometer on the International Space Station," Phys. Rev. Lett. **114**, 171103 (2015) (cit. on pp. 9, 40, 66).

[42] H. S. Ahn et al., "Discrepant Hardening Observed in Cosmic-ray Elemental Spectra," The Astrophysical Journal Letters **714**, L89 (2010) (cit. on p. 9).

[43] A. Obermeier et al., "Energy spectra of primary and secondary cosmic-ray nuclei measured with tracer," The Astrophysical Journal **742**, 14 (2011) (cit. on p. 9).

[44] K. Abe et al., "Measurements of cosmic-ray proton and helium spectra from the bess-polar long-duration balloon flights over antarctica," The Astrophysical Journal **822**, 65 (2016) (cit. on p. 9).

[45] S. Thoudam and J. R. Hörandel, "Nearby supernova remnants and the cosmic ray spectral hardening at high energies," Monthly Notices of the Royal Astronomical Society **421**, 1209 (2012) (cit. on p. 9).

[46] P. Blasi et al., "Spectral breaks as a signature of cosmic ray induced turbulence in the galaxy," Phys. Rev. Lett. **109**, 061101 (2012) (cit. on pp. 9, 55).

[47] D. de Marco and T. Stanev, "On the shape of the ultrahigh energy cosmic ray spectrum," Phys. Rev. D **72**, 081301, 081301 (2005) (cit. on pp. 9, 18, 21).

[48] E. Waxman, "Gamma-ray bursts, cosmic-rays and neutrinos," Nuclear Physics B - Proceedings Supplements **87**, 345–354 (2000) (cit. on pp. 9, 18, 21).

[49] O. Deligny, "Cosmic rays around : implications of contemporary measurements on the origin of the ankle feature," Comptes Rendus Physique **15**, Ultra-high-energy cosmic rays: From the ankle to the tip of the spectrum, 367–375 (2014) (cit. on pp. 9, 17, 19).

[50] P. L. Ghia, "Highlights from the Pierre Auger Observatory," Proceedings of Science **ICRC2015**, 034 (2016) (cit. on p. 9).

[51] J. Abraham et al., "Measurement of the Depth of Maximum of Extensive Air Showers above $10^{18}$ eV," Phys. Rev. Lett. **104**, 091101 (2010) (cit. on pp. 9, 19).

[52] C. Jui, "Summary of Results from the telescope Array Experiment," PoS **ICRC2015**, 035 (2016) (cit. on pp. 9, 19).

[53] C. Jui, "Cosmic Ray in the Northern Hemisphere: Results from the Telescope Array Experiment," J. Phys. Conf. Ser. **404**, 012037 (2012) (cit. on p. 9).

[54] R. U. Abbasi et al., "Measurement of the Flux of Ultrahigh Energy Cosmic Rays from Monocular Observations by the High Resolution Fly's Eye Experiment," Phys. Rev. Lett. **92**, 151101 (2004) (cit. on p. 9).

[55] W. D. Apel et al., "Ankle-like feature in the energy spectrum of light elements of cosmic rays observed with kascade-grande," Phys. Rev. D **87**, 081101 (2013) (cit. on pp. 9, 19).

[56] D. Harari, "The flux suppression at the highest energies," Comptes Rendus Physique **15**, Ultra-high-energy cosmic rays: From the ankle to the tip of the spectrum, 376–383 (2014) (cit. on p. 10).

[57] B. R. Dawson et al., "The energy spectrum of cosmic rays at the highest energies," in European physical journal web of conferences, Vol. 53, European Physical Journal Web of Conferences (June 2013), p. 01005 (cit. on p. 10).

[58] K. Greisen, "End to the cosmic-ray spectrum?" Physical Review Letters **16**, 748–750 (1966) (cit. on p. 10).

[59] G. T. Zatsepin and V. A. Kuz'min, "Upper Limit of the Spectrum of Cosmic Rays," ZhETF Pisma Redaktsiiu **4**, 114 (1966) (cit. on p. 10).

[60] R. U. Abbasi et al., "First observation of the greisen-zatsepin-kuzmin suppression," Phys. Rev. Lett. **100**, 101101 (2008) (cit. on p. 10).

[61] Barcikowski, E. et al., "Mass composition working group report," EPJ Web of Conferences **53**, 01006 (2013) (cit. on pp. 10, 19).

[62] W. Baade and F. Zwicky, "Cosmic rays from super-novae," Proceedings of the National Academy of Sciences of the United States of America **20**, 259–263 (1934) (cit. on p. 10).

[63] V. L. Ginzburg and S. I. Syrovatsky, "Origin of Cosmic Rays," Progress of Theoretical Physics Supplement **20**, 1–83 (1961) (cit. on p. 11).

[64] G. F. Krymskii, "A regular mechanism for the acceleration of charged particles on the front of a shock wave," Akademiia Nauk SSSR Doklady **234**, 1306–1308 (1977) (cit. on p. 11).

[65] W. I. Axford et al., "The acceleration of cosmic rays by shock waves," International Cosmic Ray Conference **11**, 132–137 (1977) (cit. on p. 11).

[66] R. D. Blandford and J. P. Ostriker, "Particle acceleration by astrophysical shocks," Astrophysical Journal **221**, L29–L32 (1978) (cit. on p. 11).

[67] R. A. Treumann, "Fundamentals of collisionless shocks for astrophysical application, 1. Non-relativistic shocks," The Astronomy and Astrophysics Review **17**, 409–535 (2009) (cit. on p. 11).

[68] Caprioli, D. et al., "On the escape of particles from cosmic ray modified shocks," Monthly Notices of the Royal Astronomical Society **396**, 2065 (2009) (cit. on p. 11).

[69] D. Caprioli et al., "Comparison of different methods for non-linear diffusive shock acceleration," Monthly Notices of the Royal Astronomical Society **407**, 1773 (2010) (cit. on p. 11).

[70] Malkov, M. A. and Drury, L. O., "Nonlinear theory of diffusive acceleration of particles by shock waves," Reports on Progress in Physics **64**, 429 (2001) (cit. on p. 11).

[71] L. O. Drury et al., "The gamma-ray visibility of supernova remnants. A test of cosmic ray origin," Astronomy and Astrophysics **287**, 959–971 (1994) (cit. on p. 11).

[72] Giuliani, A. et al., "AGILE detection of GeV $\gamma$-ray emission from the SNR W28," Astronomy and Astrophysics **516**, L11 (2010) (cit. on p. 12).

[73] A. Giuliani et al., "Neutral Pion Emission from Accelerated Protons in the Supernova Remnant W44," The Astrophysical Journal Letters **742**, L30 (2011) (cit. on p. 12).

[74] A. A. Abdo et al., "Fermi LAT Discovery of Extended Gamma-Ray Emission in the Direction of Supernova Remnant W51C," The Astrophysical Journal Letters **706**, L1 (2009) (cit. on p. 12).

[75] A. A. Abdo et al., "Fermi Large Area Telescope Observations of the Supernova Remnant W28 (G6.4-0.1)," The Astrophysical Journal **718**, 348 (2010) (cit. on p. 12).

[76] A. A. Abdo et al., "Gamma-Ray Emission from the Shell of Supernova Remnant W44 Revealed by the Fermi LAT," Science **327**, 1103–1106 (2010) (cit. on p. 12).

[77] A. A. Abdo et al., "Observation of Supernova Remnant IC 443 with the Fermi Large Area Telescope," The Astrophysical Journal **712**, 459 (2010) (cit. on p. 12).

[78] M. Ackermann et al., "Detection of the characteristic pion-decay signature in supernova remnants," Science **339**, 807–811 (2013) (cit. on p. 12).

[79] S. Gabici et al., "Gamma rays from molecular clouds," Astrophysics and Space Science **309**, 365–371 (2007) (cit. on p. 12).

[80] S. Gabici et al., "Broad–band non–thermal emission from molecular clouds illuminated by cosmic rays from nearby supernova remnants," Monthly Notices of the Royal Astronomical Society **396**, 1629 (2009) (cit. on p. 12).

[81] L. Nava and S. Gabici, "Anisotropic cosmic ray diffusion and gamma-ray production close to supernova remnants, with an application to W28," Monthly Notices of the Royal Astronomical Society **429**, 1643–1651 (2013) (cit. on p. 12).

[82] Maurin, D. et al., "A database of charged cosmic rays," Astronomy and Astrophysics **569**, A32 (2014) (cit. on pp. 13, 53).

[83] M. Aguilar et al., "Precision measurement of the boron to carbon flux ratio in cosmic rays from 1.9 gv to 2.6 tv with the alpha magnetic spectrometer on the international space station," Physical Review Letters **117** (2016) 10.1103/PhysRevLett.117.231102 (cit. on pp. 13, 16).

[84] A. N. Kolmogorov, "The local structure of turbulence in incompressible viscous fluid for very large reynolds numbers," Proceedings of the Royal Society of London A: Mathematical, Physical and Engineering Sciences **434**, 9–13 (1991) (cit. on p. 13).

[85] R. Cowsik and B. Burch, "Positron fraction in cosmic rays and models of cosmic-ray propagation," Phys. Rev. D **82**, 023009, 023009 (2010) (cit. on p. 16).

[86] R. Cowsik et al., "The origin of the spectral intensities of cosmic-ray positrons," The Astrophysical Journal **786**, 124 (2014) (cit. on p. 16).

[87] R. Cowsik and T. Madziwa-Nussinov, "Spectral intensities of antiprotons and the nested leaky-box model for cosmic rays in the galaxy," The Astrophysical Journal **827**, 119 (2016) (cit. on p. 16).

[88] R. Yang et al., "Radial distribution of the diffuse $\gamma$-ray emissivity in the Galactic disk," Phys. Rev. D **93**, 123007 (2016) (cit. on pp. 16, 38, 58, 61–66, 68, 73, 89).

[89] F. Acero et al., "Development of the Model of Galactic Interstellar Emission for Standard Point-source Analysis of Fermi Large Area Telescope Data," The Astrophysical Journal Supplement Series **223**, 26 (2016) (cit. on pp. 16, 38, 58, 61–63, 66–68, 73, 89).

[90] M. Vietri, *Foundations of high-energy astrophysics*, Theoretical Astrophysics (University of Chicago Press, 2008) (cit. on pp. 18, 23, 25, 40, 61, 93).

[91] R. Lovelace, "Dynamo model of double radio sources," Nature **262**, 649–652 (1976) (cit. on p. 18).

[92] Aharonian, F. A. and Belyanin, A. A. and Derishev, E. V. and Kocharovsky, V. V. and Kocharovsky, Vl. V., "Constraints on the extremely high-energy cosmic ray accelerators from classical electrodynamics," Physical Review D **66** (2002) 10.1103/PhysRevD.66.023005 (cit. on p. 18).

[93] D. Allard et al., "On the transition from galactic to extragalactic cosmic-rays: spectral and composition features from two opposite scenarios," Astroparticle Physics **27**, 61–75 (2007) (cit. on pp. 18, 21).

[94] E. G. Berezhko and H. J. Völk, "Spectrum of cosmic rays produced in supernova remnants," The Astrophysical Journal Letters **661**, L175 (2007) (cit. on p. 19).

[95] W. D. Apel et al., "Kneelike structure in the spectrum of the heavy component of cosmic rays observed with kascade-grande," Phys. Rev. Lett. **107**, 171104 (2011) (cit. on p. 19).

[96] S. Berezhnev et al., "The Tunka-133 {EAS} Cherenkov light array: Status of 2011," Nuclear Instruments and Methods in Physics Research Section A: Accelerators, Spectrometers, Detectors and Associated Equipment **692**, 3rd Roma International Conference on Astroparticle Physics, 98–105 (2012) (cit. on p. 19).

[97] R. U. Abbasi et al., "Indications of proton-dominated cosmic-ray composition above 1.6 eev," Phys. Rev. Lett. **104**, 161101 (2010) (cit. on p. 19).

[98] E. Berezhko et al., "Composition of cosmic rays at ultra high energies," Astroparticle Physics **36**, 31–36 (2012) (cit. on p. 19).

[99] V. Berezinsky et al., "Dip in {UHECR} spectrum as signature of proton interaction with {CMB}," Physics Letters B **612**, 147–153 (2005) (cit. on p. 20).

[100] Allard, D. et al., "Uhe nuclei propagation and the interpretation of the ankle in the cosmic-ray spectrum," Astronomy and Astrophysics **443**, L29–L32 (2005) (cit. on p. 20).

[101] R. Aloisio et al., "Ultra high energy cosmic rays: The disappointing model," Astroparticle Physics **34**, 620–626 (2011) (cit. on p. 20).

[102] M. Lemoine, "Extragalactic magnetic fields and the second knee in the cosmic-ray spectrum," Phys. Rev. D **71**, 083007 (2005) (cit. on pp. 20, 21).

[103] J. Skilling, "Cosmic ray streaming. I - Effect of Alfven waves on particles," Monthly Notices of the Royal Astronomical Society **172**, 557–566 (1975) (cit. on pp. 23, 24).

[104] R. Blandford and D. Eichler, "Particle acceleration at astrophysical shocks: A theory of cosmic ray origin," Physics Reports **154**, 1–75 (1987) (cit. on pp. 23, 91).

[105] G. Zank, *Transport processes in space physics and astrophysics*, Lecture Notes in Physics (Springer New York, 2013) (cit. on pp. 23, 91, 93).

[106] H. Alfvén, "Existence of Electromagnetic-Hydrodynamic Waves," Nature **150**, 405–406 (1942) (cit. on p. 23).

[107] Yan, H. and Lazarian, A., "Scattering of Cosmic Rays by Magnetohydrodynamic Interstellar Turbulence," Physical Review Letters **89** (2002) 10.1103/PhysRevLett.89.281102 (cit. on p. 24).

[108] Benjamin D. G. Chandran, "Weak compressible magnetohydrodynamic turbulence in the solar corona," Physical Review Letters **95** (2005) 10.1103/PhysRevLett.95.265004 (cit. on p. 24).

[109] C. F. Kennel and F. Engelmann, "Velocity space diffusion from weak plasma turbulence in a magnetic field," The Physics of Fluids **9**, 2377–2388 (1966) (cit. on p. 24).

[110] V. S. Berezinskii et al., *Astrophysics of cosmic rays*, edited by V. L. Ginzburg (North-Holland, 1990) (cit. on p. 25).

[111] R. Schlickeiser, *Cosmic ray astrophysics*, Astronomy and Astrophysics Library (Springer Berlin Heidelberg, 2002) (cit. on p. 25).

[112] J. Ballet, "X-ray synchrotron emission from supernova remnants," Advances in Space Research **37**, Astrophysics, 1902–1908 (2006) (cit. on p. 26).

[113] Y. Uchiyama et al., "Extremely fast acceleration of cosmic rays in a supernova remnant," Nature **449**, 576–578 (2007) (cit. on p. 26).

[114] J. Skilling, "Cosmic Rays in the Galaxy: Convection or Diffusion?" Astrophysical Journal **170**, 265 (1971) (cit. on p. 26).

[115] D. G. Wentzel, "Cosmic-ray propagation in the galaxy: collective effects," Ann. Rev. Astron. Astrophys. **12**, 71–96 (1974) (cit. on p. 26).

[116] J. A. Holmes and D. W. Sciama, "The confinement of galactic cosmic rays by alfvén waves," Monthly Notices of the Royal Astronomical Society **170**, 251–260 (1975) (cit. on p. 26).

[117] M. D'Angelo et al., "Grammage of cosmic rays around galactic supernova remnants," Phys. Rev. D **94**, 083003 (2016) (cit. on pp. 26, 37, 52, 54, 89).

[118] Caprioli, D., "Cosmic-ray acceleration and propagation," Proceedings of Science **ICRC2015** (2016) (cit. on p. 26).

[119] L. Spitzer, *Physical processes in the interstellar medium* (1978) (cit. on p. 26).

[120] J. Skilling, "Cosmic ray streaming. III - Self-consistent solutions," Monthly Notices of the Royal Astronomical Society **173**, 255–269 (1975) (cit. on p. 26).

[121] P. Blasi et al., "High-energy cosmic ray self-confinement close to extra-galactic sources," Physical Review Letters **115** (2015) 10.1103/PhysRevLett.115.121101 (cit. on pp. 29, 77, 90).

[122] A. J. Farmer and P. Goldreich, "Wave damping by magnetohydrodynamic turbulence and its effect on cosmic-ray propagation in the interstellar medium," The Astrophysical Journal **604**, 671 (2004) (cit. on pp. 30, 34, 38, 42, 43).

[123] V. S. Ptuskin and V. N. Zirakashvili, "Limits on diffusive shock acceleration in supernova remnants in the presence of cosmic-ray streaming instability and wave dissipation," Astronomy and Astrophysics **403**, 1–10 (2003) (cit. on pp. 30, 37).

[124] J. Wiener et al., "Cosmic Ray Heating of the Warm Ionized Medium," Astrophysical Journal **767**, 87, 87 (2013) (cit. on p. 30).

[125] E. G. Zweibel, "The microphysics and macrophysics of cosmic rays," Physics of Plasmas **20**, 055501 (2013) (cit. on p. 30).

[126] N. Krall and A. Trivelpiece, *Principles of plasma physics*, International series in pure and applied physics v. 0-911351 (McGraw-Hill, 1973) (cit. on pp. 31, 95).

[127] L. O'C Drury et al., "Limits on diffusive shock acceleration in dense and incompletely ionised media.," Astronomy and Astrophysics **309**, 1002–1010 (1996) (cit. on p. 31).

[128] P. Jean et al., "Positron transport in the interstellar medium," Astronomy and Astrophysics **508**, 1099–1116 (2009) (cit. on pp. 33, 43, 45).

[129] P. Goldreich and S. Sridhar, "Toward a theory of interstellar turbulence. 2: Strong alfvenic turbulence," Astrophysical Journal **438**, 763–775 (1995) (cit. on p. 34).

[130] P. Goldreich and S. Sridhar, "Magnetohydrodynamic turbulence revisited," Astrophysical Journal **485**, 680 (1997) (cit. on pp. 34, 35).

[131] R. Benzi and U. Frisch, "Turbulence," Scholarpedia **5**, 3439 (2010) (cit. on p. 35).

[132] V. Ptuskin et al., "On leaky-box approximation to {galprop}," Astroparticle Physics **31**, 284–289 (2009) (cit. on pp. 41, 55, 56).

[133] K. M. Ferrière, "The interstellar environment of our galaxy," Rev. Mod. Phys. **73**, 1031–1066 (2001) (cit. on pp. 42, 45).

[134] K. M. Ferrière, "Global model of the interstellar medium in our galaxy with new constraints on the hot gas component," The Astrophysical Journal **497**, 759 (1998) (cit. on pp. 43–45).

[135] "Aladdin, numerical database of atomic and molecular data," (cit. on pp. 43, 72).

[136] R. M. Kulsrud and C. J. Cesarsky, "The Effectiveness of Instabilities for the Confinement of High Energy Cosmic Rays in the Galactic Disk," Astrophysical Letters **8**, 189 (1971) (cit. on p. 43).

[137] F. A. Aharonian and A. M. Atoyan, "Broad-band diffuse gamma ray emission of the galactic disk," Astronomy and Astrophysics **362**, 937–952 (2000) (cit. on pp. 58, 59).

[138] F. A. Aharonian and A. M. Atoyan, "On the emissivity of π^o^-decay gamma radiation in the vicinity of accelerators of galactic cosmic rays.," Astronomy and Astrophysics **309**, 917–928 (1996) (cit. on pp. 58, 73).

[139] S. R. Kelner et al., "Energy spectra of gamma rays, electrons, and neutrinos produced at proton-proton interactions in the very high energy regime," Phys. Rev. D **74**, 034018 (2006) (cit. on p. 59).

[140] D. A. Green, "Constraints on the distribution of supernova remnants with galactocentric radius," Monthly Notices of the Royal Astronomical Society **454**, 1517 (2015) (cit. on pp. 60, 61).

[141] S. Recchia et al., "On the radial distribution of Galactic cosmic rays," Monthly Notices of the Royal Astronomical Society **462**, L88–L92 (2016) (cit. on p. 61).

[142] W. B. Atwood et al., "The large area telescope on the fermi gamma-ray space telescope mission," The Astrophysical Journal **697**, 1071 (2009) (cit. on p. 62).

[143] A. R. Bell and S. G. Lucek, "Cosmic ray acceleration to very high energy through the non-linear amplification by cosmic rays of the seed magnetic field," Monthly Notices of the Royal Astronomical Society **321**, 433 (2001) (cit. on pp. 76, 79).

[144] M. A. Riquelme and A. Spitkovsky, "Nonlinear Study of Bell's Cosmic Ray Current-Driven Instability," The Astrophysical Journal **694**, 626 (2009) (cit. on pp. 79, 84).

[145] Marcowith, A. et al., "Turbulence and particle acceleration in collisionless supernovae remnant shocks - ii. cosmic-ray transport," Astronomy and Astrophysics **453**, 193–202 (2006) (cit. on p. 79).

[146] K. Dolag et al., "Constrained simulations of the magnetic field in the local universe and the propagation of ultrahigh energy cosmic rays," Journal of Cosmology and Astroparticle Physics **2005**, 009 (2005) (cit. on pp. 82, 84).

[147] A. Neronov and I. Vovk, "Evidence for Strong Extragalactic Magnetic Fields from Fermi Observations of TeV Blazars," Science **328**, 73–75 (2010) (cit. on p. 84).

[148] Taylor, A. M. et al., "Extragalactic magnetic fields constraints from simultaneous GeV-TeV observations of blazars," Astronomy and Astrophysics **529**, A144 (2011) (cit. on p. 84).

[149] E. Armengaud, "Ultrahigh energy nuclei propagation in a structured, magnetized universe," Physical Review D **72** (2005) 10.1103/PhysRevD.72.043009 (cit. on p. 84).

[150] D. Caprioli et al., "The contribution of supernova remnants to the galactic cosmic ray spectrum," Astroparticle Physics **33**, 160–168 (2010) (cit. on p. 88).

[151] E. Amato and P. Blasi, "A kinetic approach to cosmic-ray-induced streaming instability at supernova shocks," Monthly Notices of the Royal Astronomical Society **392**, 1365–2966 (2009) (cit. on p. 95).

[152] J. Plemelj, *Problems in the sense of riemann and klein*, Sense of Riemann & Klein: Interscience T (Interscience Publishers, 1964) (cit. on p. 98).

[153] W. H. Press et al., *Numerical recipes 3rd edition: the art of scientific computing*, 3rd ed. (Cambridge University Press, New York, NY, USA, 2007) (cit. on p. 102).